A TECHNIQUE FOR STUDYING INTERACTIONS BETWEEN A SUPERSONIC BODY AND BLAST WAVES APPROACHING OBLIQUELY

By

RUSI JAL DAMKEVALA

Bachelor of Engineering
Gujarat University
Ahmedabad, India
1960

Master of Engineering
Indian Institute of Science
Bangalore, India
1962

Submitted to the Faculty of the
Graduate College of the
Oklahoma State University
in partial fulfillment of
the requirements for
the Degree of
DOCTOR OF PHILOSOPHY
May, 1967

A TECHNIQUE FOR STUDYING INTERACTIONS BETWEEN A SUPERSONIC BODY AND BLAST WAVES APPROACHING OBLIQUELY

Thesis Approved:

Glen W. Zumwalt
Thesis Adviser

Ladislaus J. Fila

R. L. Lowery

Dale D. Grosvenor

D. D. Duncan
Dean of the Graduate College

PREFACE

This work completes the development of a technique for studying side-on and oblique shock-on-shock interactions using a projectile and a shock tube. Complete sets of schlieren photographs were obtained for interaction at four different angles and three shock-model Mach number combinations.

The work was sponsored by the Sandia Corporation, Albuquerque, New Mexico, and their financial support of the author during the period of this work is appreciated. Besides this thesis, four analytical studies of related problems have been completed at Oklahoma State University under the same contract.

My sincere appreciation is due to my thesis adviser and doctoral committee chairman, Dr. G. W. Zumwalt, whose guidance, insight into the problem, and basic understanding of the trials and tribulations pertaining a work of this type are chiefly responsible for the fruition of this effort. I would also like to thank Professor L. J. Fila for serving on my doctoral committee and for his many helpful suggestions for the final draft of this thesis. I am also grateful to Drs. R. L. Lowery and D. D. Grosvenor for serving on my committee and Dr. K. N. Reid, Jr., for

his many suggestions and genuine interest in my work.

Messers. J. Rittmann, L. McCommon, and M. Cure helped me at various times throughout the course of the experimental work. Without their help, the completion of this work would have taken a great deal more time.

Finally, I thank Miss Velda Davis for typing the final draft of the thesis, Mr. Eldon Hardy for making many of the diagrams, and especially my wife, Cheryl, for her help in proofreading and for her patience and encouragement throughout the course of my studies at Oklahoma State University.

TABLE OF CONTENTS

LIST OF TABLES

LIST OF FIGURES

CHAPTER I

INTRODUCTION

When a moving shock wave encounters a body in supersonic flight, the resultant shock waves cannot be predicted simply by superposition of the moving shock wave onto the bow shock. It is known that high transient overpressures occur on the body surface. The estimation of these overpressures is important for two reasons: (1) The body encountering the blast wave has to be so designed as to withstand the stresses arising from such an encounter; (2) The trajectory of the body might be affected by unbalanced pressures on its surface, especially if the blast wave is encountered from other than a head-on direction. The current interest in the shock-on-shock problem, as this type of interaction is commonly termed, stems from the need for reliable data for the design of anti-missile missiles and, conversely, to program friendly missiles for evasive maneuvers when encountering an enemy anti-missile device.

It is generally accepted that theoretical prediction of the transient overpressures cannot be attempted without basic knowledge of the shock geometries resulting from the interaction process. An attempt to predict the shock pattern from purely physical reasoning was made by Smyrl (1)

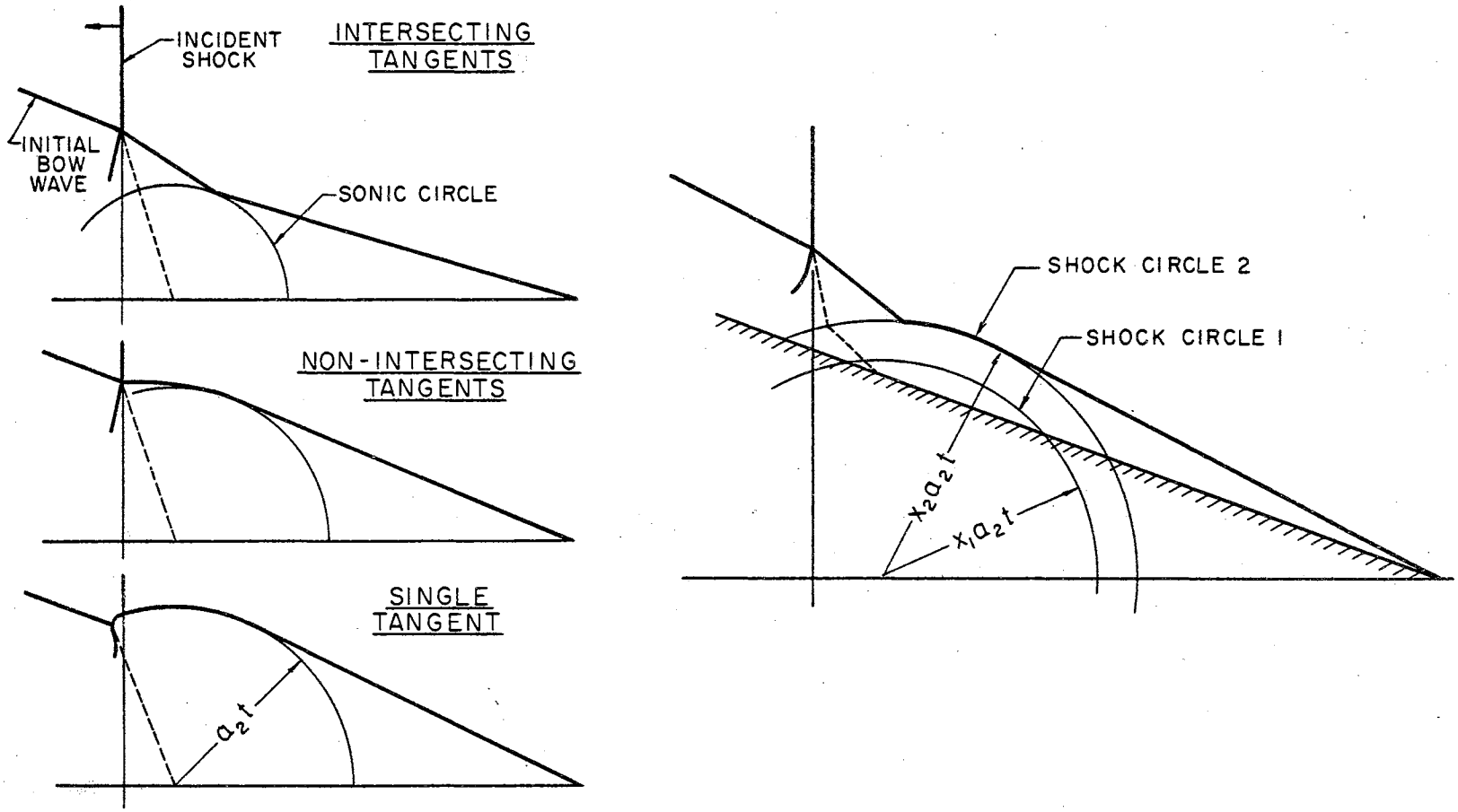

Figure 1. Comparison Between Theoretical Shock Geometries for a Wedge and Actual Geometry for a Finite Cone

who, based on this shock pattern, developed a method of calculating the pressures on the surface of a thin infinite wedge intercepting a plane blast wave. His shock patterns, however, cannot be extended simply to a finite three-dimensional body, as has been shown by Brown and Mullaney (2). Shadowgraphs of the head-on interaction between a cone-cylinder projectile and a plane blast wave show up important differences between Smyrl's picture and the actual picture for a finite body. Figure 1 shows the two geometries for the case tested by Brown and Mullaney. When the oncoming blast wave is at an angle to the axis of the body, the resulting shock geomtries should be even more difficult to predict theoretically. To date there has been no attempt to do so. The only recourse left is to obtain the pattern experimentally by shadowgraphy or schlieren photography of the simulated interaction.

Three attempts to obtain shadowgraphs of such oblique shock-on-shock interactions have previously been made (3), (4), (5). All these attempts used a shock tube mounted on the side of a supersonic windtunnel with the body immersed in the supersonic freestream. As a result, the shock wave as it emerged from the shock tube suffered considerable distortion and, more important, the amount by which the shock strength had attenuated was not predictable. The scheme used in reference (4) is shown in Figure 2. Recently, a study of a shock wave emerging into a supersonic crossflow by Tyler and Zumwalt (6) has shown

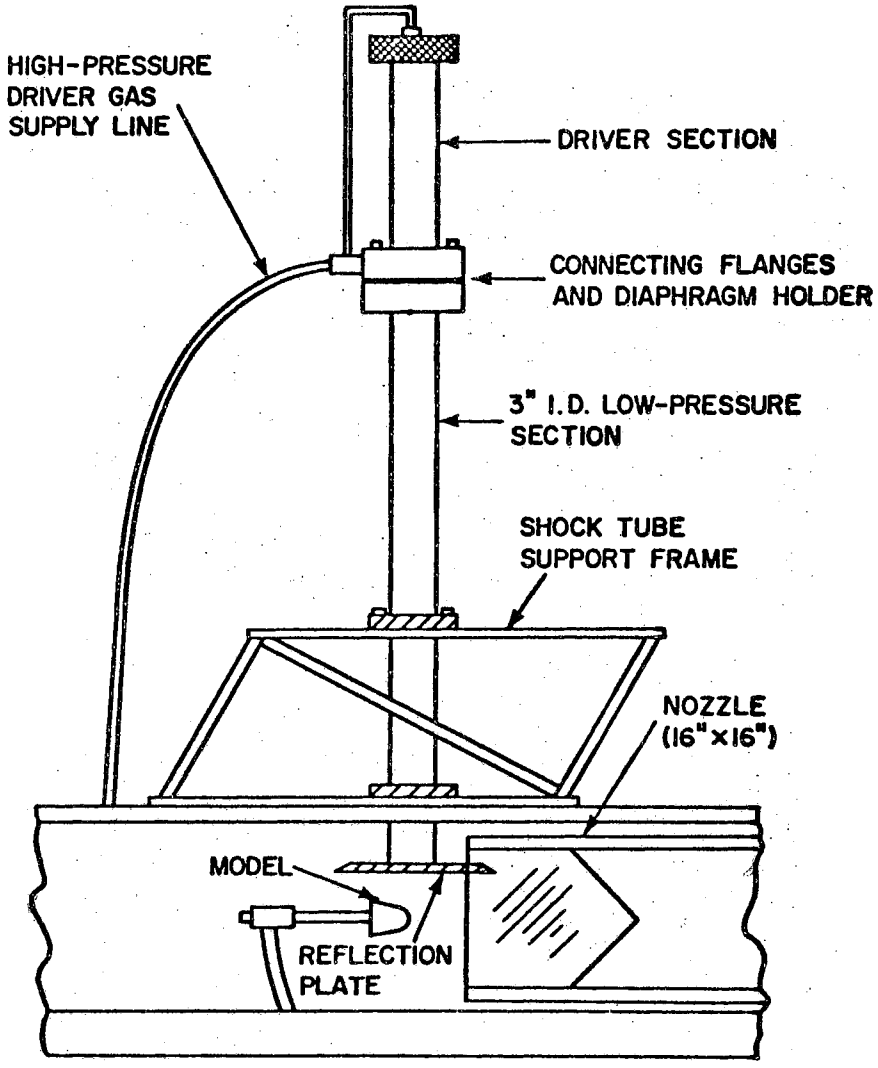

Figure 2. Arrangement for Studying Side-on Shock-on-Shock Interactions in a Wind-Tunnel

conclusively that such an experimental setup cannot produce reliable interaction geometries because the shock wave is always non-uniform and attenuates too rapidly. A different technique is clearly needed.

In the present work, the development of a technique whereby a rifle-launched model interacts with a cylindrical shock wave from a shock-tube was undertaken. The strength of the blast wave was always known and was repeatable at a given location. The interaction angle could be any angle from head-on to side-on depending on the distance from the opening in the shock tube at which the interaction was made to take place. The timing problem of obtaining coincidence of the model, shock, and schlieren spark-light at a pre-selected location had to be solved first. Schlieren pictures of adequate quality for the detection of shock waves, expansion regions, and contact surfaces had to be obtained. Methods of providing sufficient variation in missile Mach number and shock strength were needed. Then a sufficient number of interaction photographs had to be obtained so that a whole sequence of events could be studied. Only oblique interactions were studied since these were regarded as an essential step along with the study of head-on and side-on interactions and, further, are most likely to occur. Head-on interactions had already been studied and verified in detail by several authors (2), (7), (8).

Finally, an analysis, based on the bow shock angles

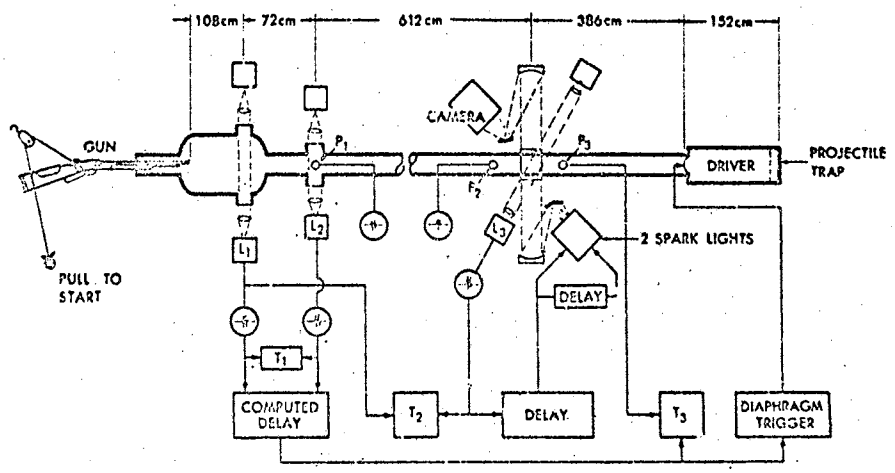

Figure 3. Schematic of Free-Flight Interaction Test Setup Used in Reference (2)

before and after interaction, was made to show how over-pressures may be estimated from photographed shock geometries.

In summary, the objectives of the work were to:

(a) Develop a technique for studying oblique shock-on-shock interactions.

(b) Using this technique, obtain a sufficient number of schlieren photographs of the interaction to prove its usefulness.

(c) Indicate a method based on the schlieren photographs for estimating transient pressures on the body during an interaction.

CHAPTER II

LITERATURE REVIEW

A survey of available literature on the subject of shock diffraction in general was made by Tyler and Walker (9) and a detailed review of most of the papers surveyed was made by Tyler and Zumwalt (6) in 1965. Only literature published on the subject of moving shocks interacting with supersonic bodies will be reviewed here.

Smyrl (1) obtained a solution for the pressure field behind an arbitrary plane shock after the shock encountered a thin airfoil moving at supersonic speed. First he considered the case of a thin infinite wedge. The shock pattern at the interaction was assumed to provide the smallest and simplest disturbed region consistent with the physical facts and for which a solution could be found. Three apparently distinct shock patterns, as shown in Figure 1, were arrived at depending on the wedge Mach number and shock strength. Numerical examples were given for various shock strengths, wedge speeds and angles of yaw. The solution was also extended to cover the case of a thin infinite airfoil of arbitrary shape.

Miles in 1963 (10) applied Whitham's method of diffraction of blasts by stationary bodies to the problem of

a blast diffracted by a thin supersonic wedge (11). The results tended to the exact results for weak blasts but were unsatisfactory for strong blasts.

Wolff (12) used coordinate transformations to make shock waves steady for the case of a flying conical body meeting a blast wave head-on. Real gas effects were included. The pressure distribution on the body as a function of time was also estimated.

Inger (13) developed an analysis that applies to the case of a hypersonic wedge encountering a relatively weak blast wave (Mach number $\cong$ 1.10). The blast could thus be treated as a small perturbation over the bow shock and the resulting linearized mathematical boundary value problem solved analytically with the pressure field appearing in explicit form. Real gas effects were included in the theory. The numerical results indicate that substantial transient pressure overshoots can occur relative to the final steady-state pressure behind the blast. He also found that real-gas effects tend to enhance slightly the pressure overshoot levels at high flight Mach numbers.

The shock-on-shock interaction problem has recently been attacked by digital computer techniques. Lax (14) proposed a practical difference scheme for shock propagation problems. He assumed that a shock can be handled as a steep gradient and also used a special difference scheme for the time derivative. Rusanov (15) in 1960 presented a

difference method that used a 'dissipative' term to obtain solutions for shock diffraction caused by a number of geometries. Rusanov's scheme was used with success by Jackomis (16) who numerically solved the flow field around a stationary finite cone as a blast wave passed over it axially. Eaton (17) also used Rusanov's scheme for solving the flow field of a supersonic cone-cylinder entering and leaving a blast diametrically.

Pierce (3) made one of the first attempts to simulate blast wave interaction in the wind-tunnel. He mounted a shock tube perpendicular to the tunnel flow to produce side-on interaction. Local shock velocities and interaction angles were measured from the shadowgraphs. Then, assuming locally two-dimensional flow, oblique shock relations were applied to find the pressure rise across the incident and reflected waves. By comparison with measured values, it was shown that good estimates of the overpressure could be obtained in this way. The measurements were made at free-stream Mach number of 1.87 and a blast wave Mach number of 2.38.

Merritt and Aronson (4) used Pierce's technique at a free-stream Mach number of 5, and obtained side-on interaction with a body of revolution. Because of the distortion of the shock by the free-stream and since no theoretical solutions were available for comparison with results for side-on interaction with bodies of revolution, they decided to study the head-on interaction first. For

the head-on case, theoretical estimates of the overpressure at the stagnation point of a hemisphere and on the surface of a wedge were obtained using normal and oblique shock relations. The shock wave from the shock tube passed over the model immersed in the steady supersonic stream at the nozzle exit. Overpressures were measured by pressure transducers embedded in the models at appropriate locations. Excellent agreement is shown between the measured and predicted overpressures at the stagnation points of these bodies.

Bingham and Davidson (5) used a double diaphragm shock tube mounted at 30, 60, 90, and 120 degrees to the centerline of a hypersonic free-jet tunnel operating at Mach 7.30. The shock tube was capable of generating shock velocities from 3600 to 13,500 fps. The method produced pressure measurements and schlieren photographs of the interaction. The results, however, could not be put to much practical use due to the distorting effects of the tunnel free-jet boundary and the wind-tunnel flow on the shock wave from the shock tube.

A numerical study of shock waves emerging into a supersonic crossflow by Tyler and Zumwalt (6) showed that wind-tunnel techniques using shock tubes mounted at angles to the test section would simulate a blast wave approaching a supersonic missile only under limited conditions. The stagnation pressure behind the shock wave has to be greater than the stagnation pressure of the supersonic

crossflow. Even then, only a portion of the emerging shock wave would approximately represent the conditions expected from a blast wave. The emerging shock wave attenuates rapidly and is distorted considerably for all conditions.

In June 1965, Brown and Mullaney (2) described a new technique developed by them at the Boeing scientific research laboratory. A smooth-bore powder gun was installed in the dump chamber of a conventional shock tube. The gun fired 0.300 caliber cone-cylinder projectiles at about 4000 fps toward the driver. The velocity of the projectile was measured near the muzzle and a computer was used to provide a proportional delay before the shock wave was started by a capacitor discharge system. The projectile and the shock wave met in a 3 inch diameter window where a two frame shadowgraph system was used to obtain photographs of the interaction. The computed delay was found to be necessary in order to account for the ±5% variation in the projectile velocity. Figure 3 shows a schematic of the test setup.

In a later paper, Brown and Mullaney (7) compared the shadowgraphs obtained by the above method with the shock geometry models proposed by Smyrl. A modification of Smyrl's model was found to be necessary for finite bodies and was suggested by them.

The same experimental technique was used by Merritt and Aronson (8) at the Naval Ordnance Laboratory at

approximately the same time. Head-on interaction between a slender cone and a plane shock wave was studied by means of a sequence of photographs taken through windows in the shock-tube wall. The magnitude of the transient pressures on the surface of the body was then obtained from calculations. Both model and shock wave Mach numbers were varied from 2 to 5. Their observations show that Mach reflection on the cone surface is obtained for all the above test conditions. The velocity of the Mach stem relative to the cone was found to be such that the stem always remained in line with the main shock front. Calculations show that for low Mach numbers the pressure behind the Mach stem is less than the new steady-state cone pressure in the flow behind the shock wave. Overpressures were not found until the model Mach number exceeded 4. The schlieren photographs of the interaction were extremely clear and accurate since the blast wave was perfectly plane.

This survey of experimental and theoretical work published to date pointed out the need for further studies, especially for the side-on and oblique blast interaction cases. The technique of using gun-launched models producing interactions in free flight appeared attractive and had been proved feasible. Once the shock geometries are known, the overpressure calculations are not difficult. This approach was, therefore, chosen for the present study.

CHAPTER III

EXPERIMENTAL TECHNIQUE

The technique uses a rifle-launched projectile and a cylindrical shock wave so timed as to interact within a five inch diameter area at a predictable time instant. The free-flying model (projectile) has the advantage of an unsupported model so that studies can be extended into the base and wake flow regions and is capable of producing aerodynamically clean supersonic flow over the body suitable for detailed optical observations. The shock wave is produced by a rather unconventional shock tube. Both the model velocity and the shock speed can be varied over a wide range simply by using varying amounts of powder load and different gases and pressure ratios across the shock tube diaphragm.

Figure 4 shows a schematic of the experimental setup. The rifle, the shock-tube and the schlieren visualization system are situated on mutually perpendicular axes intersecting in the receiver of the shock tube. The rifle launches the model which travels vertically downwards through the receiver and is stopped finally by a sand butt. A multiple spark schlieren system was used for recording the interaction, the shutter of the camera using 4 x 5

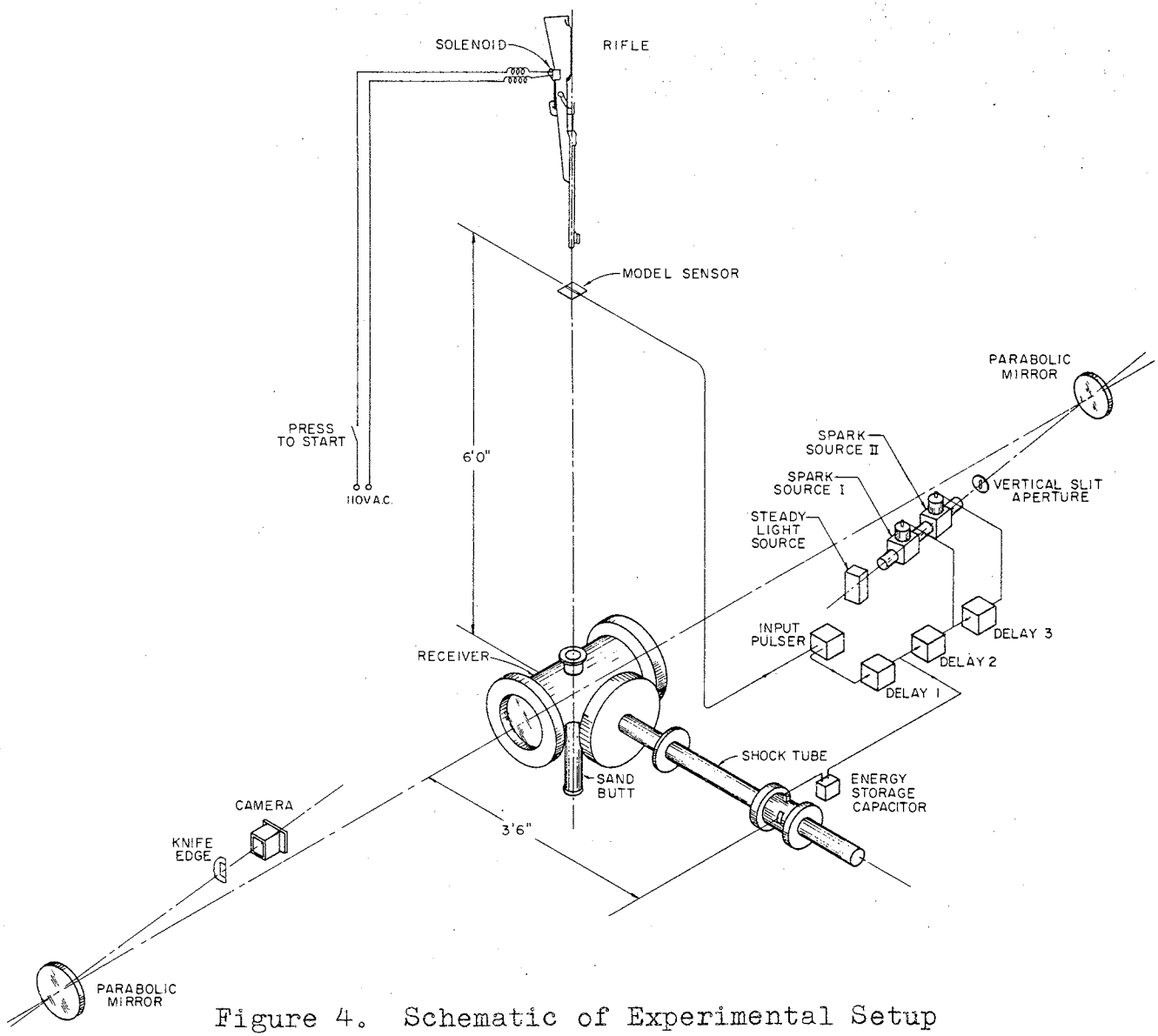

Figure 4. Schematic of Experimental Setup

inch cut film was left open during the experiment which was performed in total darkness.

The rifle was fired first. The model, upon exiting the muzzle of the rifle, broke a thin conducting strip (hereafter called the model sensor) stretched in its path. This event was translated into a fixed-voltage positive pulse by the input pulser and delayed by a preset interval in the delay unit. A thyratron 'switch' triggered the discharge of a 200 joule capacitor into the center of the diaphragm upon signal from the delayed pulse. The delay interval, of course, depended upon the difference between the shock and the model velocities. A further delay, representing the time taken by the shock wave to reach the interaction point, was now applied to the initial pulse. The output pulse triggered the spark light source so that if the model velocity were right, the shock interacted with the model at the same instant and the interaction was recorded. Thus, the success of the experiment depended on achieving repeatable and completely controllable shock and model velocities as well as repeatable intervals of time between the shock, model and spark initiations. Due to difficulties mentioned later, only one spark source was used for most of the experiments. The following paragraphs explain how this repeatability was achieved to a sufficient degree as to make the method feasible.

The sequence of firing the shock-tube after the model was launched had to be adopted for the following reason.

For a given model weight and powder load, the model velocity was repeatable within two percent. The time from the rifle firing signal until the model reaches a predetermined point in the shock tube receiver varies by ten percent (8). The time taken by the shock wave to reach a predetermined point in the shock tube after the diaphragm trigger signal is repeatable to better than one percent. Starting the shock after the model has completed its travel through the barrel thus avoids the large variable factor introduced by the action of the rifle.

In a similar technique used by Brown and Mullaney (2) for the study of head-on interaction between a free-flying model and a shock wave, the velocity of the projectile was measured near the muzzle by two light beams (L_1 and L_2 in Figure 3) and a computer was used to provide a proportional delay before the shock wave was started. However, in their setup the observation window was located twelve feet from the diaphragm and the model had to travel twenty-six feet between the light beam sensors and the point of interaction at the window. It was essential that the interaction took place behind the 3 inch diameter window. In the present setup, the shock wave travels only three feet and the model travels six feet after starting the sequence. This was made possible by the unusually short shock tube assembly mentioned earlier. The total randomness in the times involved between the initiating pulse and the actual interaction was thus considerably less than in the setup

of Figure 3 and the probability of obtaining the desired interaction at the right time and location was thus greater. The added problem and cost of providing a computed delay and the apparently successful operation of the system without such a delay finally precluded its inclusion in this setup. As an example, the time lag between the initiating pulse and the interaction was of the order of 3000 microseconds. A two percent variation in the 2000 fps projectile velocity meant a time error of 60 microseconds or a location error of 1.40 inches. Since the spark provides a beam of light five inches in diameter, the two percent variation in model velocity is theoretically acceptable. The one percent variation in shock timing gives an even smaller location error since the shock had to travel only three feet before interaction. In practice, five out of every ten successful runs yielded pictures of the interaction. Out of these five, at least one would show the desired amount of interaction.

Model Launching Technique

A Winchester Model 90, 0.375 H and H Magnum rifle was supported by a specially designed recoil mechanism and used for launching the models. Since a sub-microsecond spark was used to record the interaction, the spin imparted to the model had no influence on the quality of the photographs. Even when the model was badly out of balance because of tip distortion at high speeds, the spark was

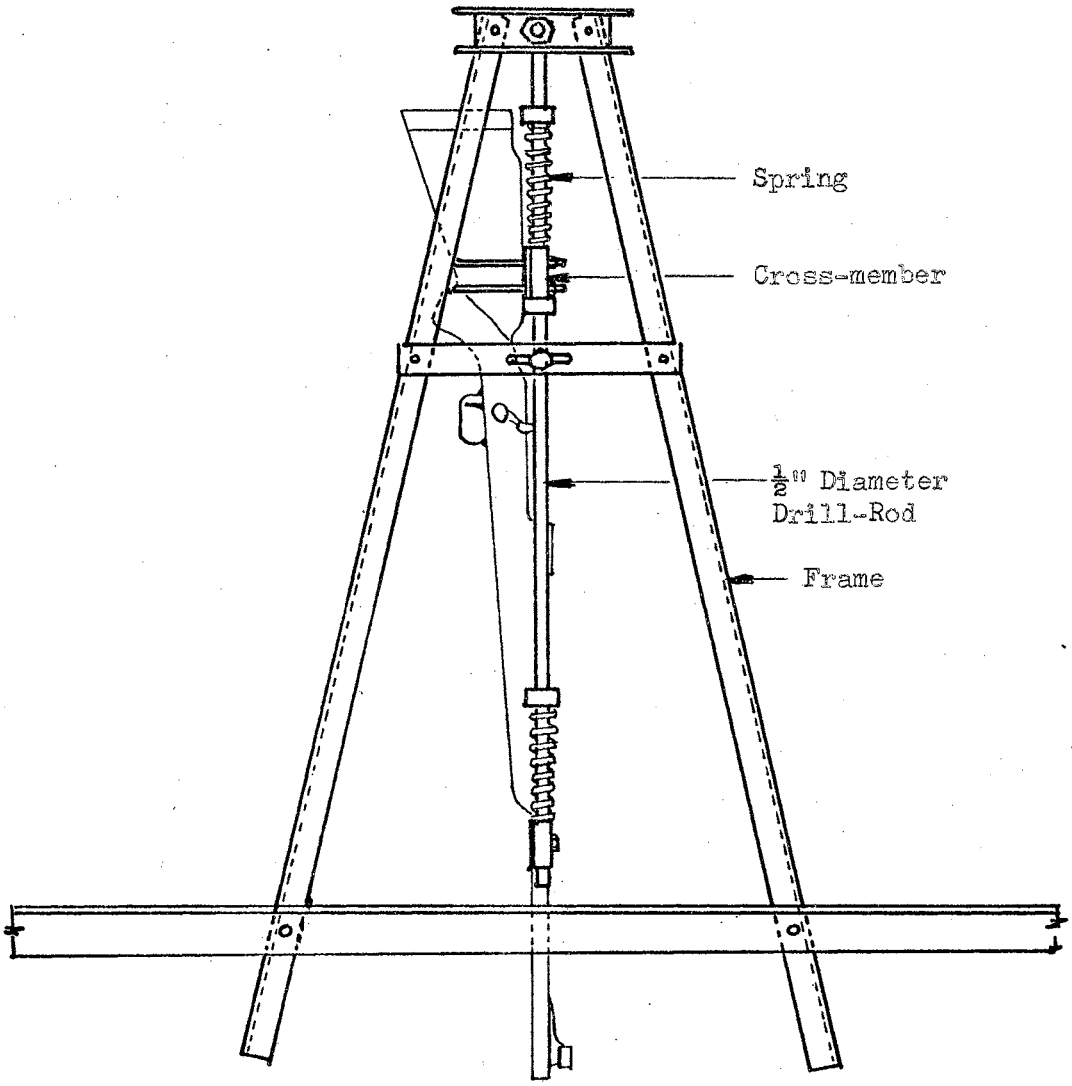

Figure 5. Rifle Recoil Mechanism

able to stop all motion effectively as seen in Figure 7(c) in which no blurring of details can be discerned. Naturally, the spinning of the smooth model also has no effect on the shock geometry around it.

The 0.375 Magnum is the largest commonly-used rifle caliber on the American continent and was chosen to permit as large a model size as possible in order to obtain clear photographs of the interaction. The model simply replaced the bullet in the cartridge and, hence, all the advantages of reloading empty cartridge cases by hand were realized. Velocities of the order of 3000 fps can be imparted to a model weighing as much as 200 grains without any danger to the rifle. The recoil force, however, was considerable and the rifle had to be mounted in such a way as to allow it to recoil about three inches. The force, estimated at 44 ft. lb. (18), was absorbed completely by four compression springs each rated at 30 lb./in. The sliding friction of the cross-members holding the rifle was sufficient to damp out excessive vibrations after the recoil. Figure 5 shows how the rifle was actually mounted. The cross-members slide freely on two one-half inch diameter drill rods. The rods were attached to a trapezoidal frame in such a way that the upper ends of the rods could be swivelled around a one inch diameter pin while the other ends could be clamped so that the rifle could be made to point downwards and about five degrees on either side of the vertical. The rifle was fixed in its place

after sighting through the bore to the interaction point in the receiver. Small changes in the direction of travel of the model could be made at this time. The frame was made out of 1½" equal angle sections and was mounted on two 3" angle beams running across the roof trusses.

A solenoid pulled the trigger of the rifle with a steel 'finger' upon actuation by a push button switch. The solenoid was fixed to the rifle stock by means of two 3" long bolts.

Table I (p. 65) shows the different model velocities used in the study. The most extensive interaction studies were made with a 215.0 grain model at 2120 fps. For this, the cartridge cases were loaded with 55 grains of DuPont No. 4320 smokeless rifle powder. Figure 6 shows the relation between the muzzle velocity and amount of powder used. Actual measurements of velocity were performed on a 270 grain model (a .375 caliber round-nose bullet) using different amounts of 4320 rifle powder.

The corresponding velocity for a model of any other weight can be estimated by assuming that the kinetic energy of the model as it leaves the muzzle depends only on the amount of powder used to impart this velocity. If V_1 is the known velocity, the unknown velocity V_2 can be calculated as follows:

$$K.E. = \tfrac{1}{2} m_1 V_1^2 = \tfrac{1}{2} m_2 V_2^2$$

$$V_2 = \sqrt{\frac{m_1}{m_2}}\, V_1 = \sqrt{\frac{w_1}{w_2}}\, V_1 .$$

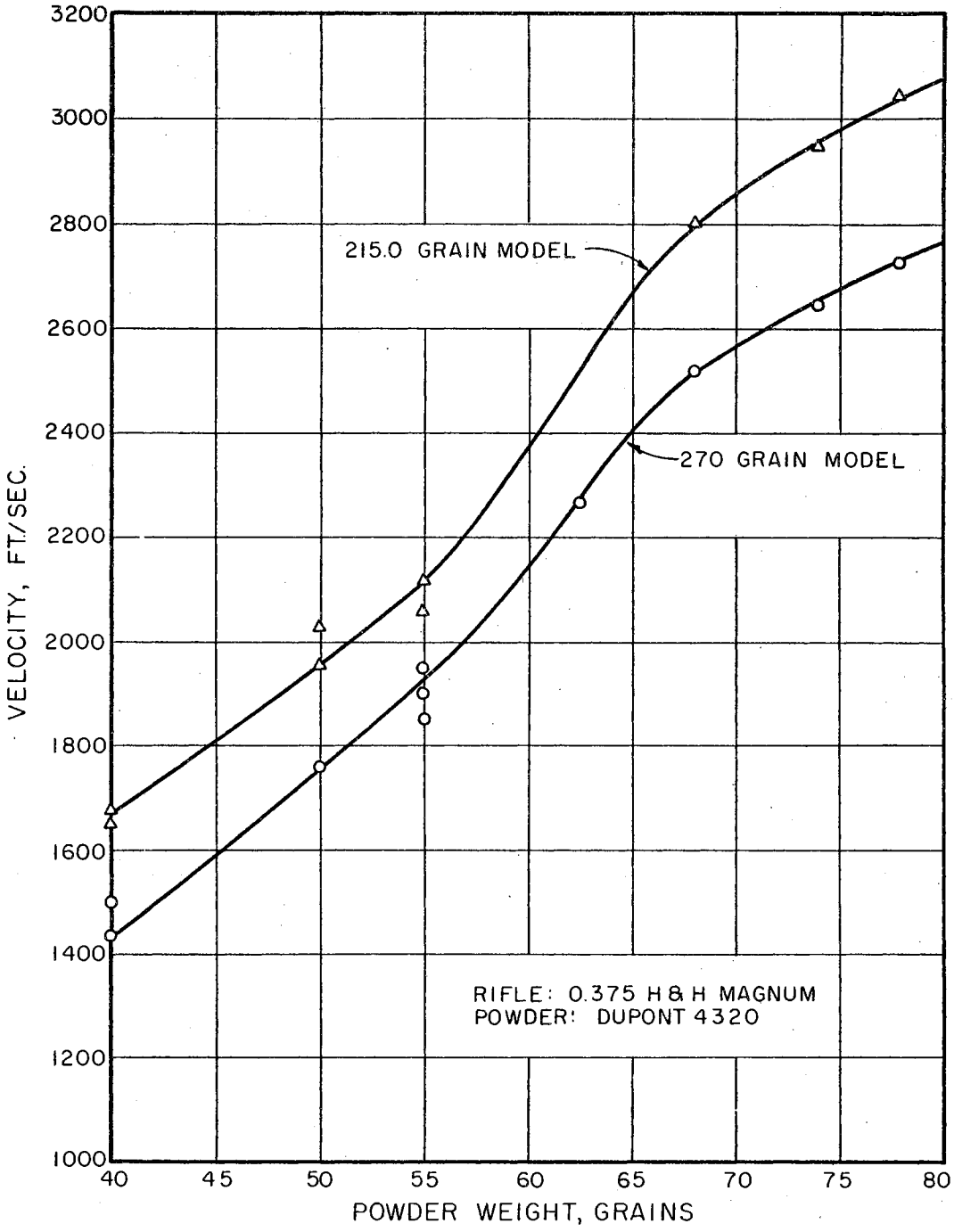

Figure 6. Relation Between Powder Weight and Model Velocity

The relation between powder weight and model velocity is more difficult to predict. The rate of increase of velocity depends on the burning rate of the powder, barrel length of the rifle and the size of the case. Powder amounts of less than 40 grains show incomplete burning in the barrel length, hence the need for actual measurement. The measured values agreed quite well with those in Reference (18).

Model Fabrication

The model was made by machining the ogival forebody of a 0.375 caliber 270 grain round-nose bullet into a 19.5° semi-angle cone. Typical model dimensions and general appearance can be seen in Figure 7. The standard of finish of the conical forebody had great influence on the aerodynamic cleanliness of the flow around the body, especially at higher model velocities. Uniform finish also naturally tends to give less variation in weights between models. The lead used in the manufacture of these bullets was able to attain a high degree of polish right on the lathe itself. The average variation in the weights of the models used was kept within 0.2 percent by using carefully repeatable machining techniques. Any finished models differing from the average weight by more than this margin were either rejected or used for trial runs only. The average weight of these models was 215.0 grains.

The soft conical nose of the model was able to

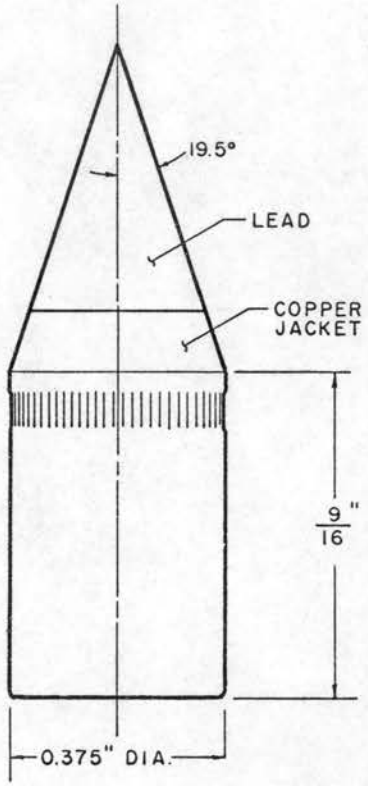

(a) Dimensions

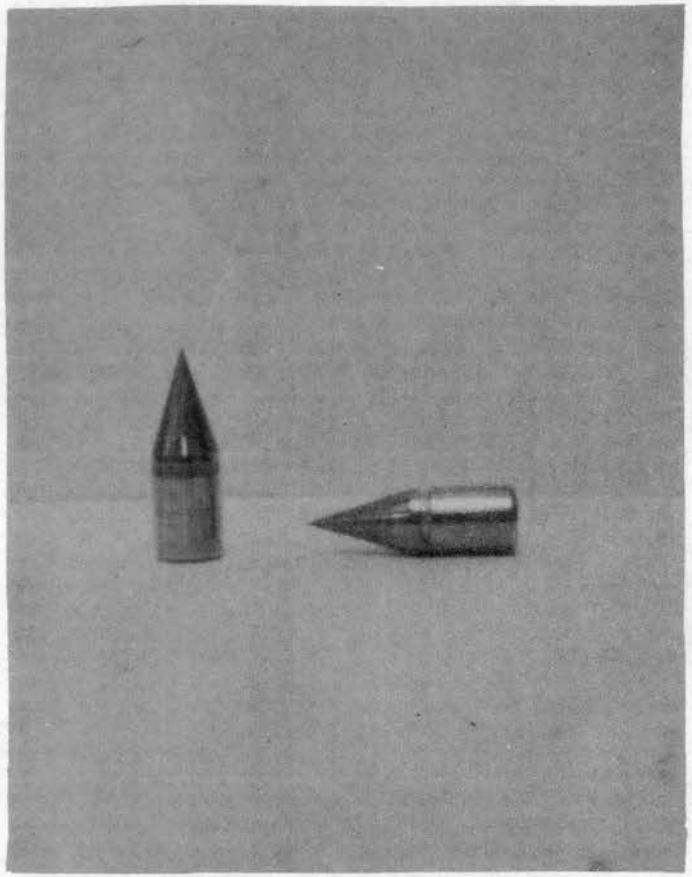

(b) Appearance

Figure 7. The Model

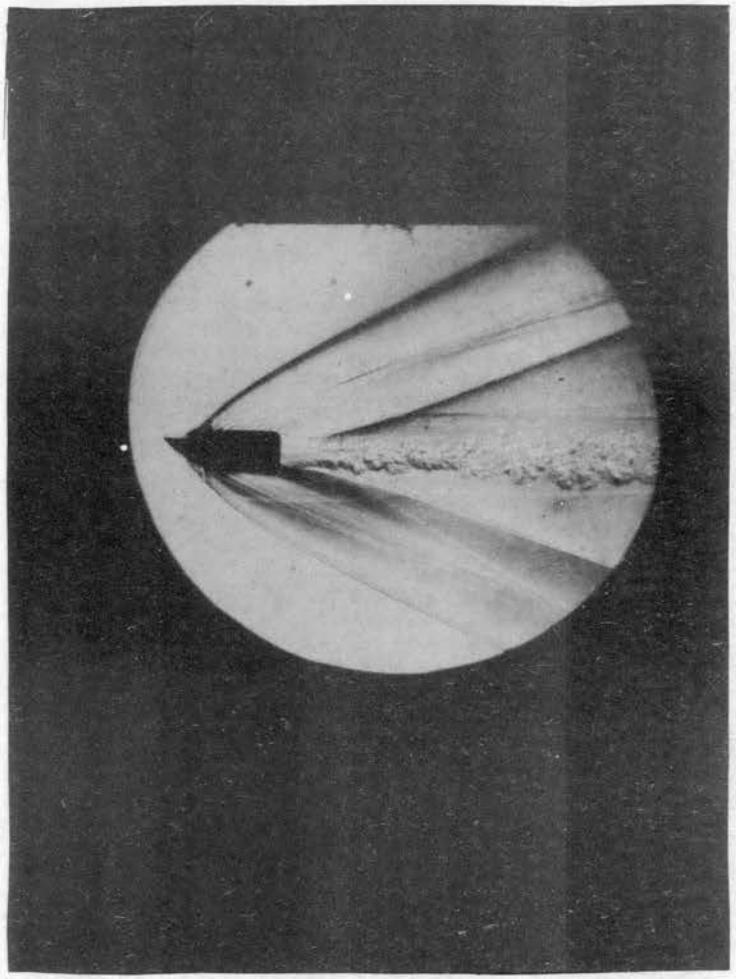

(c) Schlieren Photograph at 3000 fps

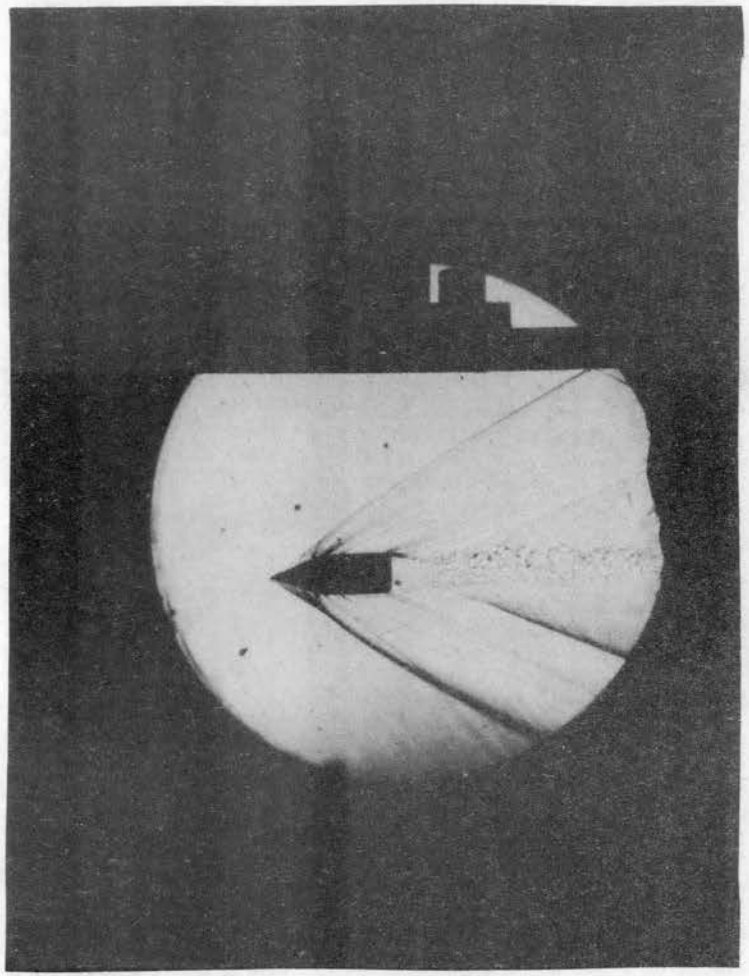

(d) Schlieren Photograph at 2710 fps

Figure 7. (Continued)

withstand the impact of the sensor strip without too much distortion except at the highest velocities. Figure 7(c) shows one of the models traveling at 3000 fps. There was no distortion at slightly lower velocities (2800 fps) as evidenced in Figure 7(d).

Model Sensor Strip

The arrival of the model at a given location can be sensed either by a mechanical or a photosensitive device. Photoelectric sensors are more convenient and do not cause any interference with the motion of the body itself. Mechanical methods, however, are to be preferred due to lower cost and trouble-free operation. The method which was used here can best be described as "breaking a circuit." A one-eighth inch wide strip of aluminum foil was glued onto a piece of light cardboard and placed in the path of the model. The two ends of the strip were connected to a pulser unit that generated a controlled pulse of fixed width and strength whenever the conductor was broken.

The placement of this strip was not critical, but care had to be taken not to place it too close to the muzzle. The gases that follow the model out of the barrel expand very rapidly and overtake the model in a very short distance. The force of these expanding hot gases is sufficient to rupture the thin strip prematurely even when supported on a thin card. When it was found necessary to

place the sensor strip closer than about ten inches from the muzzle, the card was supported on an aluminum disc with a one inch diameter hole in the center to permit the model to pass through. The clamps connecting the conducting strip to the pulser should be firmly attached and make a good electrical contact.

Sand Butt

After interaction with the blast wave, the model was stopped by means of a sand butt. A 28 inch long, 4 inch diameter steel pipe placed at the lower end of the receiver was packed tightly with fine sand to a depth of 20 inches. The surface of the sand was covered to a depth of three inches by a plastic compound to prevent the sand from flying back into the receiver upon impact from the model. Used models that tended to collect at the same spot in the sand butt were periodically removed.

Shock Tube

The shock tube which was used in this work was adapted from one assembled by G. Lazalier as a Master's degree thesis project (19). Its chief features are summarized below.

Design

The main consideration for the design of this shock tube was to obtain an unusually short assembly for the

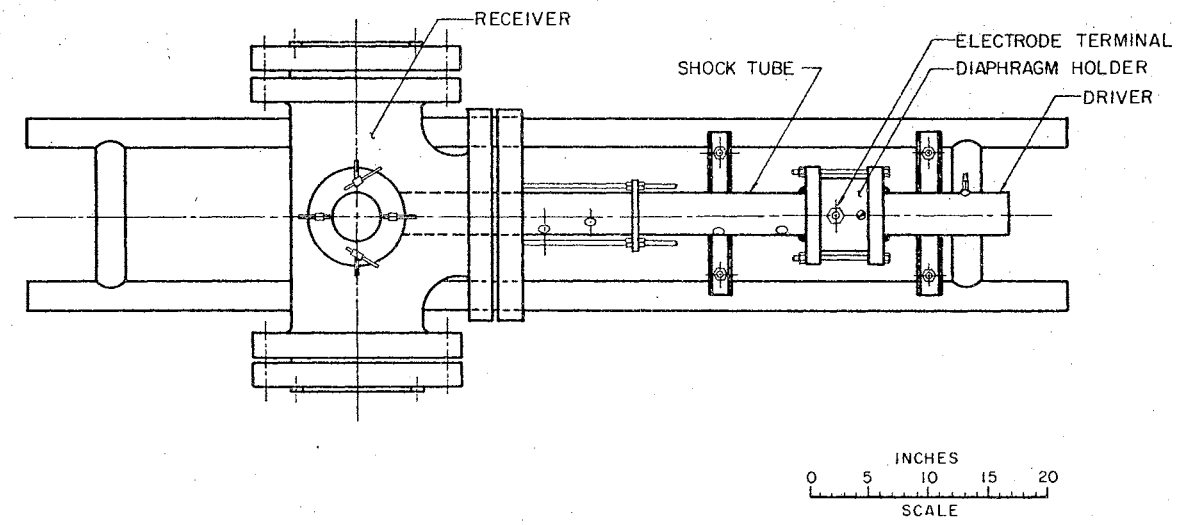

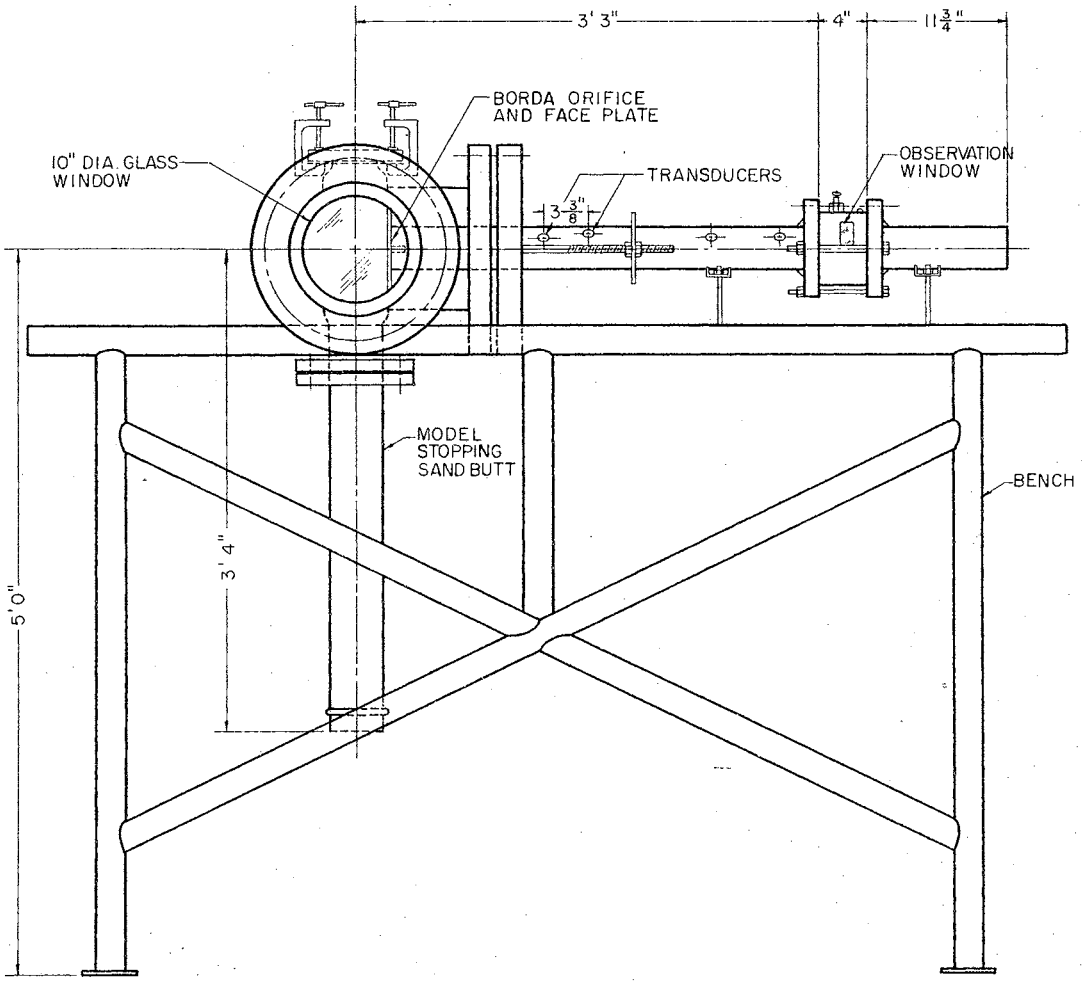

Figure 8. Shock Tube

conservation of laboratory space and to be able to obtain clean shocks in the receiver section before the rarefaction wave caught up with the shock wave. Windows suitable for schlieren observation of the shock wave were to be provided in the receiver. To obtain high shock Mach numbers using relatively small pressure ratios across the diaphragm, a double diaphragm configuration was selected, using helium in the driver and intermediate sections and rarefied air in the shock channel. A maximum workable pressure ratio P_4/P_1 of 200:1 was chosen as the upper limit of operation for the shock tube. The driver section was designed for a working pressure of 400 psia. Pressure burst type diaphragms were to be used and, hence, no consideration was given to diaphragm bursting techniques.

In the present configuration, an electrical system of bursting diaphragms by means of precisely timed pulses had to be incorporated. A single diaphragm was found adequate for the desired range of shock wave Mach numbers. Freon was used in the driven channel to increase the model Mach numbers and aid flow visualization at low pressures due to its greater density. For example, freon-114 is 5.78 times denser than air at atmospheric pressure and temperature while the acoustic velocity in pure freon-114 is only 416 fps at 86° F. Hence, a model traveling through freon-114 would have a Mach number 2.74 times that in air.

Description of the Shock-Tube

Figure 8 shows the side view and planform of the shock-tube. The driver and the shock channel are made out of 3" I.D. hydraulic tubing having a nominal wall thickness of 3/8 inch. The driver section is almost 12 inches long including the flange at the diaphragm end. The shock channel is 3 feet long and has a similar flanged end for connection to the driver. The channel is kept in alignment with the driver tube by a four inch long $5\frac{3}{4}$ inch I.D. cylindrical sleeve that fits onto short bosses projecting from the faces of the flanges. Figure 9 shows the diaphragm holder assembly and the method of joining the driver and the channel sections together. The diaphragm is held in place between two "Quick-serts"* on the driver side of the assembly. A second diaphragm can be inserted between the two other "Quick-serts" if double diaphragm operation is desired. Four 3/4 inch diameter bolts hold the two flanges together with the diaphragm holder sandwiched between them. The "Quick-sert" holding the diaphragm from the driven side has been modified slightly by reducing its thickness by 3/4 inch and replacing the removed material with a 3/4 inch thick plexiglass ring. Two small windows were cut out in the sleeve so that the spacing of the spark gap could be viewed

*Made by Black, Sivalls and Bryson, Inc., Kansas City, Mo.

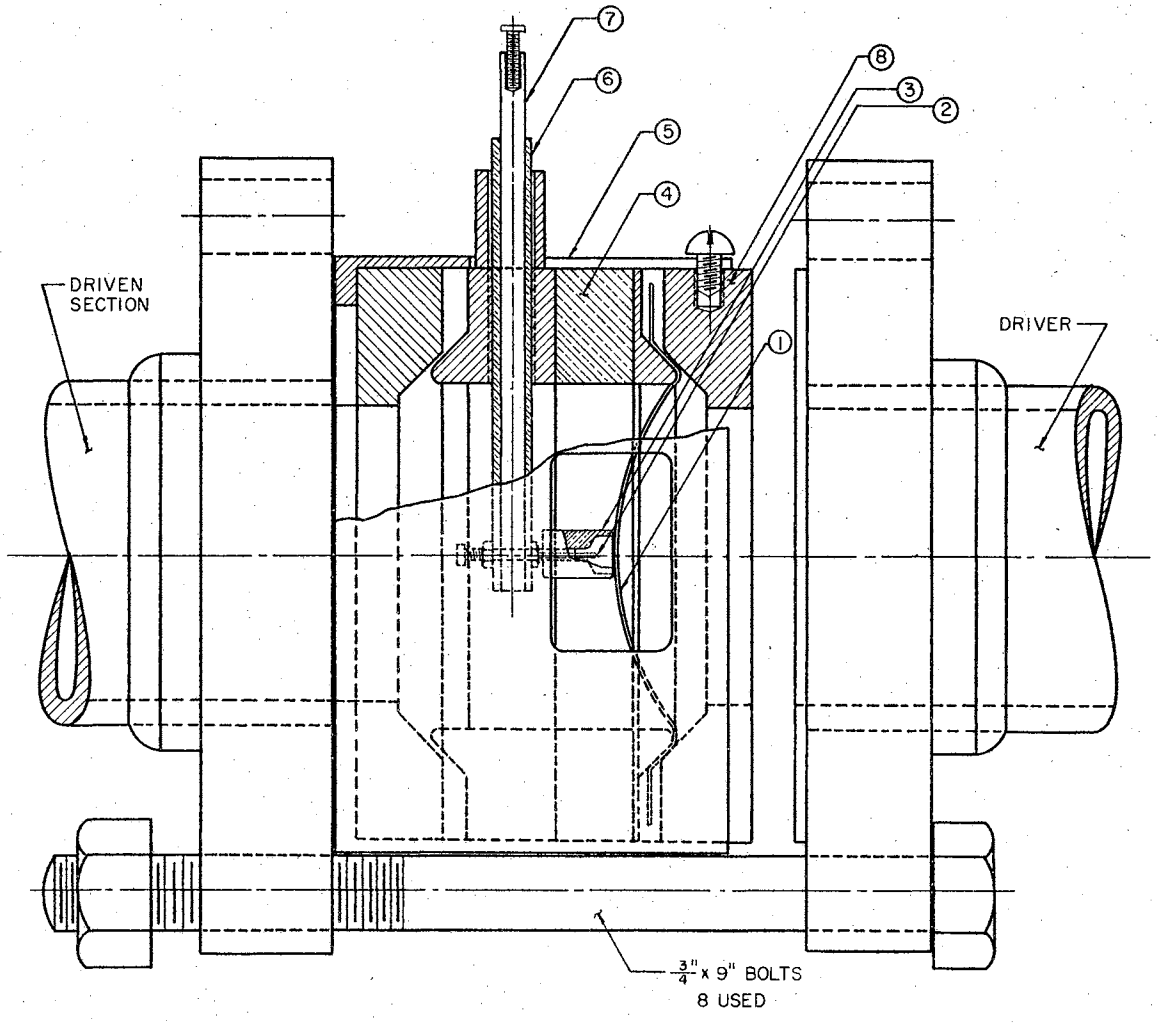

① - DIAPHRAGM
② - GRAPHITE TIP OF ELECTRODE
③ - SPACER
④ - PLEXIGLASS RING
⑤ - BRASS SLEEVE
⑥ - INSULATING SLEEVE
⑦ CONDUCTOR ROD
⑧ QUICK-SERT

INCHES
0 1 2 3
SCALE

Figure 9. Details of Diaphragm Holder Assembly

through the plexiglass ring after the shock tube had been pressurized. Other details of the spark gap and the diaphragm bursting technique are given later in the chapter. The B. S. and B. "Quick-serts" were chosen because they were recommended for use with the pressure burst type scored monel diaphragms originally intended to be used. However, they were found to grip any diaphragm material very effectively due to their tapered gripping surfaces and, hence, were retained for use in the present configuration also.

After traveling through the channel, the shock wave emerged into the receiver section through a Borda orifice. Figure 10 shows details of the orifice. The opening is $2\frac{1}{2} \times \frac{1}{2}$ inches in size. The face plate prevents the emerging shock from spreading upstream of the orifice location in the receiver. The orifice helps make the shock wave cylindrical as it emerged into the receiver and allows only the straight middle section of the shock wave in the tube to enter the receiver. Both of these properties help to create the sharp, well-defined shock wave seen in the schlieren photographs. An effort to make the shock wave truly cylindrical by placing glass walls in the receiver to prevent the shock from spreading sideways was unsuccessful.

The receiver, resembling a conventional shock tube "dump tank", was made of a commercially available ten inch cast steel tee section. The strength of the tee was

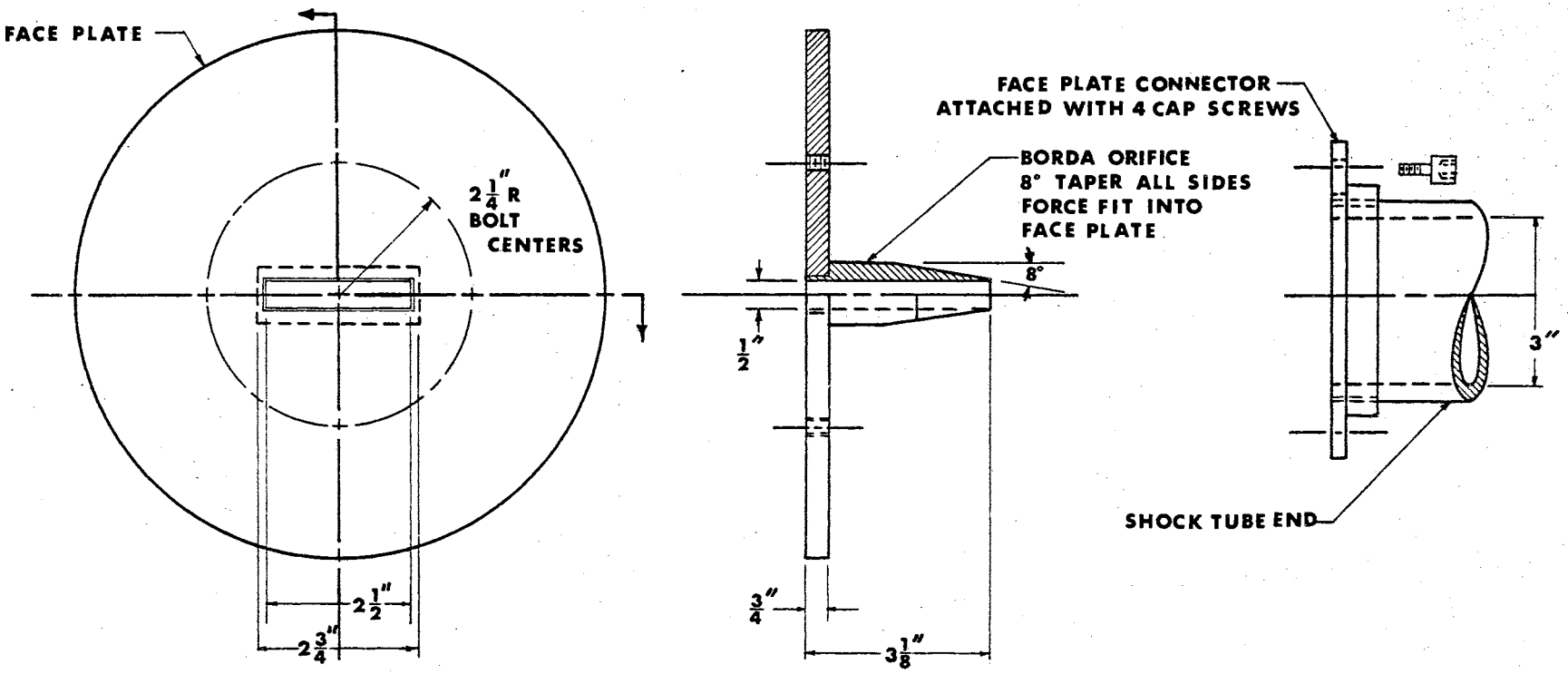

Figure 10. Borda Orifice and Face Plate Assembly

much in excess of that required by the shock tube assembly. The main advantage of using such a heavy section was that it provided a large mass to counteract the recoil when the diaphragm ruptured. Ten inch diameter plate glass windows of one-half inch thick first quality glass were provided at each end of the crossbar of the tee. The shock tube channel enters the receiver through a blind flange sealed by a sliding O-ring arrangement. All the other joints also were sealed for vacuum by means of O-rings. Openings were provided at the top and bottom sides of the receiver for model entry and exit. The top opening had a 4 inch diameter flange welded to it. A thin metal diaphragm was clamped between the face of this flange and a steel ring to provide isolation between the gas in the receiver and the atmosphere outside. The projectile was able to pierce the thin diaphragm (two layers of 0.001" thick aluminum foil) without any problem. This method worked well and proved to be much simpler than making special enclosures to maintain vacuum around the rifle and along the path of the projectile when low receiver pressures were used. The sand butt tube was connected to the lower opening in the receiver.

The entire shock tube assembly was mounted on a strong bench made out of $2\frac{1}{2}$" diameter steel pipes so that the centerline of the shock tube was raised five feet above floor level. The pressure indicating gauges and a relief valve were fixed on a panel mounted on the driver

end of the stand. Helium driver pressure was obtained by using 2200 psi bottles of helium. Freon-114 gas was supplied from a bottle at 13 psig. The connection between the freon bottle and the receiver was made by a flexible polyethylene tubing while the helium was supplied to the driver through a high-pressure conduit. A Welch Duo-Seal vacuum pump was used for evacuating the receiver and the vacuum was measured by a mercury U-tube manometer.

Two Kistler type 701 quartz pressure transducers were located $3\frac{3}{8}$" apart in the shock tube wall for measurement of shock velocities.

Diaphragm Material

The shock tube was operated in the single diaphragm configuration. At first it was proposed to use B. S. and B. prescored monel safety discs rated at 250 psig as the diaphragm material and a plunger mechanism to rupture these diaphragms at the appropriate time. The diaphragms were guaranteed by the manufacturer to burst at pressures within ± 5 psia of the rated pressure. While these diaphragms would be ideally suited for pressure-burst-type operation, the expense of quality control to assure bursting within the specified narrow range could hardly be justified when they were to be ruptured mechanically or electrically at a fixed pressure below the rated spontaneous bursting pressure.

The mechanical system for breaking diaphragms that

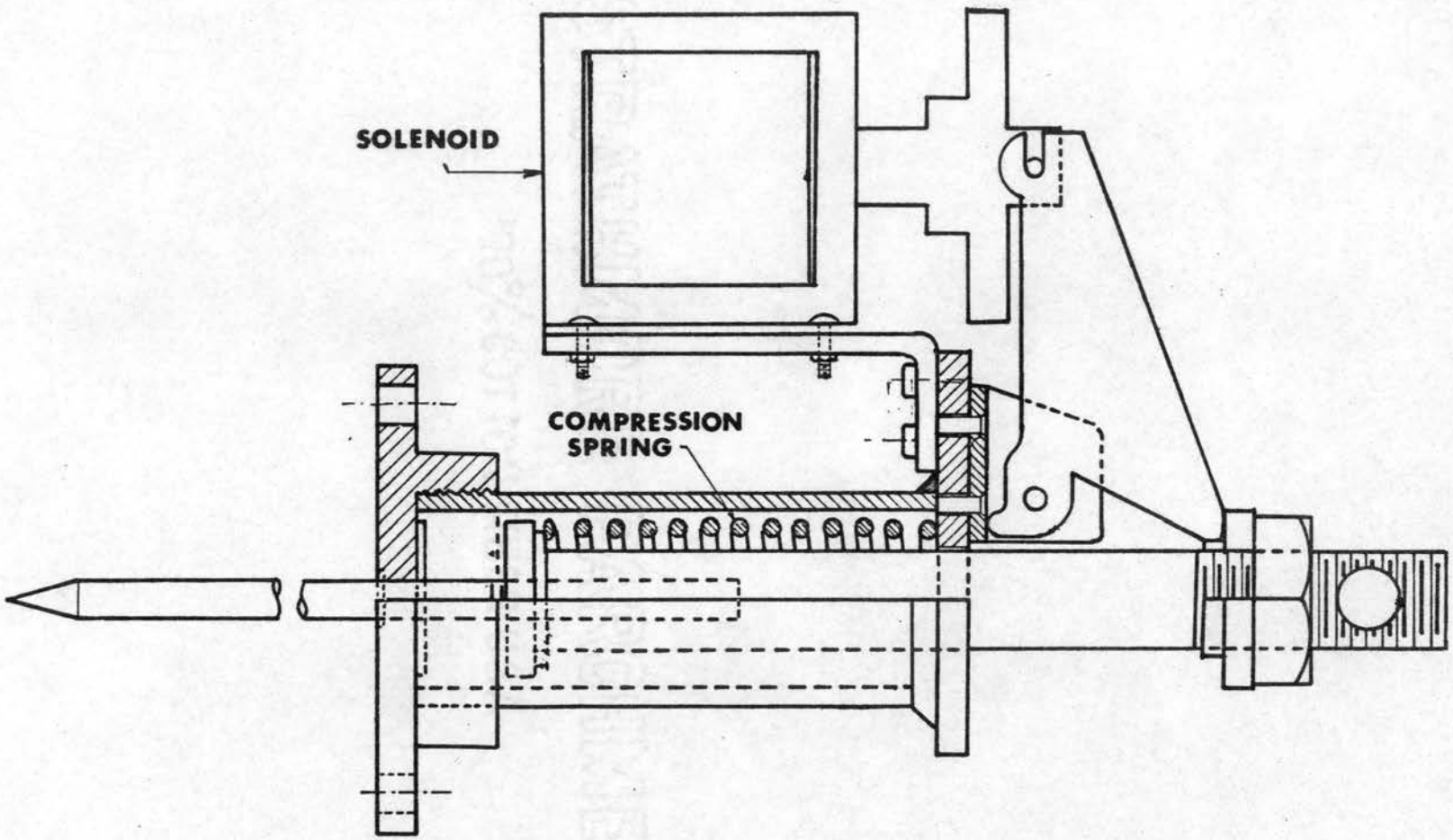

Figure 11. Mechanical Diaphragm Rupturing Method

was tried at first is shown in Figure 11. It was affixed to the closed end of the driver, the plunger went completely through the driver tube and its tip remained about one-half inch from the diaphragm center. This system could rupture the 250 pound rated diaphragms with a repeatability in timing of ±150 microseconds. This variation was found to be too great for obtaining photographs of the interaction within a reasonable number of tries. Another problem that was encountered was that the plunger took about 10 milliseconds to travel the one-half inch to the diaphragm after the initiating signal was applied to the solenoid. A smaller mass of plunger could reduce this delay somewhat but the delay in the trip mechanism or the frictional losses could not be reduced. The rifle would have to be mounted at least twenty feet above the shock tube in that case, since it had to be fired first. It was finally decided to try bursting the diaphragms electrically.

The scored safety discs had to be abandoned, however, due to their high cost and difficulties with maintenance of pressure in the driver at the exact value for sufficiently long periods. Moreover, it was observed that the driver pressure required for reliable bursting with the available energy capacitors differed with individual diaphragms even though they were manufactured under close tolerances. Finally, the use of Freon-114 as the driven gas removed the necessity of using high driver pressures

to obtain strong shocks for flow visualization.

Bradley, et al., (20) have reported the use of thin aluminum foil to obtain high repeatability in opening time of diaphragms burst electrically. A 0.001" thickness gave a variation in opening time after application of the trigger signal of less than ±15 microseconds in a 1" diameter shock tube. This thickness naturally supported very small pressures, but more than one thickness can be used. Trials conducted here indicated good results with as many as nine layers of 0.001" foil supporting a pressure difference of 100 psia. Of course, the diaphragm opening time increased enormously. It required 350 microseconds for a three layered diaphragm to open while the corresponding time for a single layer was 90 microseconds when a 200 joule capacitor was used. As measurements of time lags on the oscilloscope were accurate only to within ±10 microseconds, no noticeable variation in opening time could be recorded. A further discussion on diaphragm opening time measurements is given later in this chapter.

Three layers of 0.001" thick oven-tempered aluminum foil (Extra Heavy Reynolds Wrap) were used for most of the work. A pressure ratio of 20.05:1 was obtained across this diaphragm by using the driver gas at 18.0 psig (32.3 psia*) and the driven gas at 26 in. Hg vacuum (1.57 psia*).

---

*Based on 14.3 psia atmospheric pressure at Stillwater, Oklahoma.

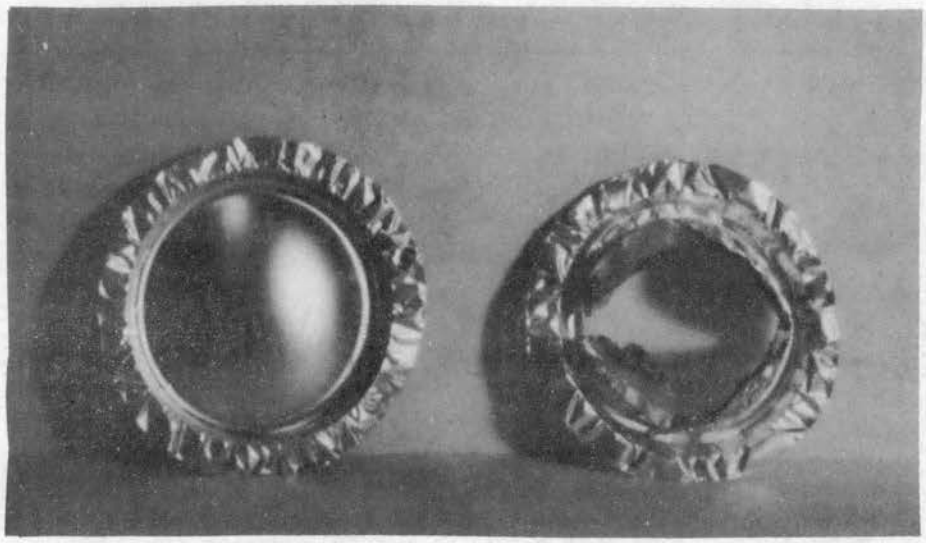

Figure 12. Aluminum Foil Diaphragm Before and After Bursting Electrically

This ratio gives a theoretical shock wave Mach number of 2.44 with air and 3.20 with Freon-114 as the driven gas, and with helium at room temperature as the driver gas in both the cases.

Figure 12 shows a typical three-layered diaphragm before and after bursting. The remarkably clean opening with four petals should be noted.

Diaphragm Bursting Technique

The electrical technique relies on melting down the center of the diaphragm instantaneously by means of an electrical arc discharge. If the diaphragm is supporting a pressure close to its maximum capacity at this time, the weakening caused by the hole in the center is sufficient to cause complete breakdown. The diaphragm holder assembly shown in Figure 9 also shows the location of the main electrode. The scheme for causing a controlled electrical discharge at an appropriate time is shown in Figure 13. The main advantage of this system is that time intervals can be controlled electronically with great precision. The pulse from the delay unit fires the thyratron. Thus, the 12 microfarad capacitor which was charged to 900 volts discharges through the thyratron and back through the primary of a step-up transformer. The 5 Henry choke between the power supply and the thyratron plate acts as a wall to the discharging current due to its large reactance to rapid rate of change but allows the d.c. voltage to be

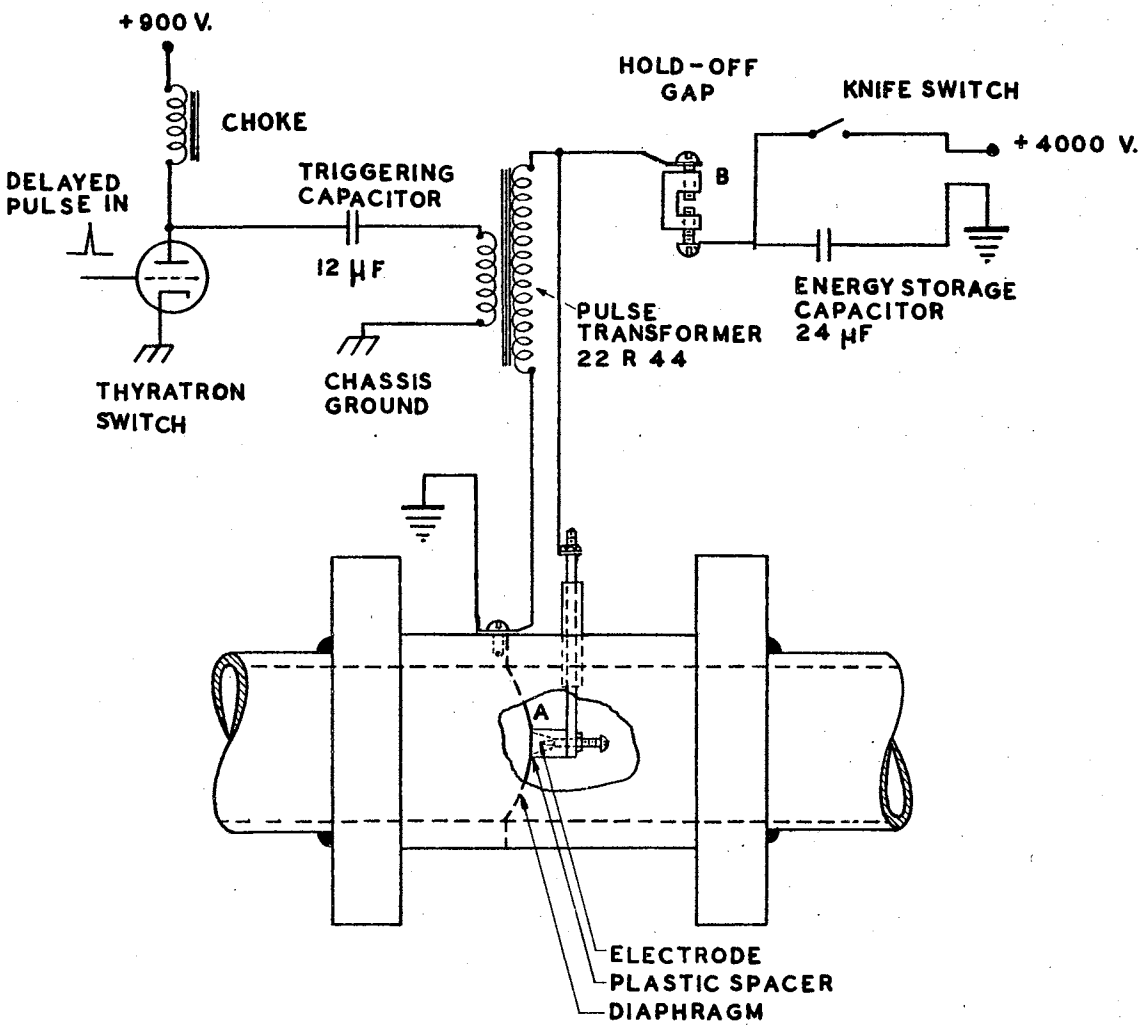

Figure 13. Arrangement for Electrical Bursting of Diaphragms

transmitted through to recharge the triggering capacitor. The transformer steps up the pulse voltage to about 15 Kv. which is sufficient to break down the gap between the electrode and the diaphragm. However, this spark does not have sufficient energy to melt the diaphragm material and is used only to trigger the discharge of a larger capacitor through the same gap. This is achieved in the following manner.

A hold-off gap B (Figure 13) is provided between the main gap and the positively charged terminal of a 25 microfarad energy storage capacitor. The capacitor is charged to 4 Kv. and the gaps are adjusted so that the two gaps in series are sufficient to hold off this voltage. Now, when the thyratron conducts and triggers a spark between the electrode and the diaphragm (gap A) as explained previously, the gas molecules within this gap ionize and the resistance of the gap is momentarily lowered. Hence the total resistance of the two gaps in series lowers also and allows the energy stored in the large capacitor to discharge into the diaphragm center. Of course, the hold-off gap should not be so large as to prevent the discharge even at this time.

All the energy stored in the capacitor (200 joules) does not go into melting the hole in the diaphragm. Part of it is dissipated as heat in the hold-off gap and in the sound and light emitted. In fact, the flash of light was quite a problem as it blanked out the photographic record

of the interaction so that the viewing windows in the diaphragm holder had to be covered each time. The hold-off gap was made integral with the energy storage capacitor, as was the pulse transformer, all of which was enclosed in a light-tight box. The intense heat that melts the diaphragm also affects the electrode and, hence, the tip of the electrode had to be specially designed. The tip is made of graphite pencil lead and can be changed or resharpened easily. It is inserted into a tight-fitting hole in a 1 inch long, 8-32 machine screw, so that the gap can be adjusted easily by turning the screw. A spacer made of one-half inch diameter plexiglass rod is screwed onto the machine screw as shown in Figure 9. The spacer holds the diaphragm at the correct distance from the graphite tip as the diaphragm might not always buldge to the same extent under similar pressure conditions. The spacer and the electrode have to be adjusted in position so that the diaphragm just touches the spacer under the required driver pressure. This can be viewed through the windows in the diaphragm holder. The best gap width for the setup used was 0.10" under 26" Hg vacuum and 0.05" under atmospheric pressure. The electrode is held in position by a one-fourth inch diameter mild steel rod which also acts as the conductor. A sleeve of delrin slipped over the rod screws into the "Quick-sert" to hold the rod in place. A screw terminal is provided at the other end of the rod. Another screw terminal on the

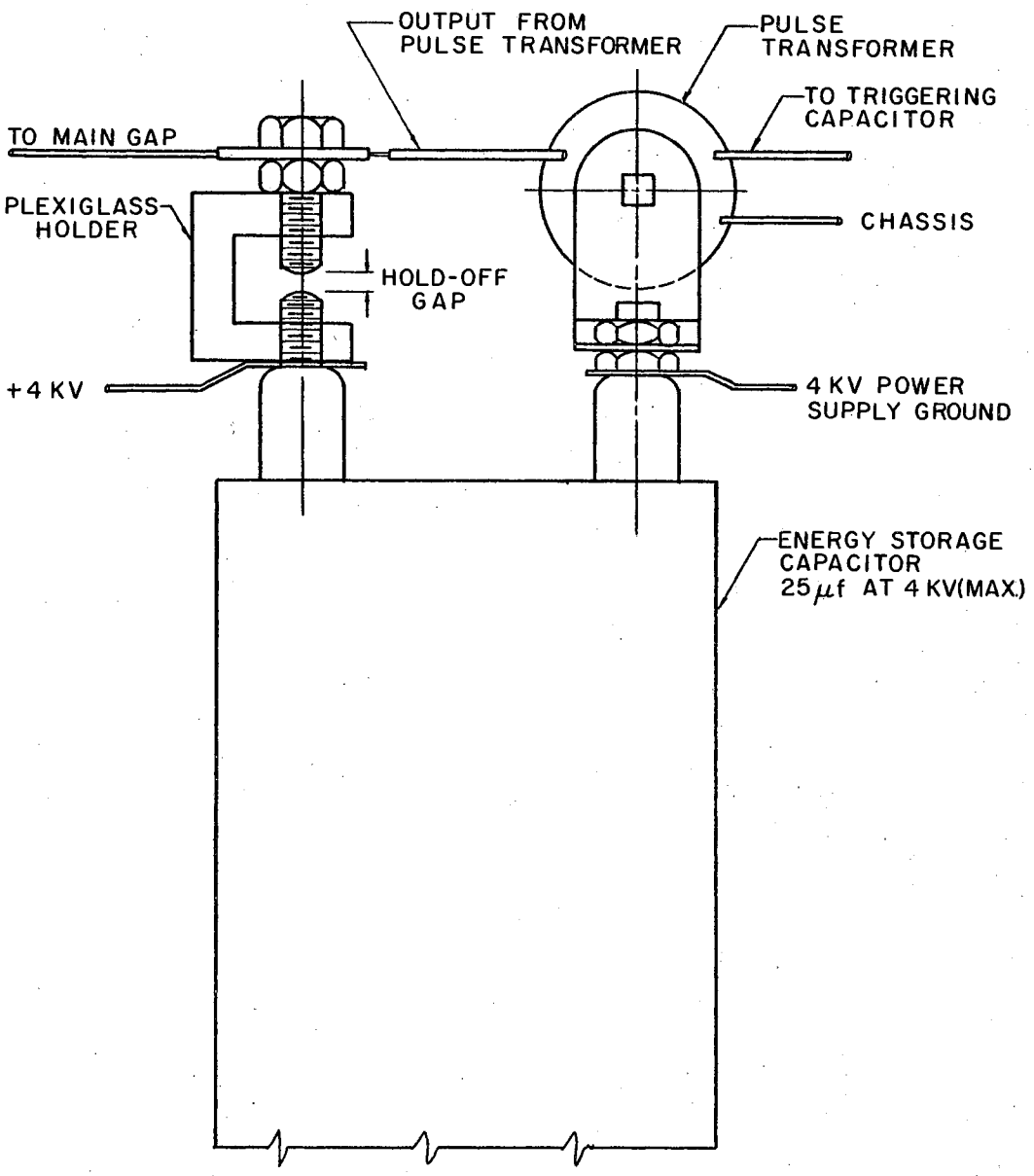

Figure 14. Details of Hold-off Gap

sleeve of the diaphragm holder provides the grounding terminal. The diaphragm makes electrical contact with this terminal.

The hold-off gap construction was simple and is shown in Figure 14. A U-shaped plexiglass piece was screwed onto one of the terminals on the energy storage capacitor. The gap is formed between the terminal and a screw which is connected to the main electrode terminal by a heavy but flexible copper wire. This gap is about 0.10 inch wide. This gap as well as the main or triggering gap have to be adjusted from time-to-time as the heat of the sparks across them melts the screws and deteriorates the graphite tip. A complete change of the graphite tip was found to be necessary after about fifty discharges due to the graphite becoming too brittle and forming hairline cracks.

The unusually large capacitance of the triggering capacitor was helpful in improving the reliability of triggering the main spark. A 0.5 microfarad capacitor could be used in its place but the gap adjustment would become too critical. There is also a lower limit on the size of the main gap since extremely small gaps would not produce sufficient ionization of the surrounding gas under the triggering spark to lower significantly the resistance of the gap. On the other hand, if the gap is too large, then the triggering spark occurs across the hold-off gap and the energy storage capacitor is discharged through the secondary winding of the pulse transformer without ever

reaching the diaphragm.

Another difficulty, not directly related to the technique, that was encountered was that if the energy storage capacitor and the schlieren light source capacitors were both charged from the same power supply, the large voltage surge when the energy capacitor discharged also discharged the spark source capacitor. The power supply had to be left connected to the capacitors because otherwise the charge slowly reduced due to tiny leakage paths inside the capacitor. This difficulty was solved by using a double throw knife switch to charge the energy capacitor first to 4 KV. and then to connect the spark source capacitor to the power supply while leaving the energy capacitor connected to the supply through a 5 megohm resistor. In this way, the voltage of the spark source was not restricted to the 4 KV. maximum on the other capacitor. The current passing through the 5 meg resistor was sufficient to replace any charge lost from the capacitor through leakage.

The ground potential of the diaphragm bursting circuit was kept floating and not connected to the chassis for the delay units. This prevented spurious triggering of the spark source when the diaphragm burst.

The Optical System

The optical system was designed around 6 inch diameter parabolic mirrors with a 36 inch focal length which were available at the time the work was started.

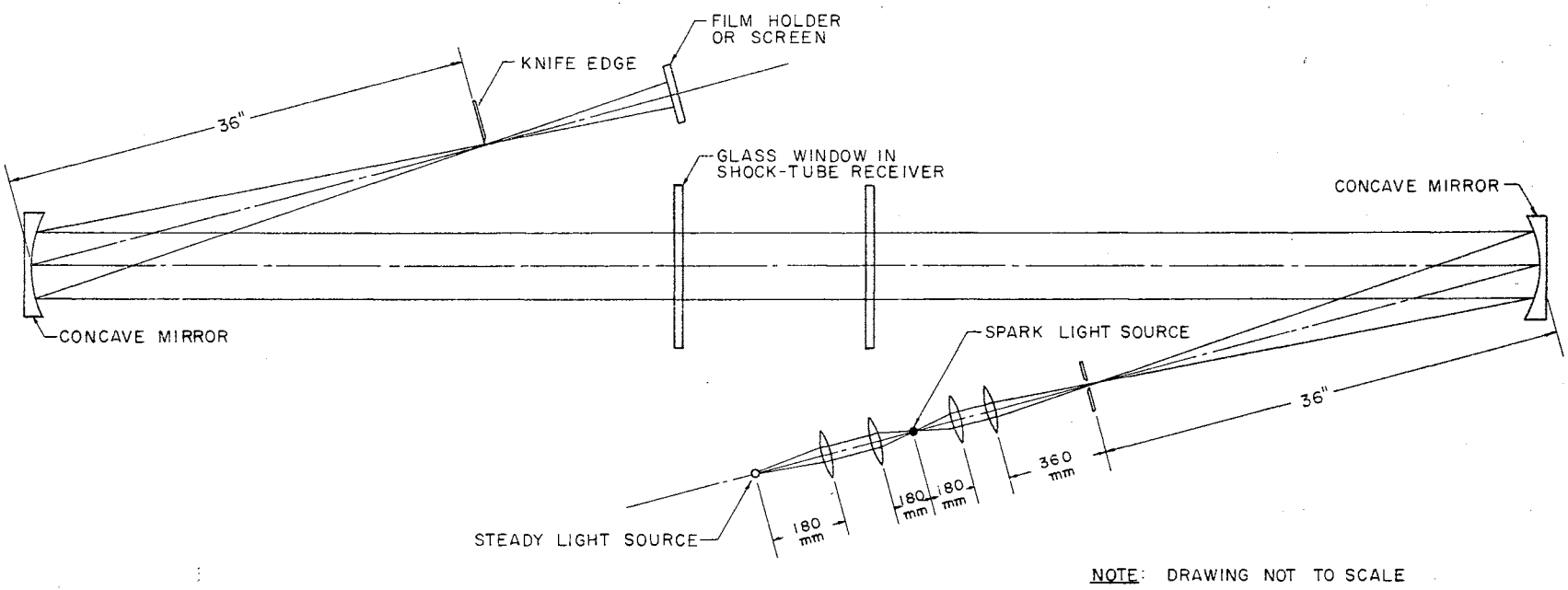

Figure 15. Schlieren Arrangement

Schlieren visualization technique was deemed necessary because the receiver pressure was so low as to make shadowgraphy too indistinct. The spark light source was designed such that identical units could be added in series if a multiple light source unit is desired at a later time. In fact, a dual light source was used for the calibration of the shock strength as the shock wave propagated in the receiver of the shock tube. But for the actual interaction photographs, only a single spark source was used.

The arrangement of the spark source and mirrors is shown in Figure 15. The steady light source was used only for alignment and adjustment of the sensitivity of the system. The steady light source is a mercury vapor lamp with its own power supply. The steady light was focussed on the spark gap and from then on the light followed the same path as the light from the spark source. The spark was refocussed on a vertical slit aperature to cut off extraneous light and to make the light more of the point source type since the spark is usually in the form of a thin line. The aperture is at the focus of the parabolic mirror so that the reflected light would be a 5 inch diameter beam of parallel light. This beam of light was focussed on a vertical knife edge after passing through the test section. Finally, the light fell on a 5" x 4" cut film piece. For spark photography, the lights in the room were turned off and the unexposed film left open.

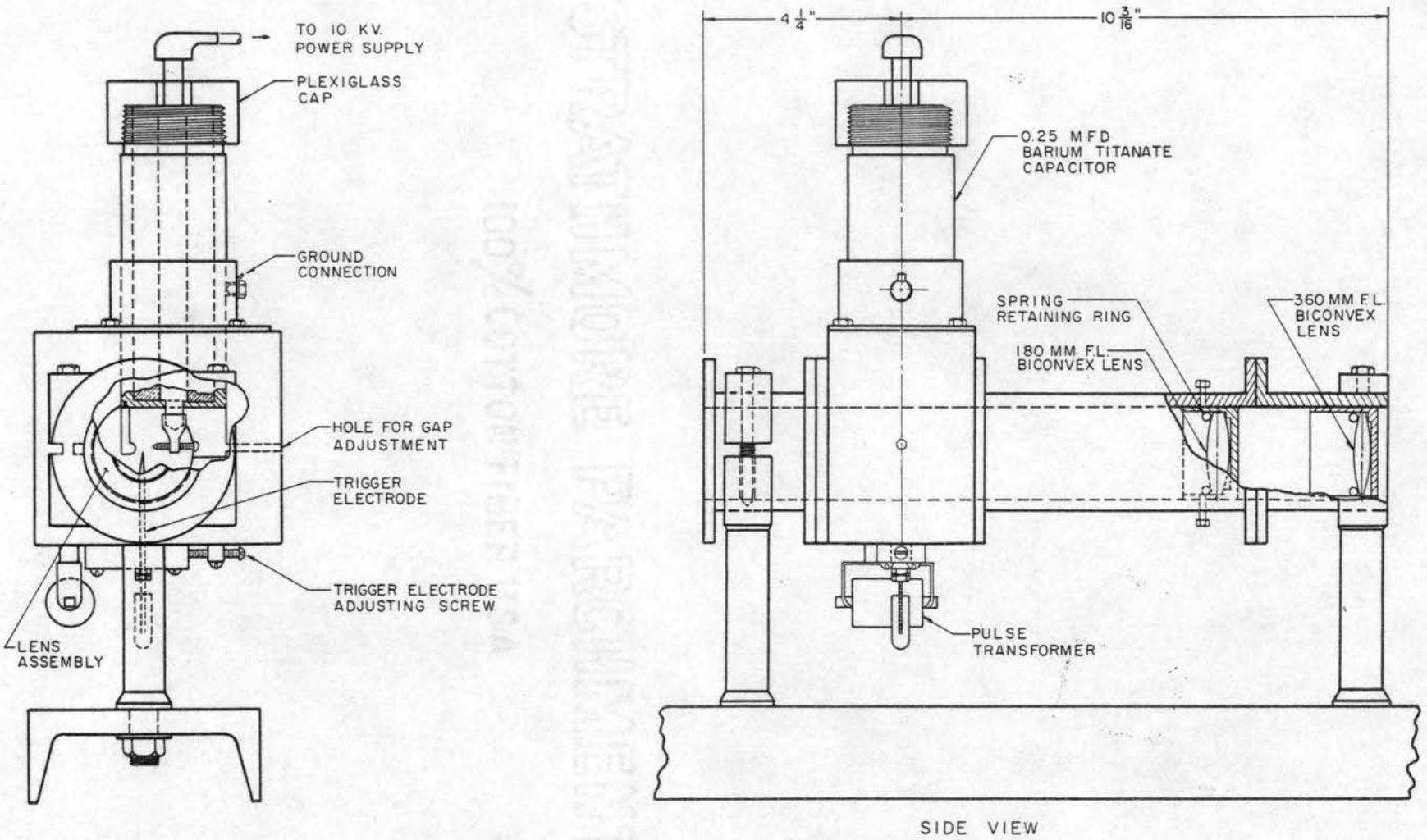

Figure 16. Spark Light Source Assembly

A typical spark source assembly is shown in Figure 16. The main block of the spark source was machined out of plexiglass painted black on the outside. The lenses were mounted in specially machined aluminum holders with spring retainers sliding in aluminum tubes. Achromatic lenses were used throughout. The spark source capacitor was made by inserting a 2 inch diameter, seven inch long, cylinder of barium titanate into a 2 inch I.D. copper tube which formed the outer or ground electrode. The other electrode was a 7/8" diameter copper rod inserted through a hole on the axis of the barium titanate cylinder. The electrode projects one inch out of the capacitor on the sparking side and a size 8-32 screw threaded through it forms the sparking electrode. The air gap was about 1/4 inch long when the capacitor was charged to 6000 V.

Higher voltages could be used (upto 10 KV.) permitting larger spark gaps and giving a brighter spark, but the intensity of the light obtained at 6 KV. was found to be adequate for schlieren pictures of good contrast on Kodak Tri-X film as well as on Polaroid ASA 3000 film. The use of barium titanate as the dielectric material gives an effective light intensity nine hundred times greater than that obtained from a RG8U coaxial cable dimensioned for the same 10^{-7} second effective light duration during discharge (21). The gain in intensity is apparently due to both the higher capacity of the barium titanate cable and its very low characteristic impedance.

The design of the barium titanate capacitor used here is similar to one used by Wilson and Heimenz (22) for a multiple spark light source.

The spark source assembly was affixed to a stand to make its height the same as the centerline of the shock tube. The steady light source was mounted on this stand also, but can be slid on an optical bench so as to permit readjustment in case more than one spark source needs to be used. The individual lens holders can also be adjusted since they slide inside the aluminum light guides.

Optical Spark Circuitry and Delay Units

The method of triggering the light source spark was similar to that used for triggering the diaphragm rupture but differed considerably in its physical design. Whereas it was necessary to create an intensely hot spark for diaphragm rupturing, it now became necessary to have all the light energy from the discharge concentrated at one spot. The triggering gap and the hold-off gap were both combined into one gap. The circuit is shown in Figure 17. Triggering is achieved by means of a high-voltage spark between the ground electrode of the capacitor and an electrode within the gap connected to the secondary of the pulse transformer. The gap is too large to permit the discharging of the barium titanate capacitor charged to 6 KV. except when the effective gap resistance is lowered by ionization of air by the triggering spark. The

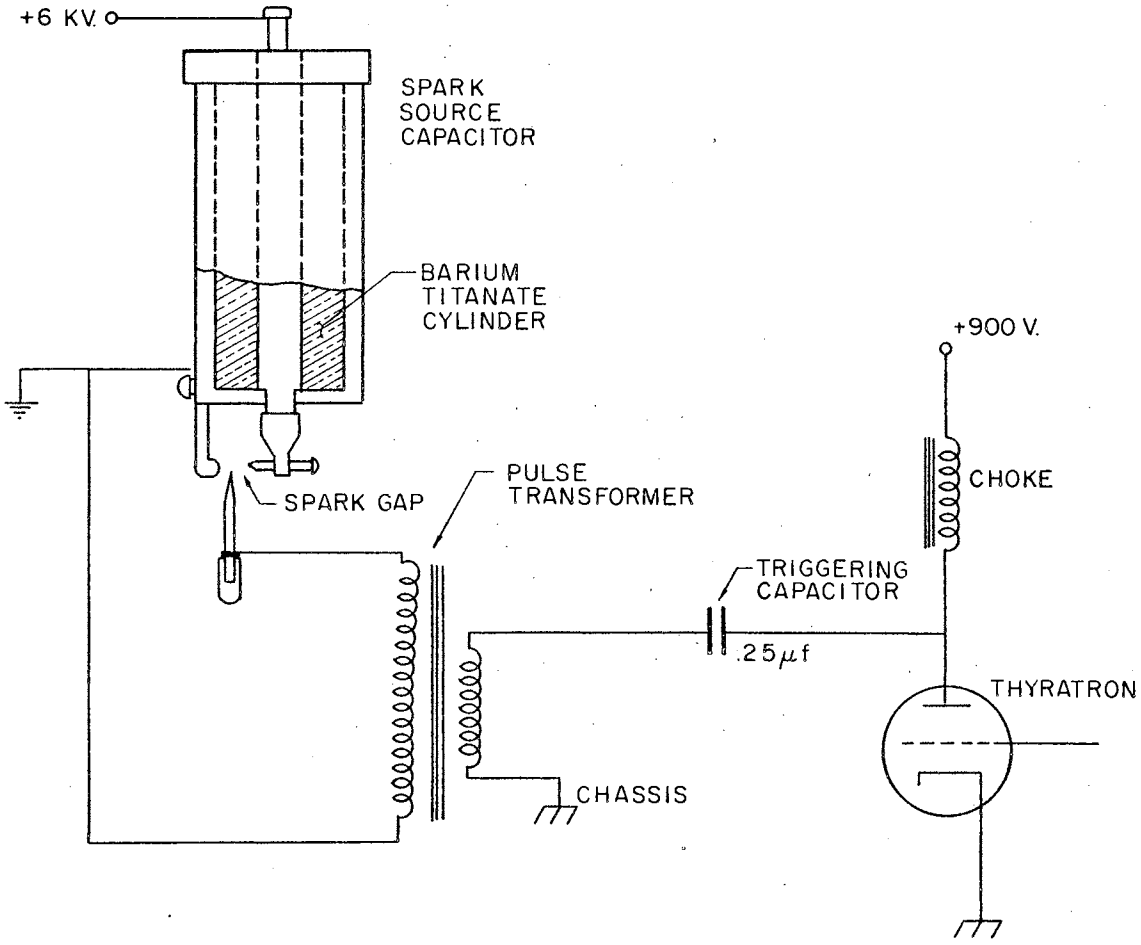

Figure 17. Schematic Showing Operation of Spark Light Source

placement of the triggering electrode is very critical in this arrangement. It is generally about midway between the two electrodes, slightly favoring towards the ground electrode. Best results were obtained when the pulse transformer was mounted on the spark source assembly itself and the leads from the thyratron to the triggering capacitor were completely shielded. The high-voltage ground was also isolated from the chassis ground to prevent spurious triggering.

The barium titanate capacitor seems to have a very high leakage rate so that the high voltage power supply had to be left directly connected to the capacitor to maintain the voltage across its electrodes. When more than one spark source had to be used, a 200 Kilo-ohm wire-wound resistantance was connected between the high-voltage electrodes of the capacitors and the capacitor nearest to the steady light source connected to the power supply. In this way, the intensity of the spark from the capacitor farther from the mirror increases, since the spark light has to travel through more lenses. This also prevents simultaneous triggering of all the spark sources when the delay between the two sparks is not very large.

The delay unit and the thyratron were mounted on the same chassis. A schematic of a typical such unit is shown in Figure 18. At least two such units were needed, one for the diaphragm rupturing signal and one for the spark source signal. The range of delay obtained depended on

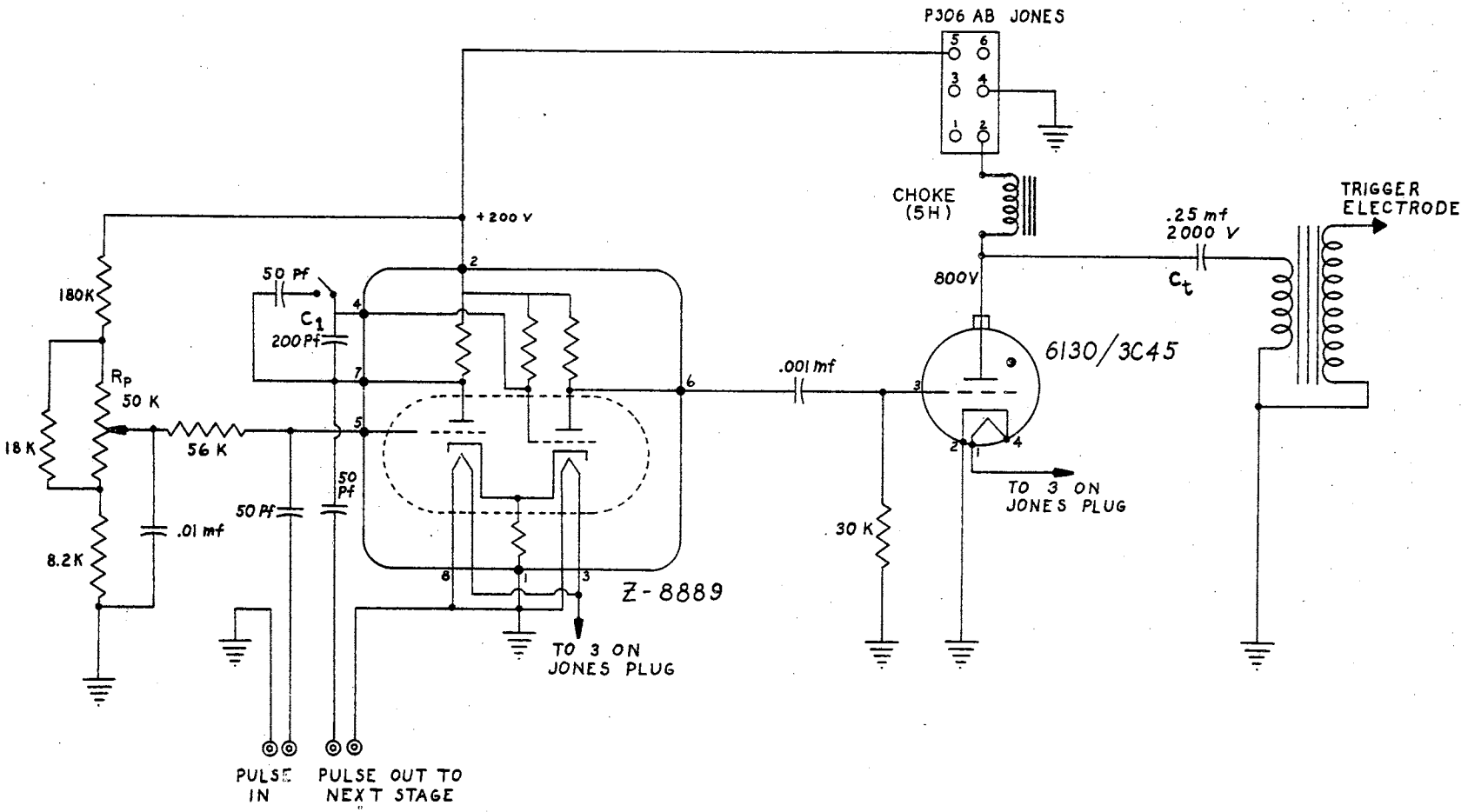

Figure 18. Schematic of Delay Unit With Thyratron

the value of the capacitor C_1 and, hence, could be easily changed when necessary. Fine adjustment of the delay within the range set by the capacitor was obtained by adjusting the potentiometer R_p. Typically, the range of the first delay (the delay between the initiating signal from the model sensor to the diaphragm rupturing signal) was from 50 to 1500 microseconds while the range of the second delay (the delay between the diaphragm rupturing signal and the spark source triggering signal) was from 1700 to 3000 microseconds. The delay unit actually is a monostable multivibrator employing a type 5963 dual-triode tube. The operation of a monostable multivibrator is explained in Appendix I. It will be noted here that the circuit converts the 27 volt positive pulse applied at the input grid into a delayed 90 volt positive pulse which is applied to the grid of the thyratron. This positive pulse is sufficient to trigger conduction in the thyratron, thereby discharging the capacitor C_t through the primary of the pulse transformer.

The units were assembled on 4" x 6" chassis, one unit per chassis. Each unit was shielded individually.

Input Pulser

The input pulser supplied a correctly shaped positive pulse of 27 volt amplitude to the delay unit upon excitation by the model sensor strip. The circuit of Figure 19 is a negatively biased thyratron whose conduction could be

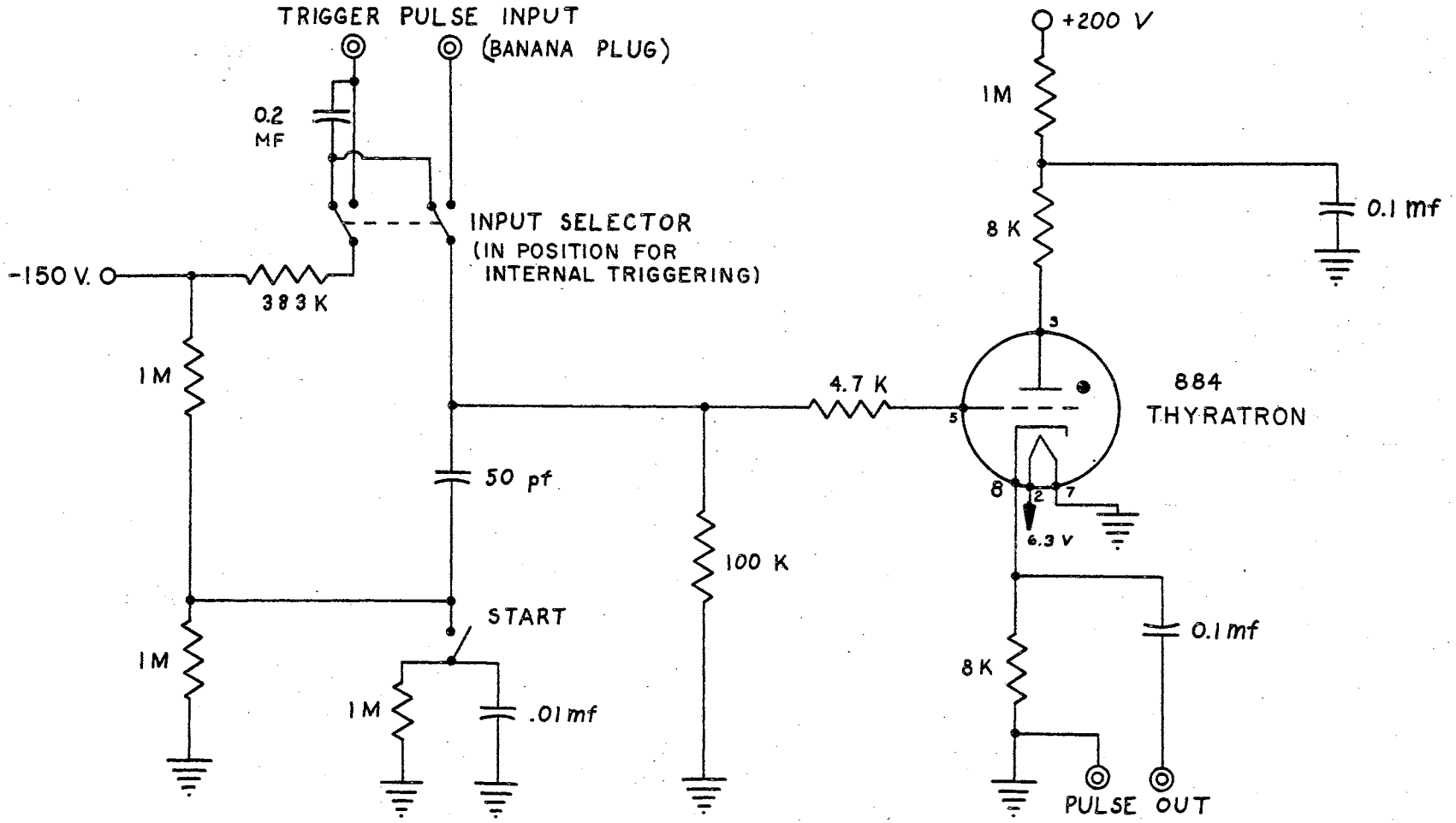

Figure 19. Schematic of Input Pulser

triggered either by breaking a short between the input jacks or by pressing the start button or by a positive pulse at the input connection. The first method was used for initiating the pulse sequence upon the model passing a given location. The internal trigger was employed for calibration and testing of the delay units. A third method of triggering could be employed when a pressure transducer was used to make the passage of the shock wave start the experimental sequence. The output pulse taken from the cathode of the thyratron was always of the same amplitude and duration regardless of the input signal.

For internal triggering the input selector switch was in the left hand position (Figure 19). This resulted in a negative bias of 30 volts on the grid of the thyratron. Depressing the start button essentially shorted out a normally negative potential of approximately 75 volts resulting in a net positive pulse to the grid of the thyratron.

For using the model passage of the sensor strip to trigger the thyratron, the input selector switch was put in the right hand position. The two ends of the sensor (p. 26) strip were connected to the two input terminals of the pulser unit. When the model cut off the strip, it also broke the connection of the negative supply to the grid of the 884 tube. Thus, the grid was suddenly brought to ground potential through its connection with the 100 kilo-ohm resistor. This was sufficient to start plate

conduction in the thyratron.

As soon as the thyratron started conducting, the 0.1 microfarad capacitor in the plate circuit was discharged through the tube and the output terminals received a net positive pulse of 27 volts peak. Conduction stopped soon as the 0.1 microfarad capacitor had discharged since the 1 megohm resistor prevented immediate recharging.

The circuit was assembled on a 4" x 5" chassis and completely shielded. The input and output conductors are also shielded to prevent unwanted triggering.

The chassis layouts for the delay units and the pulser unit were probably not optimum since they were developed and changed from time-to-time because of the problems encountered with spurious triggering, pulse amplitude adjustments, thyratron triggering problems and the like. The warm-up period required to prevent drifting was about two hours. This could be reduced considerably by using precision low-drift components instead of the standard 10 percent tolerance components in this assembly. A larger chassis might probably reduce temperature drift but could introduce shielding problems.

Power Supplies

Regulated d.c. voltage was necessary for proper and reliable operation of the delay units. The 200 volts and the -150 volts bias were both supplied by an Electronics Measurements power supply. A simple half wave rectifier

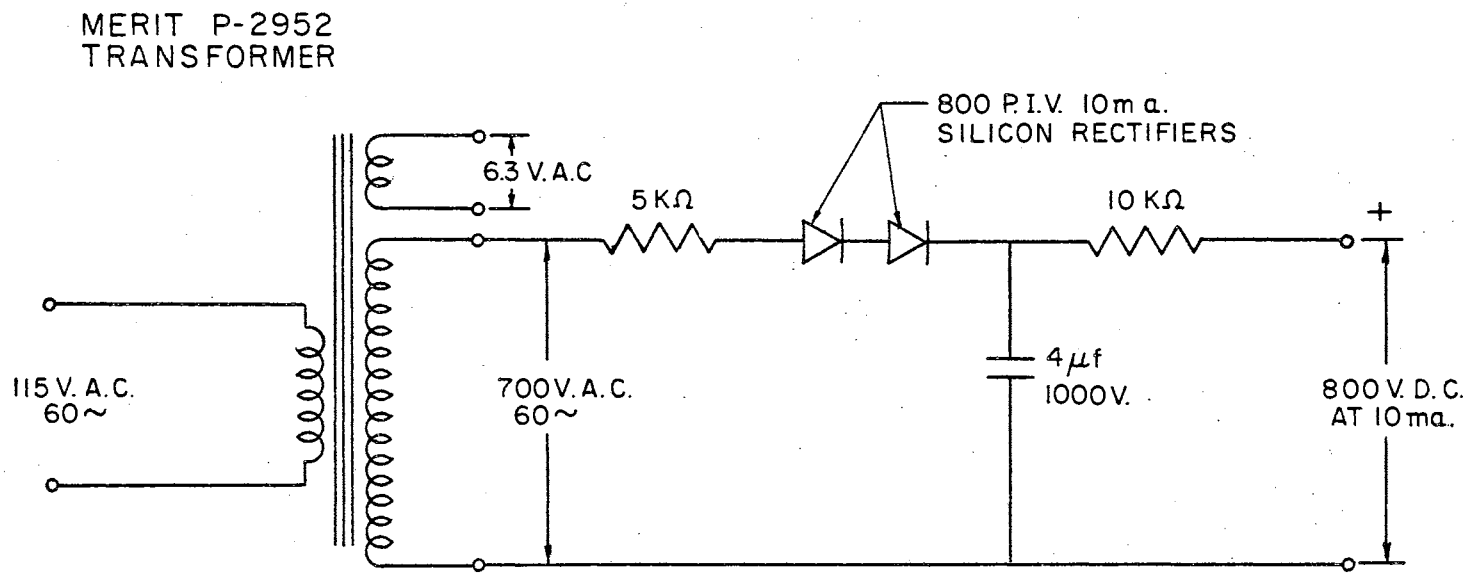

Figure 20. Schematic of 800 Volt d.c. Power Supply

supplied 800 volts d.c. This unit is shown in schematic in Figure 20. A 10 kv. regulated power supply with variable input voltage control supplied the 6 kv. to the spark source and also was used to charge the energy storage capacitor to 4 kv.

The power supply for the steady light source was made by George W. Gates and Co., Inc., L. I., N. Y. The power supply complement as well as the delay units and the energy storage capacitor were all stacked on a 3 ft. wide and 1 ft. deep stand. Figure 21 shows the complete unit along with a dual beam oscilloscope used for calibration of delays.

Measurement of Shock Velocity in the Shock Tube

Accurate measurement of shock velocity in the shock tube is necessary for the following reasons:

1. Actual values of velocity and Mach number of the shock wave generally fall short of theoretical predictions due to attenuation in the channel, energy absorbed in diaphragm opening, and the difficulty in accurate prediction of the thermodynamic constants for the mixture of gases present in the channel.
2. Knowledge of exact shock velocity is necessary for setting the delays for spark photography, etc.

In addition, it is necessary to know the exact time

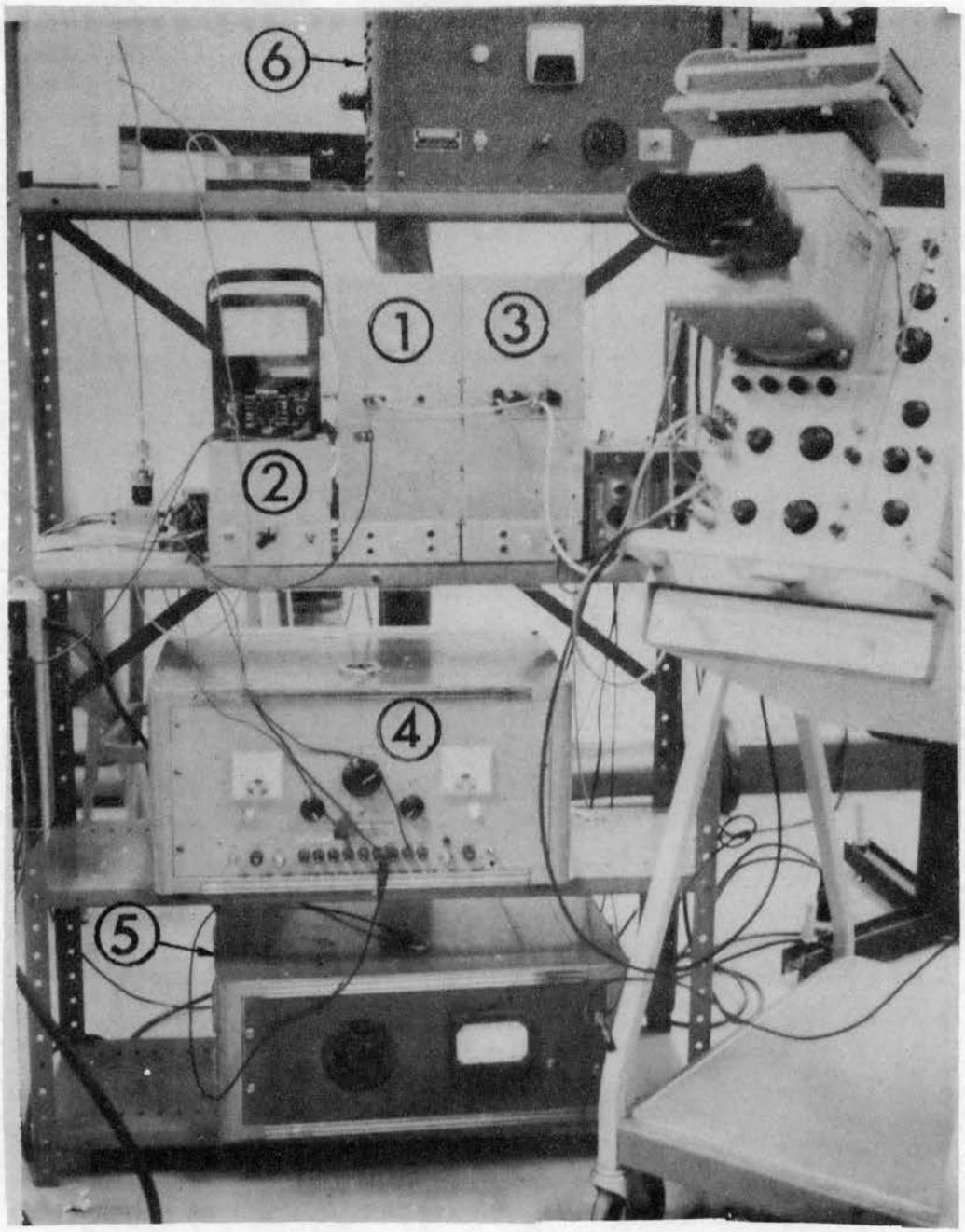

1. Input Pulser
2. 800 v. Power Supply
3. Delay Unit
4. 200 v. d.c. Regulated Power Supply
5. 10 kv. Variable Power Supply
6. Steady Light Source Power Supply

Figure 21. Electronic Equipment Rack

taken by the diaphragm to open after the trigger signal is applied for setting the delay times.

Method

Both the shock velocity and the diaphragm opening time were measured simultaneously. Two Kistler Type 502 quartz pressure transducers mounted in the shock tube wall picked up the pressure pulse from the shock wave as it passed their locations. The transducers were placed three and three-eights of an inch apart and the upstream transducer was 20.75 inches from the diaphragm location (Figure 8). The output from the transducers was recorded on a dual-beam oscilloscope after amplification. The traces on the oscilloscope were triggered by the voltage induced by the triggering pulse to the diaphragm rupturing circuit. A typical trace of the pressure history at the two transducer locations is shown in Figure 22. The lower trace is reversed in polarity for clarity, and gives the pressure history at the upstream transducer location after the diaphragm trigger signal. The shock velocity is readily obtained from this by measuring the time lag between the arrival of the shock wave at the first and the second transducer, since the distance between the two transducers is known to be 0.2808 feet. From Figure 22, the shock velocity is given by $V_s = \frac{0.2808}{0.14 \times 10^{-3}} = 2006$ fps. Since the distance from the diaphragm to the first transducer is also known, the diaphragm opening time can now be

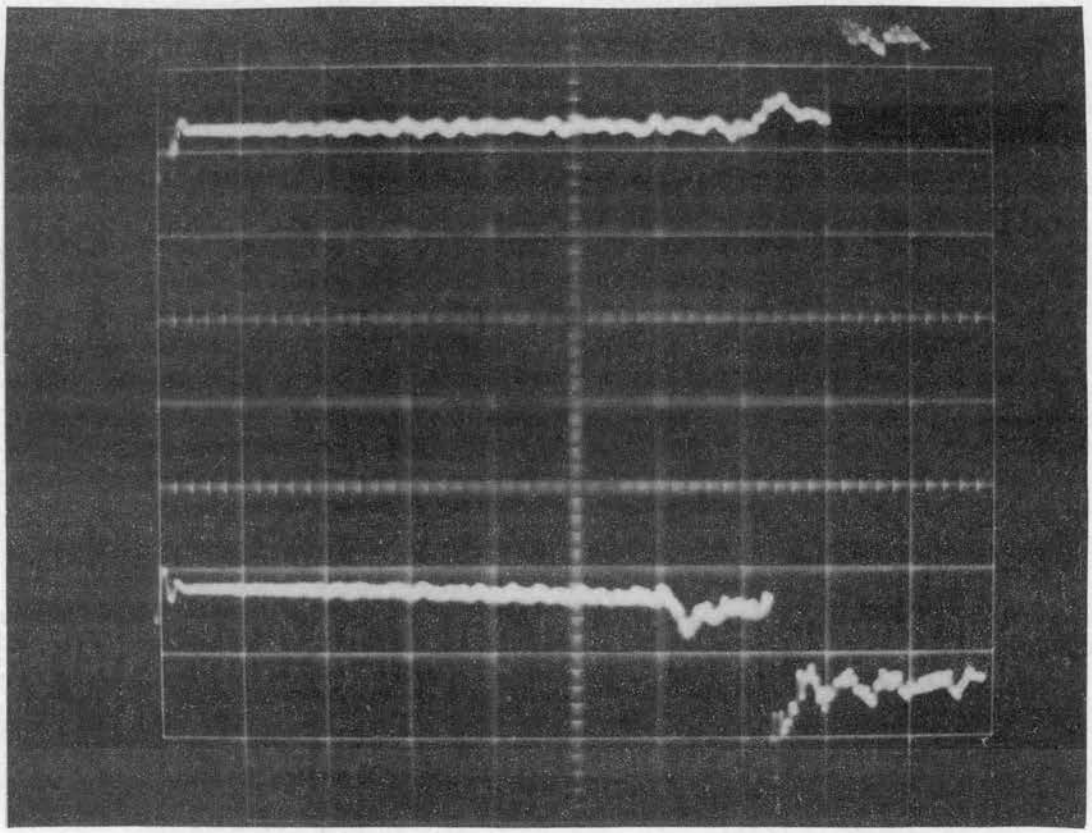

⟶ Time 0.2 ms/cm

Figure 22. Transducer Outputs for Shock Velocity Measurement

estimated. Within the measurement accuracies, it is safe to assume zero attenuation of the shock wave within the 20.75 inches it has traveled in the shock tube channel. Again, from Figure 22, the diaphragm opening time is

$$\Delta t_1 = 1.48 \times 10^{-3} - \frac{20.75}{12 \times 2006} = 0.62 \times 10^{-3} \text{ sec.}$$

Incidentally, the vertical scale of the traces gives a good indication of the strength of the shock wave if the charge amplifiers are calibrated for the transducers.

Table I gives the shock velocities and diaphragm opening times for some combinations of gases, diaphragm thicknesses and diaphragm pressure ratios. It is clear that diaphragm opening time is a strong function of the number of layers in the diaphragm. The time also depends on the receiver pressure, increasing as the pressure is reduced.

Shock Velocity in the Receiver

The shock wave, upon entering the receiver through the Borda orifice, expands in all directions and, consequently, attenuates rapidly. Therefore, the shock velocity had to be measured at various locations in the receiver where the shock would be likely to interact with the model.

Again, the method which was used for velocity measurement was direct. A double exposure of the shock wave

TABLE I

MEASURED SHOCK VELOCITIES AND DIAPHRAGM OPENING TIMES

Gas Combination in shock tube	Driver Pressure (P_4) psia	Receiver Pressure (P_1) psia	Pressure Ratio (P_4/P_1)	Number of layers of 0.001" Al.	Theo. Shock Velo. fps	Measured Shock Velo. (fps)	Diaphragm Opening Time (Microsec.)
Helium/Air	44.3	14.3	3.10	3	1550	1404	0.170
Helium/Air	76.3	14.3	5.33	6	1880	1870	0.464
Helium/Air	106.3	14.3	7.44	9	2090	2010	1.170
Helium/Air	32.3	26" vac.	20.05	3	2785	2640	0.440
Helium/Freon-114	32.3	26" vac.	20.05	3	1340	1720	0.282

Note: Actual velocity for helium/F-114 combination is greater than theoretical due to contamination of F-114 in the receiver with air. (See p. 72.)

was photographed using a dual schlieren light source. The time interval between the two light sparks was kept at 40 microseconds and the distance traveled by the shock wave during this interval measured from the photographs. The velocity was assumed to apply to the shock at the mid-point between the two picture locations. A sample of the double-exposed photograph is shown in Figure 23. The reduced quality of definition of the photograph due to double exposure should be noted.

A plot of shock velocity versus distance from the faceplate along the shock tube axis for helium/F-114 combination at a pressure ratio P_4/P_1 of 20.05 is shown in Figure 24. The region where the model interacted with the shock wave was sufficiently close to the shock tube axis to permit the use of the axial shock velocities for all calculations. Moreover, the shock wave assumes the shape of a circular arc and becomes self-similar at about three inches from the face plate, so that the shock can be assumed to be propagating uniformly in all directions. Most of the interaction photographs were obtained when the shock was in this location.

Measurement of Model Velocity

An additional model sensor and input pulser unit were required for this measurement. The time required by the model to travel the distance between the two strips was measured on an oscilloscope or digital time interval

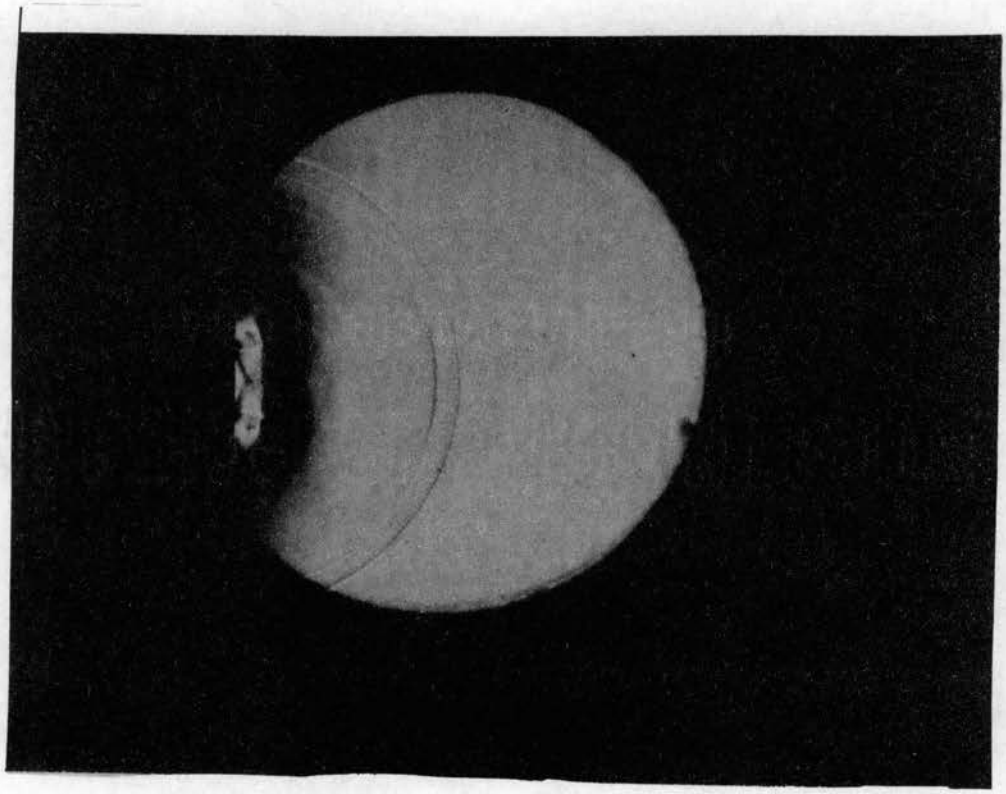

Figure 23. Double Exposure of Shock Wave in the Receiver

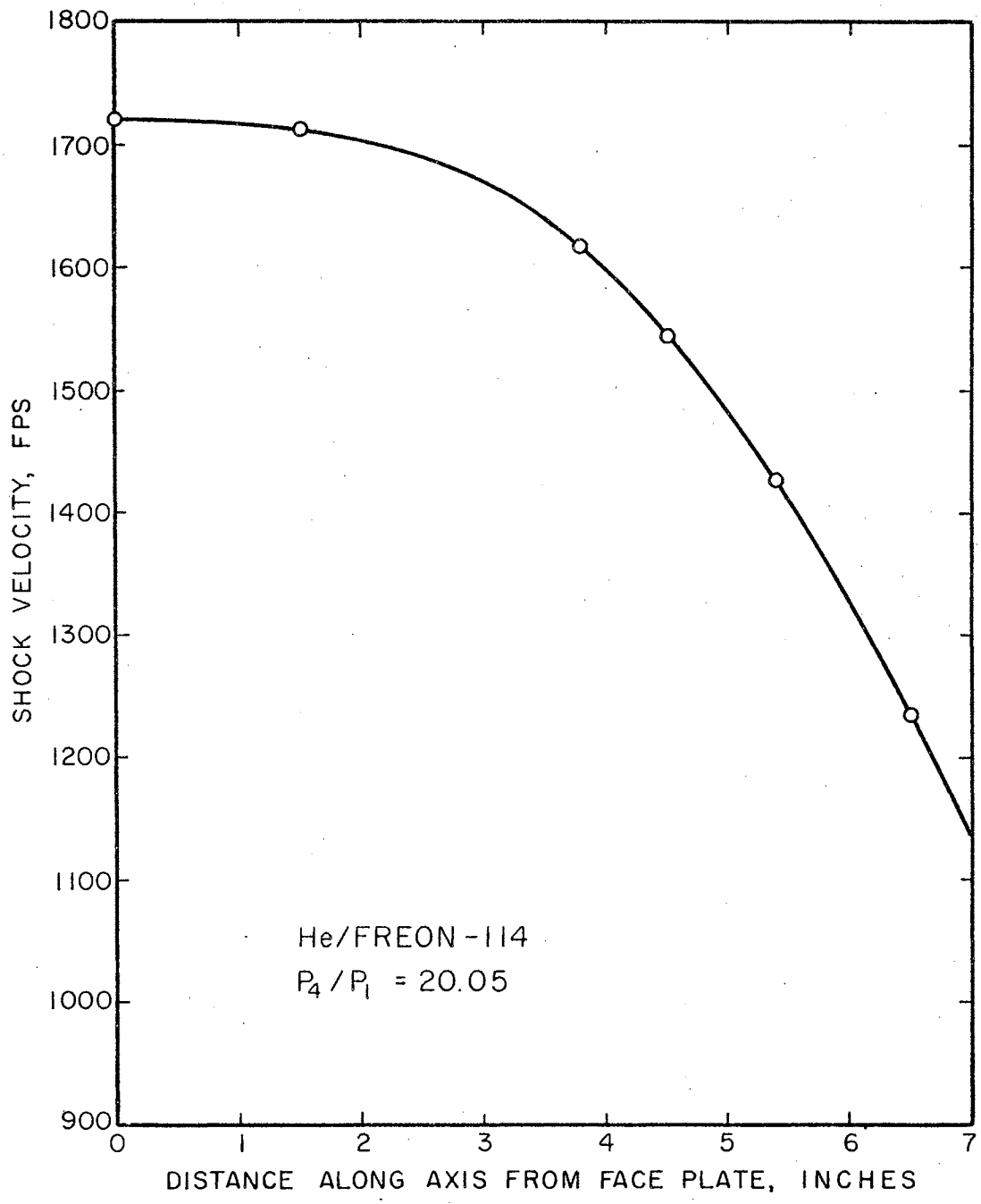

Figure 24. Shock Velocity in the Receiver

counter. The second strip was generally placed near the top of the receiver opening so that the average velocity between the muzzle and the receiver could be measured, but the location was not critical. The curves in Figure 6 were obtained in this manner. The model velocities in the tests, along with the amounts of DuPont 4320 rifle powder used are shown in Table II.

TABLE II

MODEL VELOCITIES

Weight of model (grains)	Weight of powder (grains)	Velocity fps	Mach No. in air	Mach No. in F-114 (pure)
270 (round-nose)	40	1440	1.270	3.46
224.2	40	1610	1.414	3.85
224.2	68	2710	2.390	6.51
215.0	55	2120	1.870	5.07

Calibration of the Delay Units

The time delay applied to a given pulse by the circuit of Figure 18 was measured from the time-voltage trace taken at the plate of V_1 (pin 7 of the Z-8889 unit). The

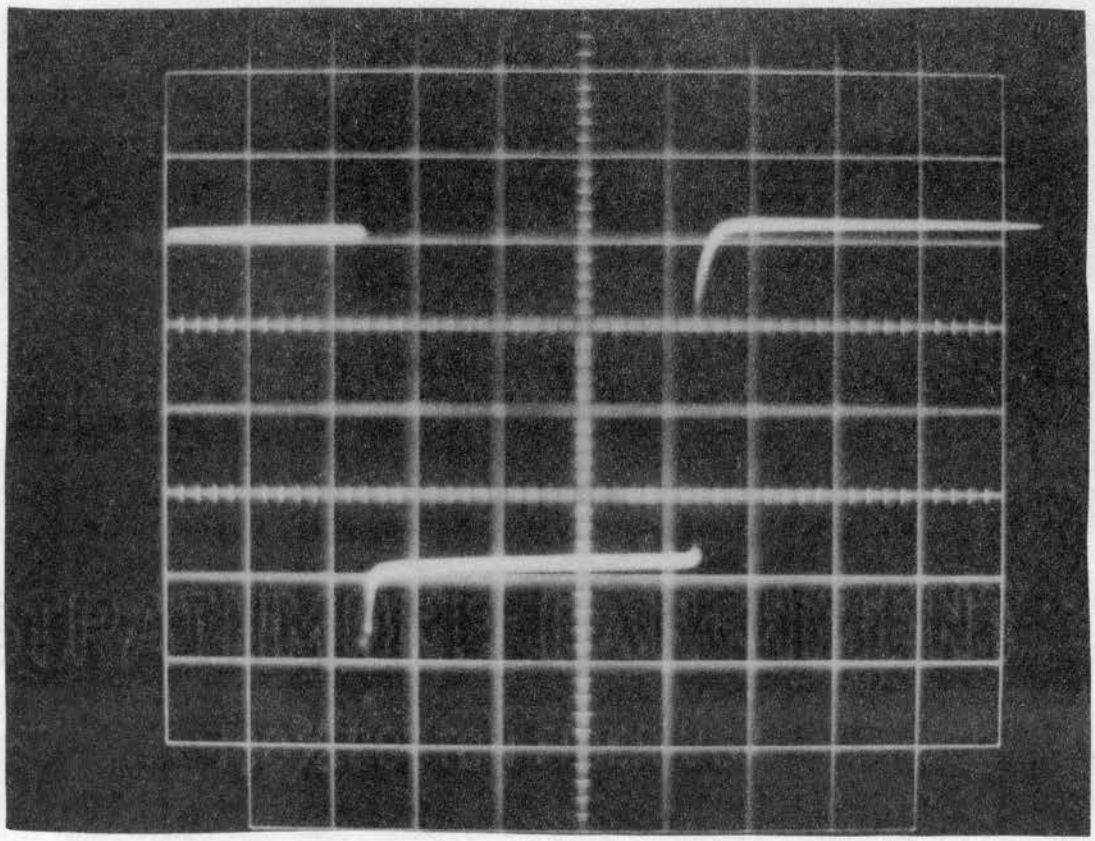

⟶ Time 0.5 ms/cm

Figure 25. Trace of Voltage at Multivibrator Plate Used for Measurement of Delay

trace was obtained at any time by pressing the internal triggering button on the input pulser unit. An oscilloscope with a reliable time scale and ultra-fast rise time made the trace shown in Figure 25 possible. Here, the trace was triggered by the input pulse to the first delay. The time from the start of the trace to the sudden voltage drop is the first delay, while the time from the sudden drop to the steep rise in voltage indicates the second delay. Although the delays can be calibrated within their entire range by this method, it was found best to check the settings before each experimental run.

Estimation of Thermodynamic Properties of Mixtures of Freon-114 and Air

At room temperature, the sonic velocity is about 1144 fps in air and 416 fps in Freon-114. For a mixture of air and Freon-114, the sonic velocity would be between these values, and would depend on the specific heat ratio γ, the gas constant R and the temperature of the mixture. The specific heat ratio and the gas constant for the mixture in the receiver at the time of the experiment were estimated as follows. The ratio of Freon-114 to air in the receiver and the shock channel was determined first from the method of filling the receiver with Freon. The receiver and the channel, which contained initially air at atmospheric pressure, were first evacuated to 2 psia. Gaseous Freon-114 was then introduced into the receiver

until the pressure was again atmospheric. This process would result in a mixture containing 86% F-114. If there were no leaks into the receiver, this concentration would essentially remain the same if the pressure of the mixture were lowered. However, the leakage rate was found to be such as could not be ignored without loss of accuracy, especially since the time required to pump the mixture down to 26 inches Hg vacuum was 11.25 minutes. This leakage rate was actually measured and was found to be 0.0597 cfm/ft^3 of receiver volume for 20 to 26 inches of vacuum. This amounts to an addition of 0.673 ft^3 of air to every ft^3 of mixture, and hence the corrected volumetric percentages were 51.4% F-114 and 48.6% air.

By using mole fractions rather than actual weights of the gases, the molecular weight M of the mixture at 1.56 psia is obtained as follows (26):

	Volumetric %	Mole Fraction	Molecular Weight	Relative Mass (mole fr. x mol. wt.)
Freon-114	51.4	0.514	170.9	87.9
Air	48.6	0.486	28.96	14.08
		Mol. wt. of mixture		101.98

The molecular weight of the mixture is obtained by adding the relative masses of Freon-114 and air.

The value of the gas constant for the mixture can be found easily now from the equation:

$R = \frac{R_o}{M}$ where R_o is the universal gas constant.

Therefore, R for the mixture is 1545/101.98 = 15.15 ft. lb/lb °R.

The other thermodynamic constants are determined from the mass fractions. Mass fraction of F-114, n_f, is 87.9/101.98 = 0.862, and the mass fraction of air in the mixture, n_a, is 14.08/101.98 = 0.138. Finally, the equations below can be used to obtain the values of c_p, c_v, and γ. Subscript f indicates the value of the constant for pure Freon-114 and the subscript a indicates the value for air.

$$C_p = n_f C_{p_f} + n_a C_{p_a}$$

$$C_v = n_f C_{v_f} + n_a C_{v_a}$$

$$\gamma = n_f \gamma_f + n_a \gamma_a$$

Relation Between Diaphragm Pressure Ratio P_4/P_1 and the Shock Mach Number for Helium/Freon Combination

The theoretical values for the shock Mach numbers and shock strengths obtained for different diaphragm pressure ratios using Freon-114 as the driven and helium as the driver gas are given by the following formulae from Reference (25).

$$\frac{P_1}{P_4} = \frac{P_1}{P_2}\left[1 - \left(\frac{P_2}{P_1} - 1\right)\sqrt{\frac{\beta_4 E_{14}}{\alpha_1 \frac{P_2}{P_1} + 1}}\right]^{\frac{1}{\beta_4}}$$

$$M_s = \left[\beta_1 \left(1 + \alpha_1 \frac{P_2}{P_1}\right)\right]^{\frac{1}{2}}$$

where $E_{14} = \dfrac{(C_v T)_1}{(C_v T)_4}$ $\qquad \alpha = \dfrac{\gamma + 1}{\gamma - 1}$

$$\beta = \frac{\gamma - 1}{2\gamma} .$$

Subscript 1 is used for the driven gas properties and subscript 4 is used for the driver gas properties. P_2 is the pressure behind the shock wave.

These equations were solved for different values of the shock pressure ratios (P_2/P_1) and plotted in Figures 26 and 27.

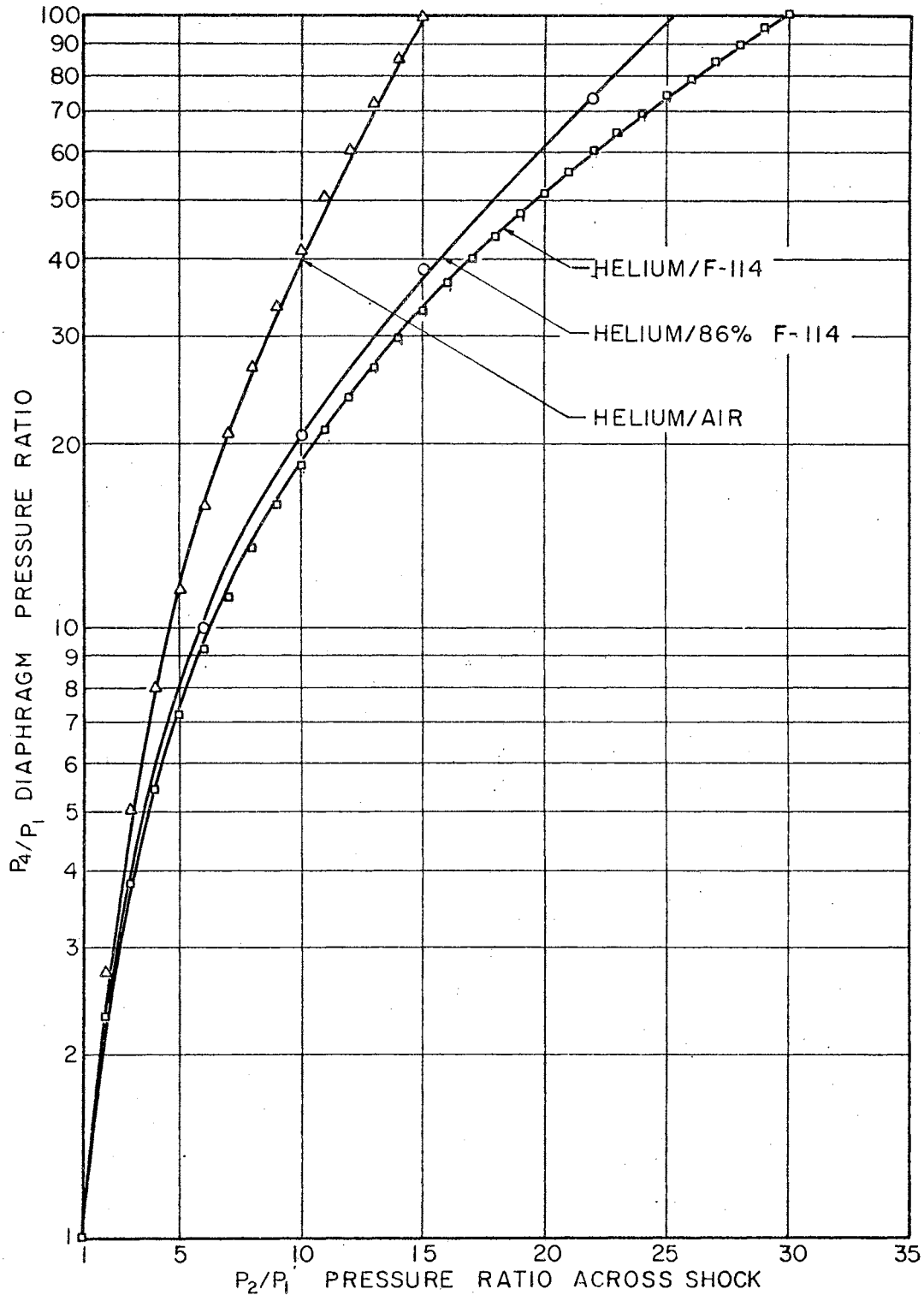

Figure 26. Shock Press Ratio Versus Diaphragm Press Ratio

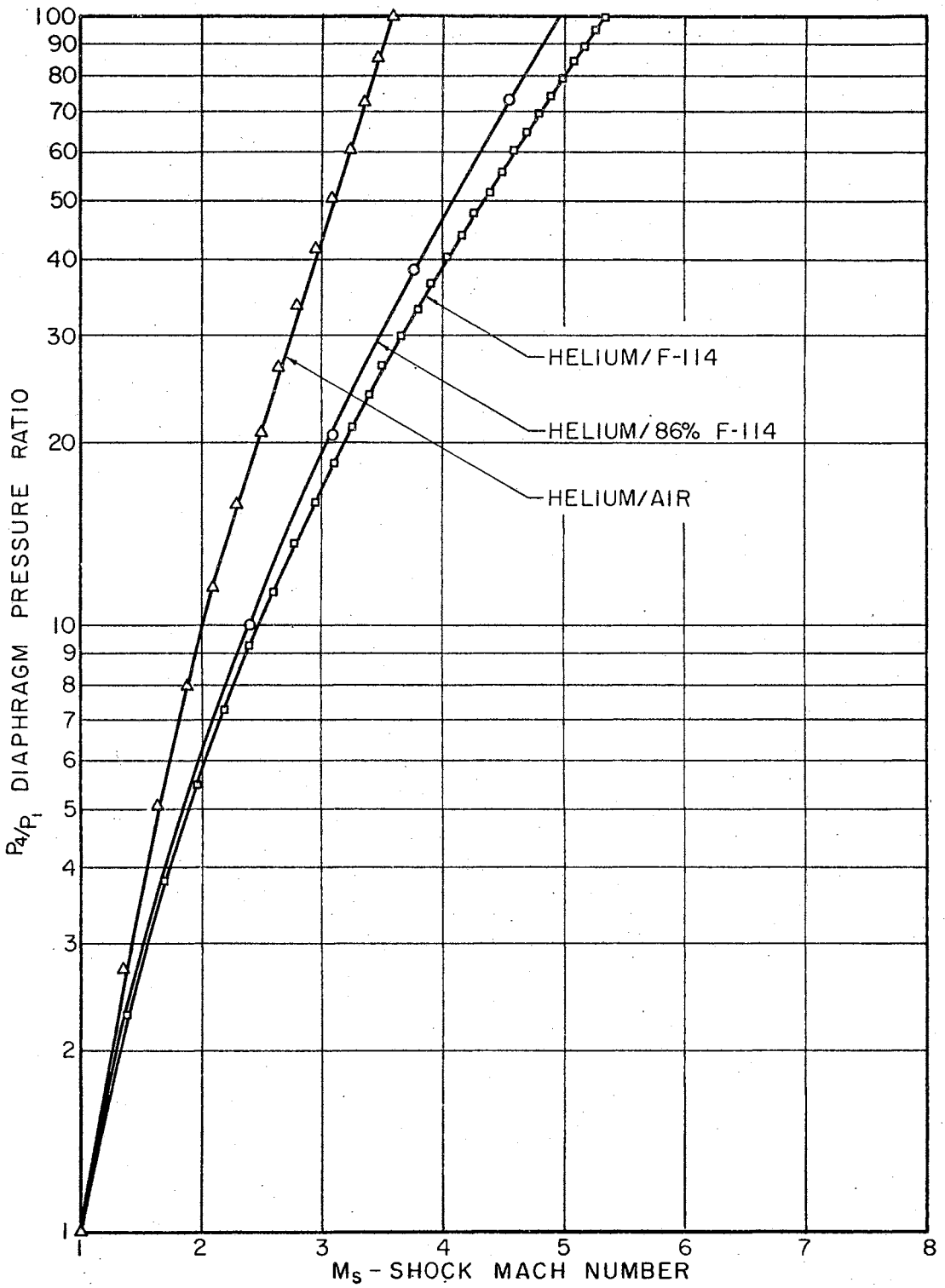

Figure 27. Shock Mach Number Versus Pressure Ratio

CHAPTER IV

EXPERIMENTAL RESULTS

Table III shows the different combinations of blast wave and model Mach numbers for which interaction photographs were obtained. Helium was used as the driver gas in all the cases.

TABLE III

TEST CONDITIONS

Blast wave Mach No.	Model Mach No.	Interaction Angle	Driven gas and pressure
1.24	1.413	65°	Air at atmospheric pressure (14.3 psia)
2.33	2.39	65°	Air at 25" Hg. vacuum
3.20	3.94	25°	Freon-114 at 26" vacuum
"	"	35°	"
"	"	80°	"

The low Mach number interaction is shown in Figure 28.

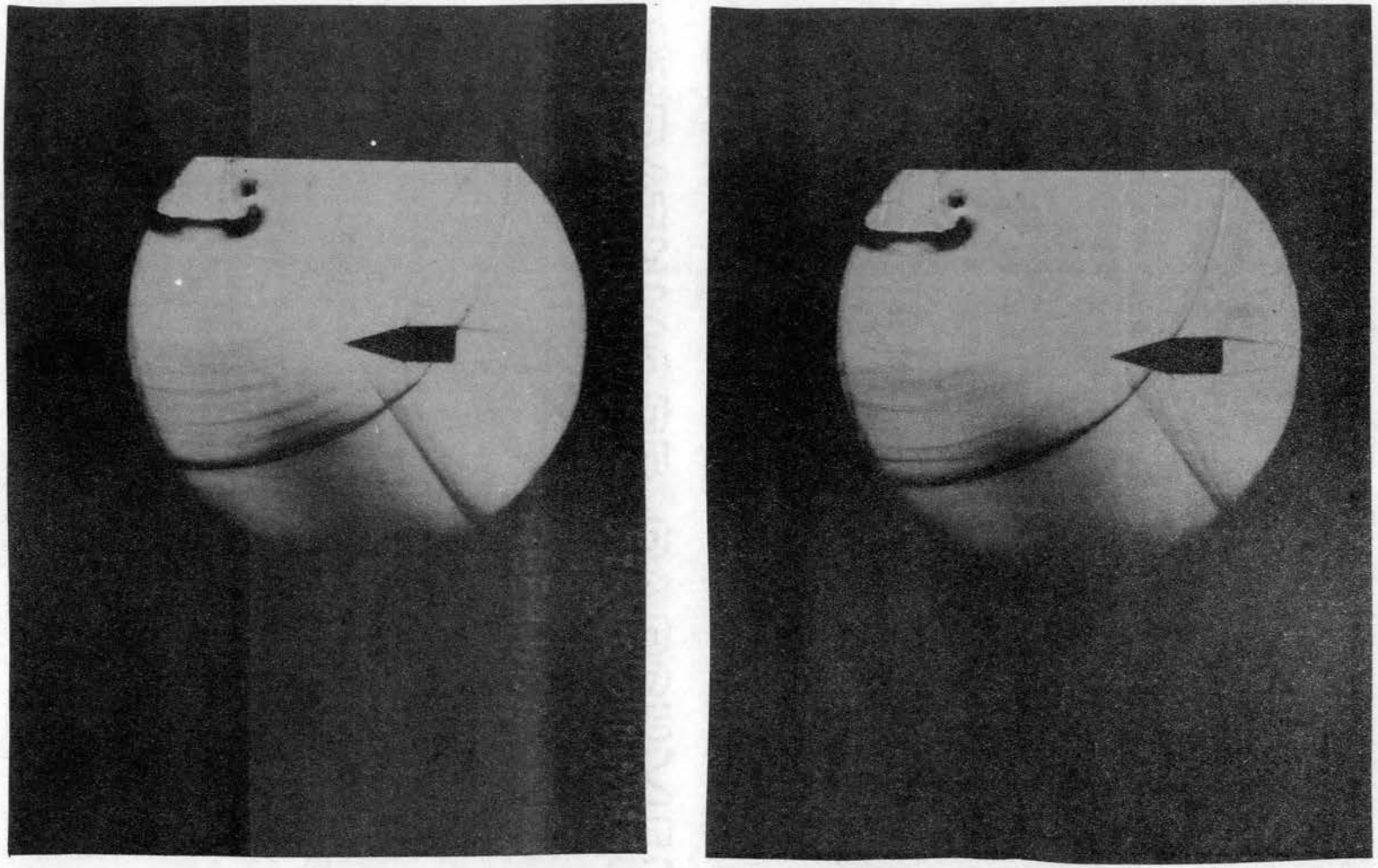

Figure 28. Schlieren Photographs of Interaction in Air
Model Mach No. 1.413
Blast Wave Mach No. 1.24
Interaction Angle 65°

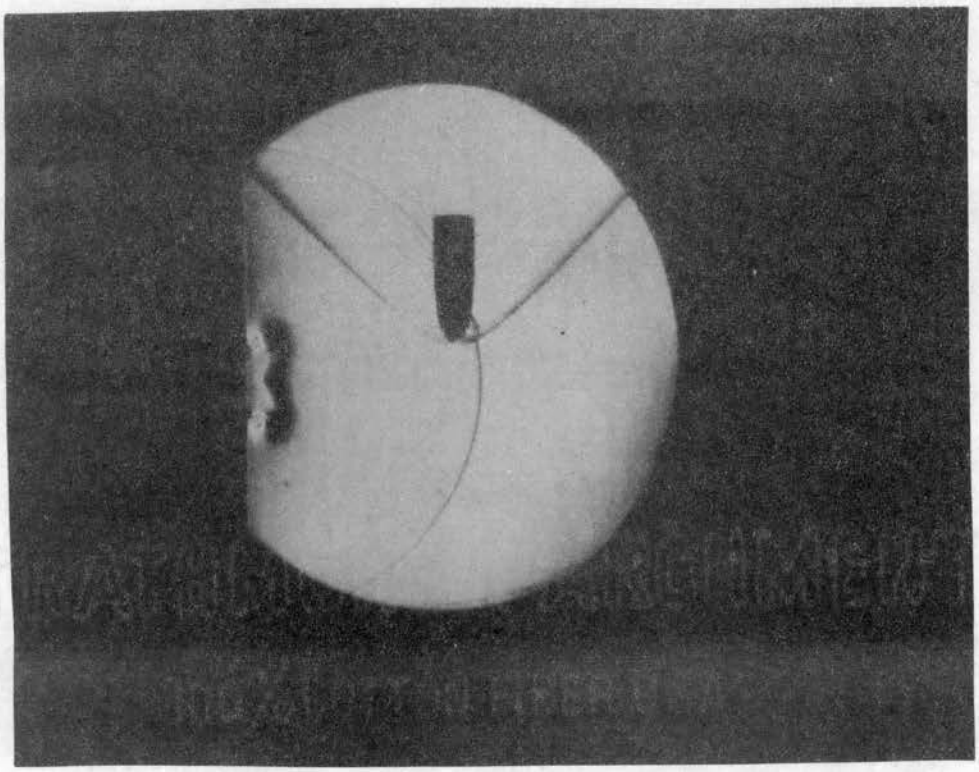

Figure 29. Schlieren Photograph of Interaction Round-Nosed Model

Very little effect can be observed on either the blast wave or the bow shock. There is normal reflection of the blast wave on the side of the model on which the blast wave hits first (hereafter termed the high-pressure side of the model). The angles of the post-blast bow wave are altered very slightly. The bow wave curves slightly outwards where the reflected blast wave intersects it. The reflected wave is highly curved, with the concave side toward the model. This is expected since the original wave is curved also. A similar interaction photograph for a round nosed model is shown in Figure 29.

The interaction at blast Mach number of 2.33 and model Mach number of 2.39 is shown in Figure 30. The interaction is almost head-on, the interaction angle being 65°. On the whole, the photographs did not have sufficient contrast to show enough detail due to the low density of air in the receiver. However, the effects mentioned for the low Mach number interaction case are seen to have been enhanced greatly. There is a sharp change in the bow wave angle close to where the reflected oblique shock meets the bow shock. This point is not so close to the conical tip as in the previous case. A contact surface is seen to have developed behind the blast wave in the vicinity of the model (Figure 30(a)). The main features are sketched in Figure 31 for clarity. Some effect on the shock geometry is also seen on the low-pressure side of the model. Very few tests were run at this Mach

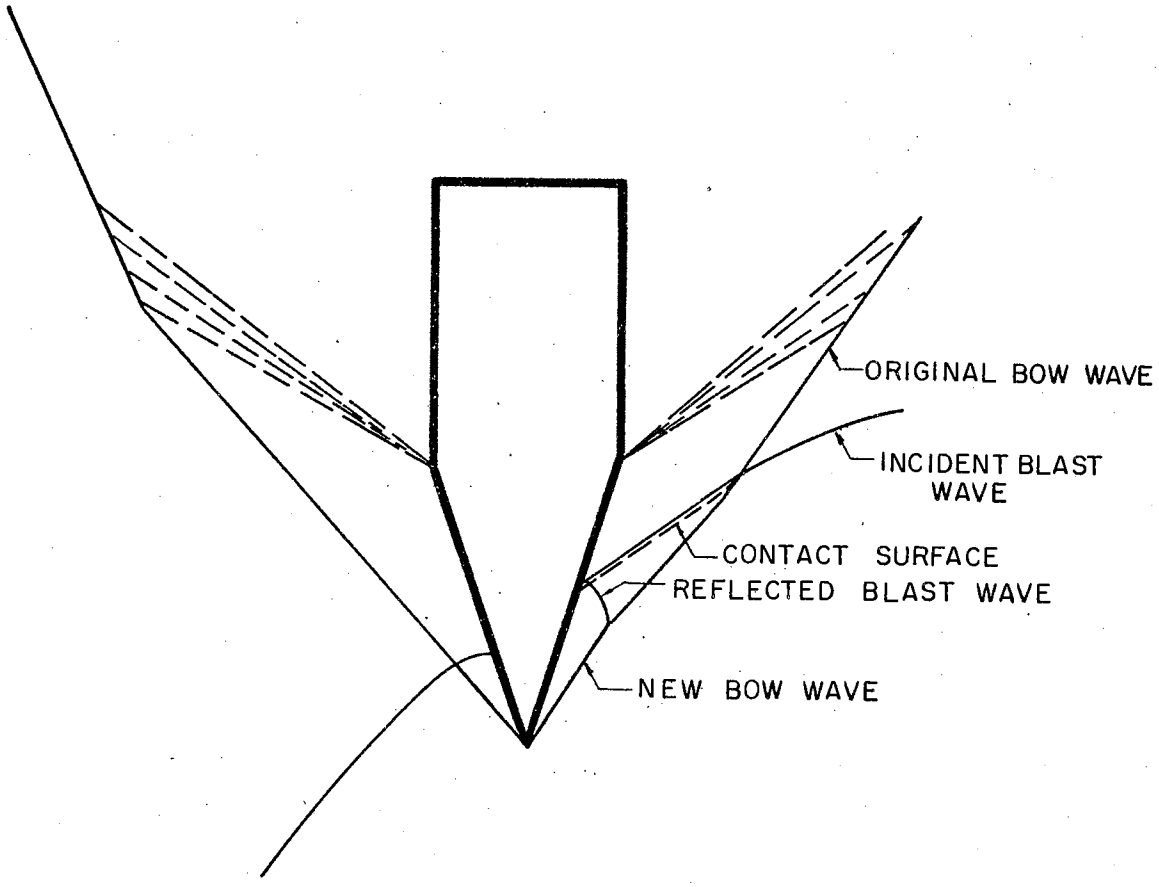

Figure 31. Sketch Showing Shock Geometry of Interaction at 65°; Model Mach No. 2.39; Blast Mach Number 2.33

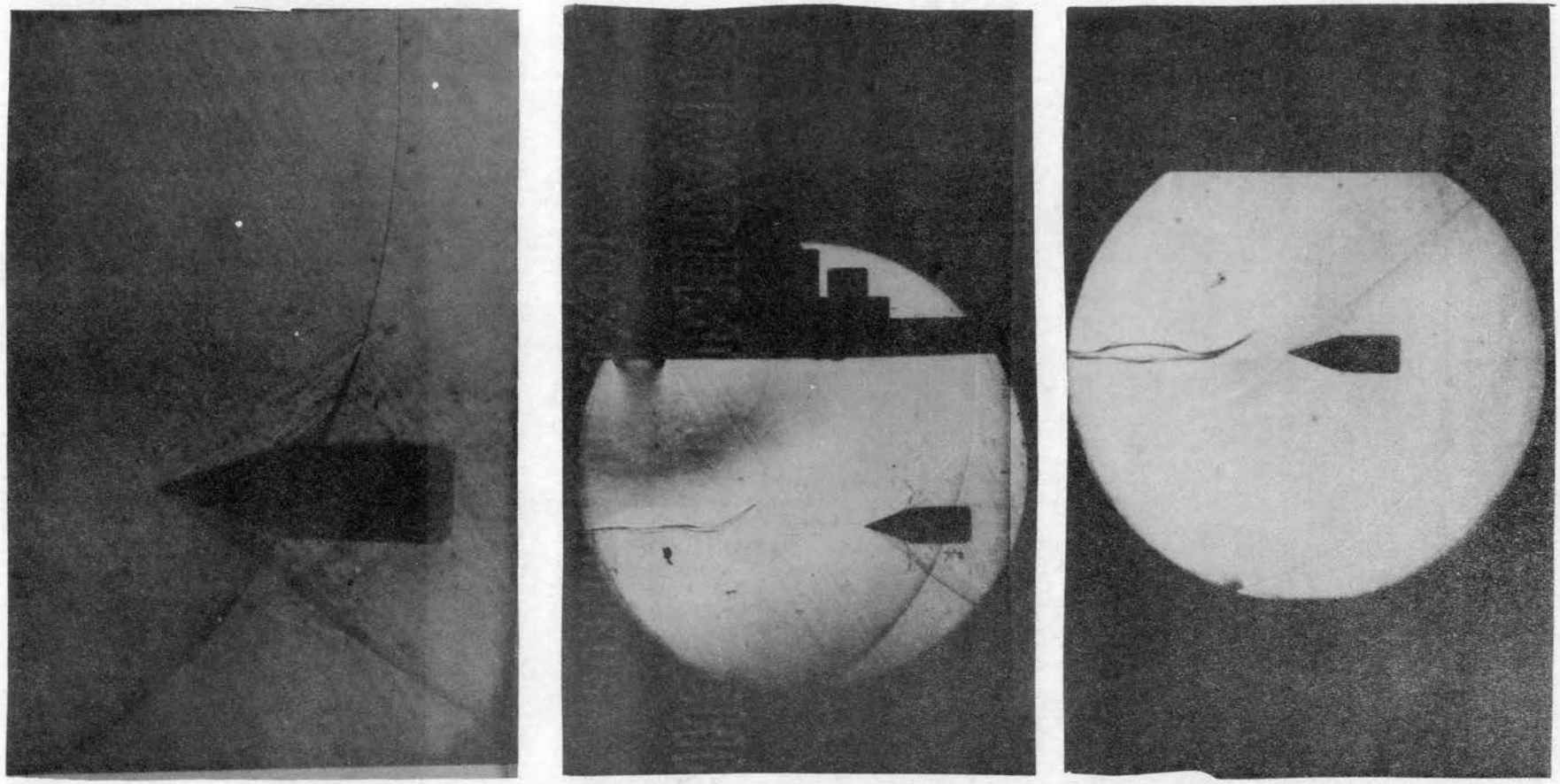

Figure 30. Schlieren Photographs of Interaction in Air
Model Mach No. 2.39
Blast Wave Mach No. 2.33
Interaction Angle 65°

number combination due to the poor visualization.

A sequence of schlieren photographs showing the interaction of a model at Mach 3.94 entering a blast region in Freon-114 atmosphere is shown in Figure 32. At the moment of interaction, the blast wave was traveling at Mach 3.14 and making an angle of 35 degrees with the axis of the model. The sequence was obtained from several separate test runs and, therefore, does not represent the same blast wave and the same model in each photograph, but the trend of events taking place at a typical oblique interaction is clear.

The second frame in Figure 32 is shown enlarged in Figure 33(a) and the main features are sketched in Figure 34. As expected, the shock geometries on the two sides of the model are very different. The bow shock after interaction on the high pressure side of the model has three distinct regions. Region I is a straight portion having a shock angle corresponding to that for the flow properties encountered by the model in the post-blast region. Region II is a portion concave towards the body and corresponds very nearly to the circumference of the "shock-circle" in Reference (6). (The shock-circle defines the extent of the disturbance caused by the intersection of the body with the blast wave. The bow wave in region I is, therefore, tangential to the shock-circle.) Region III is another straight portion joining a point on the shock circle to the intersection point of the original bow wave

(a)

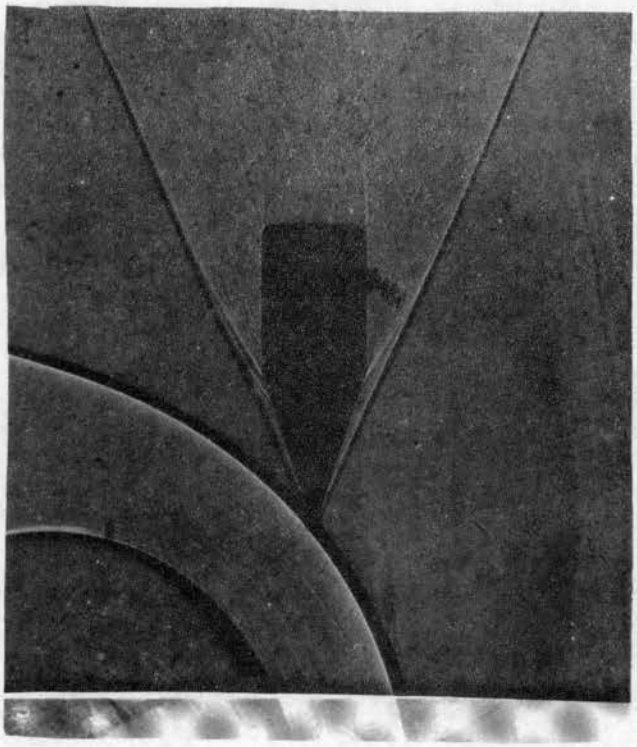

(b)

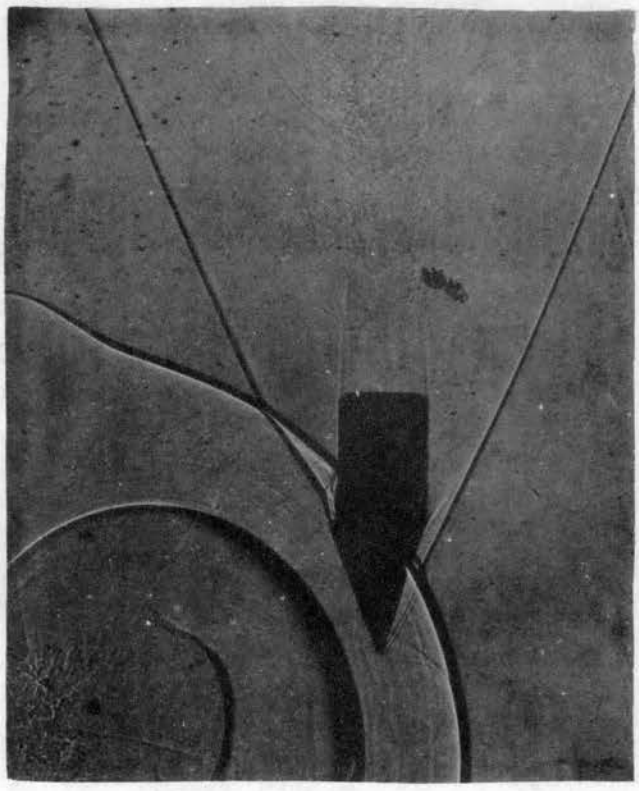

Figure 32. Schlieren Photographs of Interaction in F-114
Model Mach No. 3.94
Blast Wave Mach No. 3.14
Interaction Angle 35°

(c)

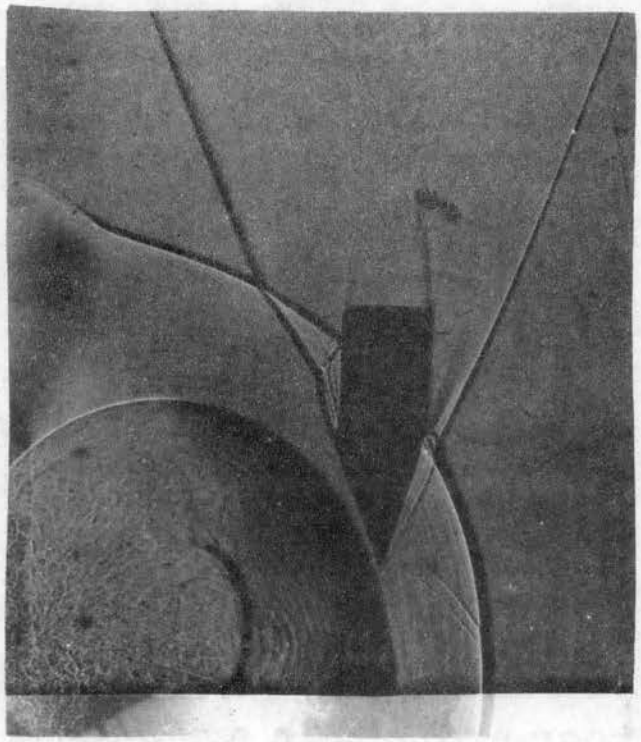

(d)

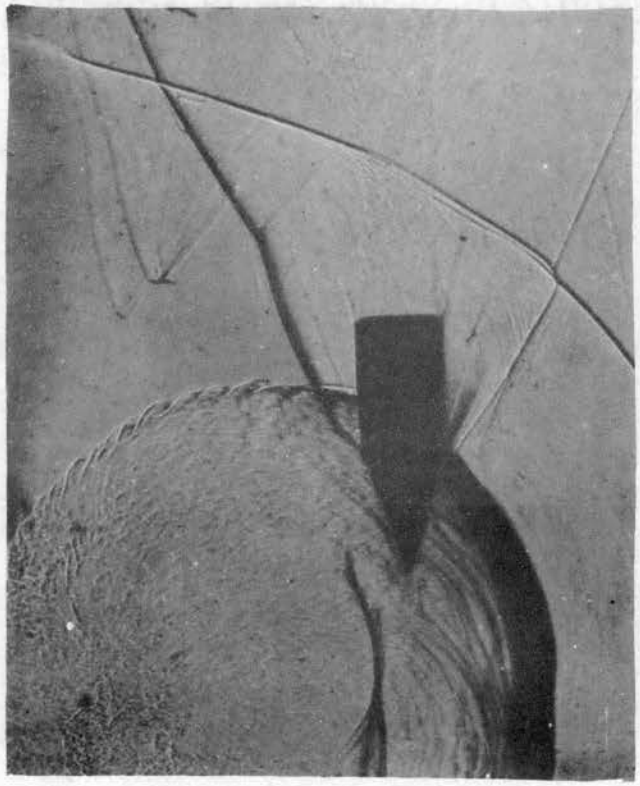

Figure 32. (Continued)

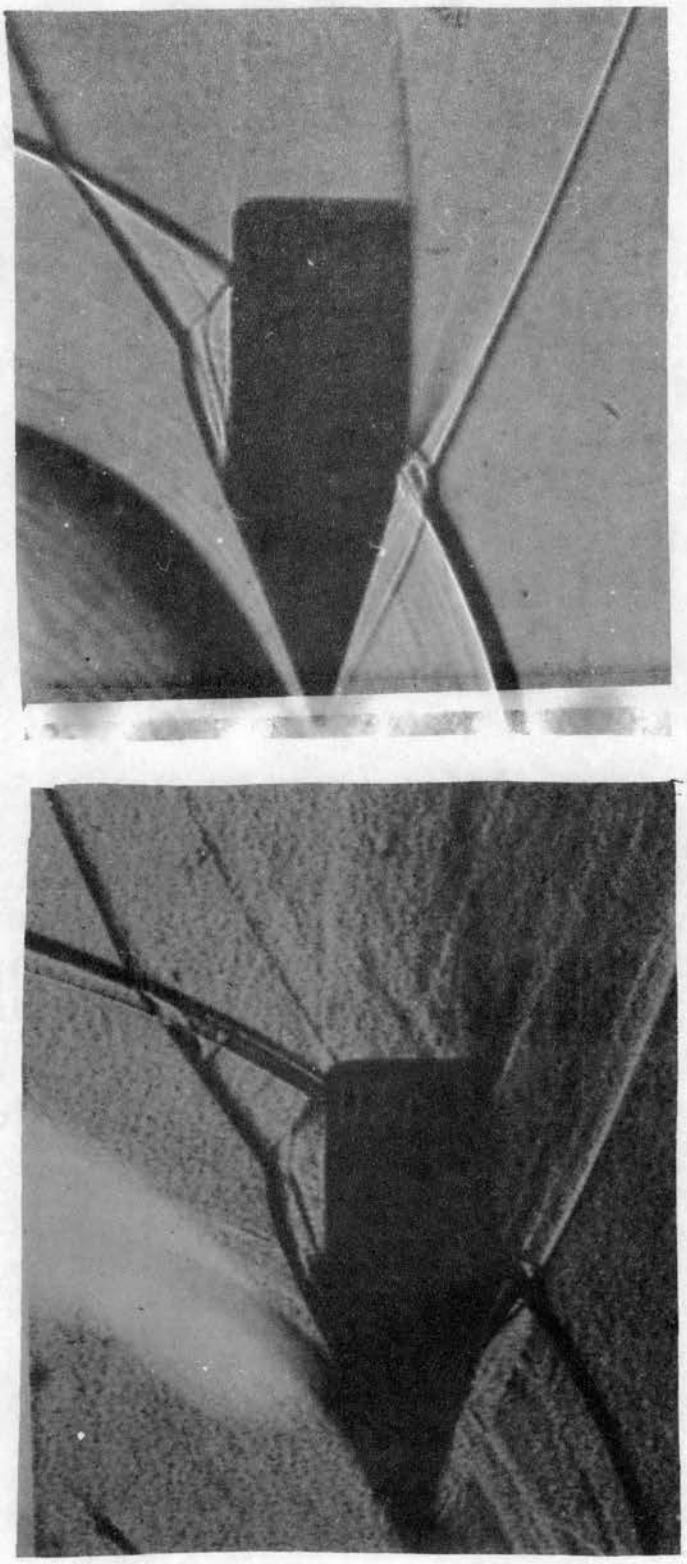

Figure 33. Enlarged Photographs of the Interaction Geometry

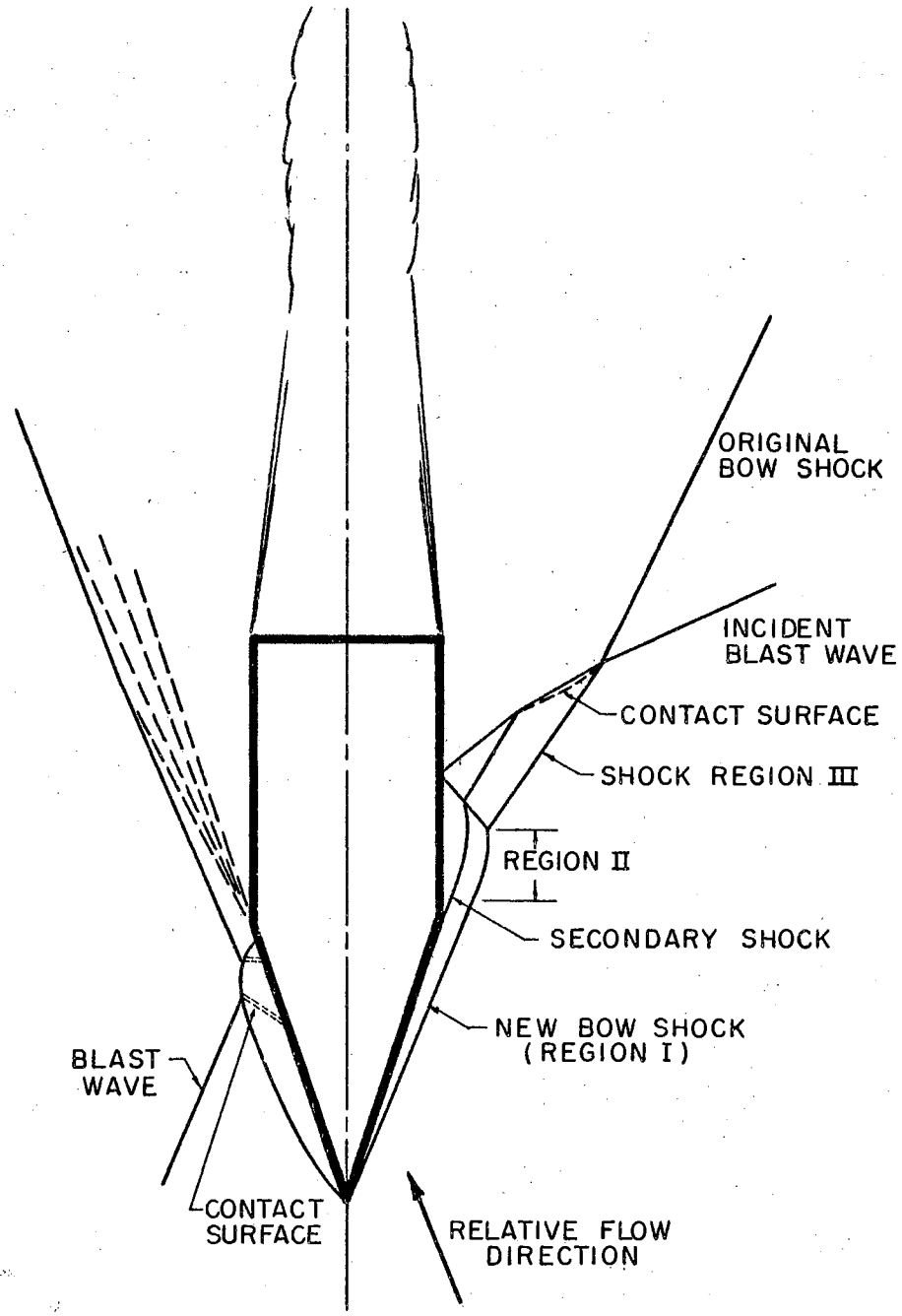

Figure 34. Sketch Showing Shock Geometry of Interaction at 35°; Model Mach Number 3.94; Blast Mach Number 3.14

and the blast wave. This general pattern is also found in head-on interactions (7), (8)*. A secondary effect of the oblique interaction is seen at the cone-cylinder junction. The cylindrical portion of the model, unlike the head-on case, is still at an angle against the flow direction so that secondary compression wave is started at this junction. Since this shock wave is inside the main shock region, it tends to intersect the new bow shock. The reflected blast wave intersects this wave and then meets the bow wave at the intersection of regions II and III. Normal reflection was observed for all cases. Finally, a contact surface is observed to start at the intersection point of the blast wave with the bow shock. This contact surface generally is very close to the blast wave and is sometimes indistinguishable.

The shock pattern on the low-pressure side is harder to evaluate. Computations show that the relative flow direction in the region behind the blast is as shown in Figure 34. The flow should, therefore, expand around the cone on this side, although the expansion angle is only about four degrees in this case. In some of the interaction photographs, this region can be seen clearly and no bow shock is seen on the low pressure side of the cone (Figure 33(b)). But generally, the blunt tip of the model and the high-pressure relief from the other side produce a

---

*See also Figure 2.

bow shock, slightly detached from the tip and bulging outwards. Several slip lines are seen between the detached shock and the cone surface. The flow in this region has been accelerated so that the blast wave in this region is pushed forward slightly ahead of the blast wave outside the interacted region. The bow shock finally curves inwards and meets the original bow wave, forming a region resembling a Mach reflection with the accelerated blast wave as the Mach stem. The pattern is self-similar until the blast wave clears the conical portion.

Figure 35 shows the schematic of the next stage of the interaction. The model has completely passed through the blast wave. The secondary shock wave from the cone-cylinder junction on the high-pressure side has disappeared and the reflected blast wave portion has become attached to the junction of regions II and III and is traveling with it. Region II is now less curved since it has traveled further from the cone surface that originated the disturbance causing the curvature. The curved shock on the low-pressure side has become straighter. It meets the blast wave further out from where the original bow wave meets it, and the intermediate portion has turned more sharply. A contact surface has formed in the wake region as shown. The distortion of the blast wave by the wake is also clearly seen.

Comparison with the shock geometries for head-on interaction shows much similarity on the high-pressure side

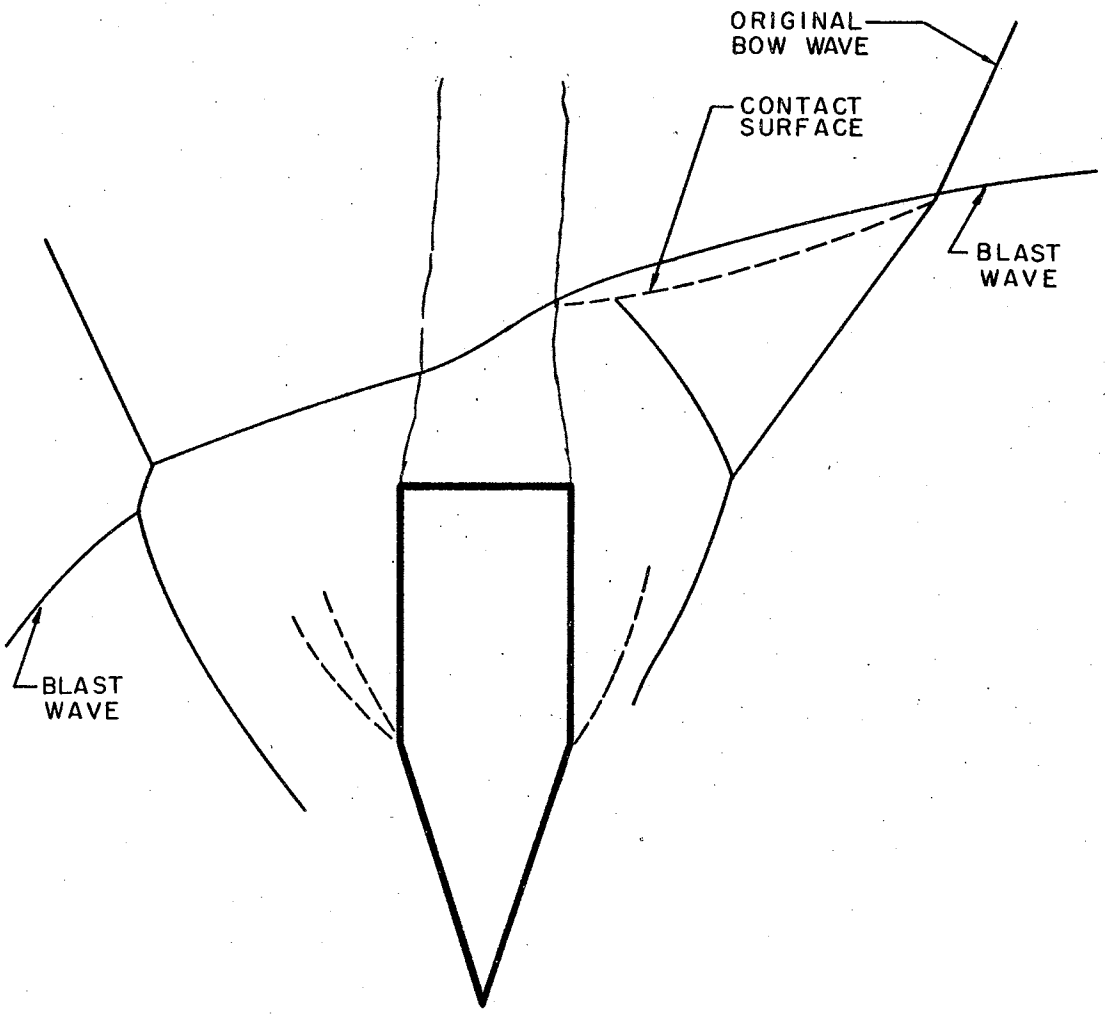

Figure 35. Sketch Showing Geometry After Model has Passed Through

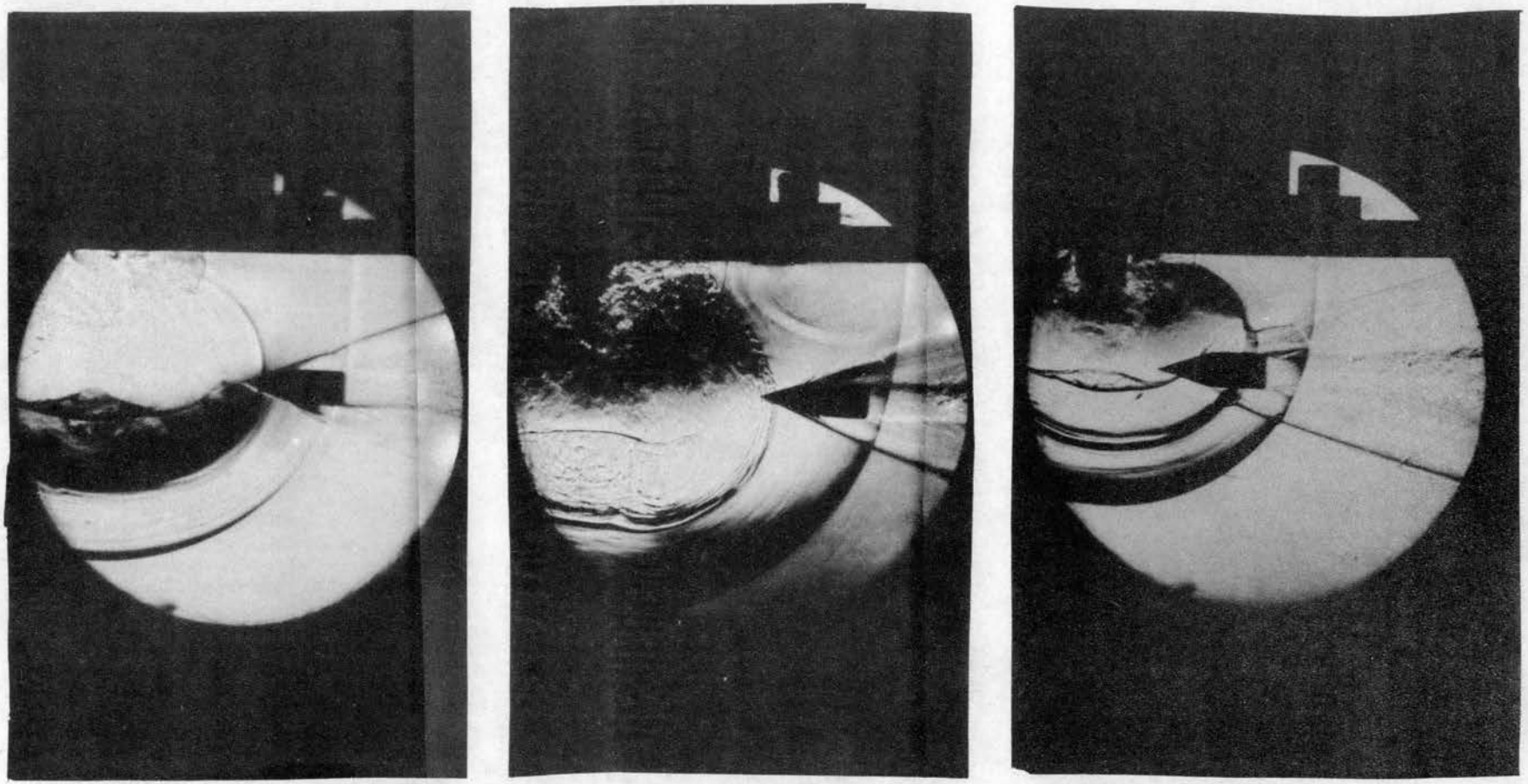

Figure 36. Schlieren Photographs of
Interaction in F-114
Model Mach No. 3.94
Blast Wave Mach No. 3.14
Interaction Angle 80°

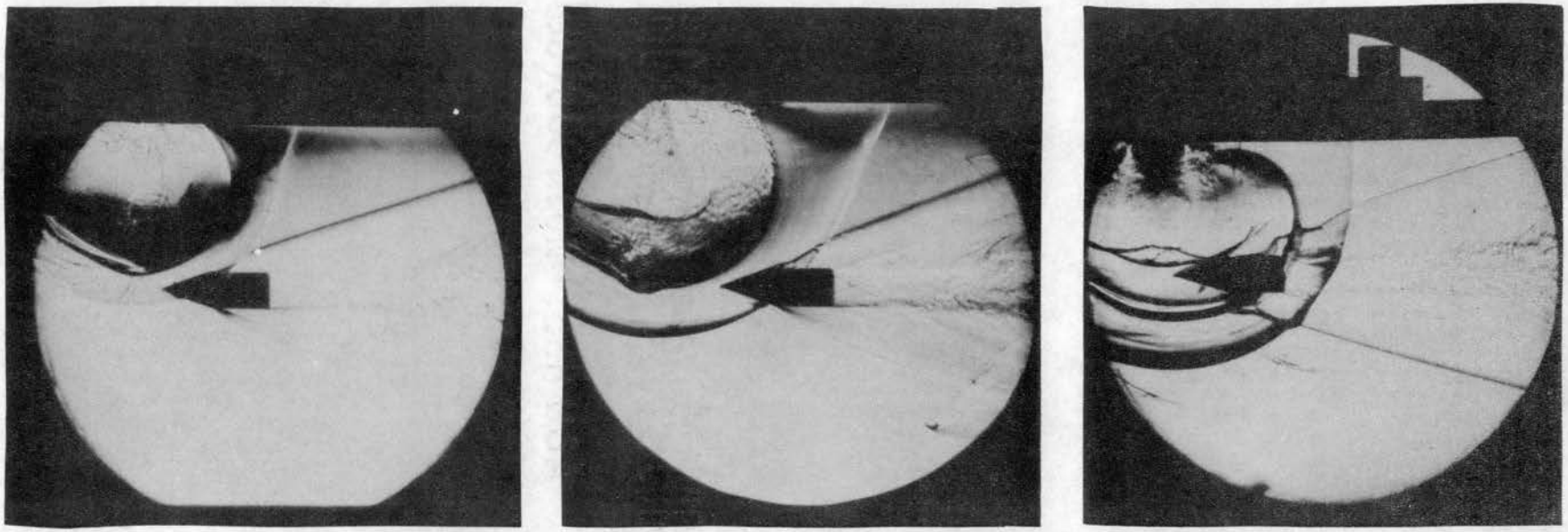

Figure 37. Schlieren Photographs of
Interaction in F-114
Model Mach No. 3.94
Blast Wave Mach No. 3.14
Interaction Angle 25°

but the pattern on the other side is quite different. This difference must cause considerable pressure differences between the two sides of the model and a possible change in the direction of its travel. Figure 36 shows interaction between a model and blast wave at an angle of 80° (90° being head-on). A sequence of interactions at approximately 25° is shown in Figure 37.

Estimation of Pressure on the Conical Nose

An estimate based on the shock angles measured from Figure 34 was made for the conical forebody, the main steps of which are presented below. A detailed derivation of the thermodynamic constants R and γ which are needed for the calculations was presented in Chapter III. Data:

M_c = Model Mach number = 3.94

M_b = Blast Mach number = 3.14

Blast wave makes an angle of 35° with the model axis.

Velocity Behind Blast Wave

The blast wave velocity is read off from Figure 24 which gives measured blast velocities at different locations in the receiver. This is found to be 1695 fps. After superimposing on the entire flow an equal velocity in the opposite direction, the corresponding steady (locally) normal shock is obtained as in Figure 38. The velocity behind the shock wave V_y' is obtained from the Prandtl relation:

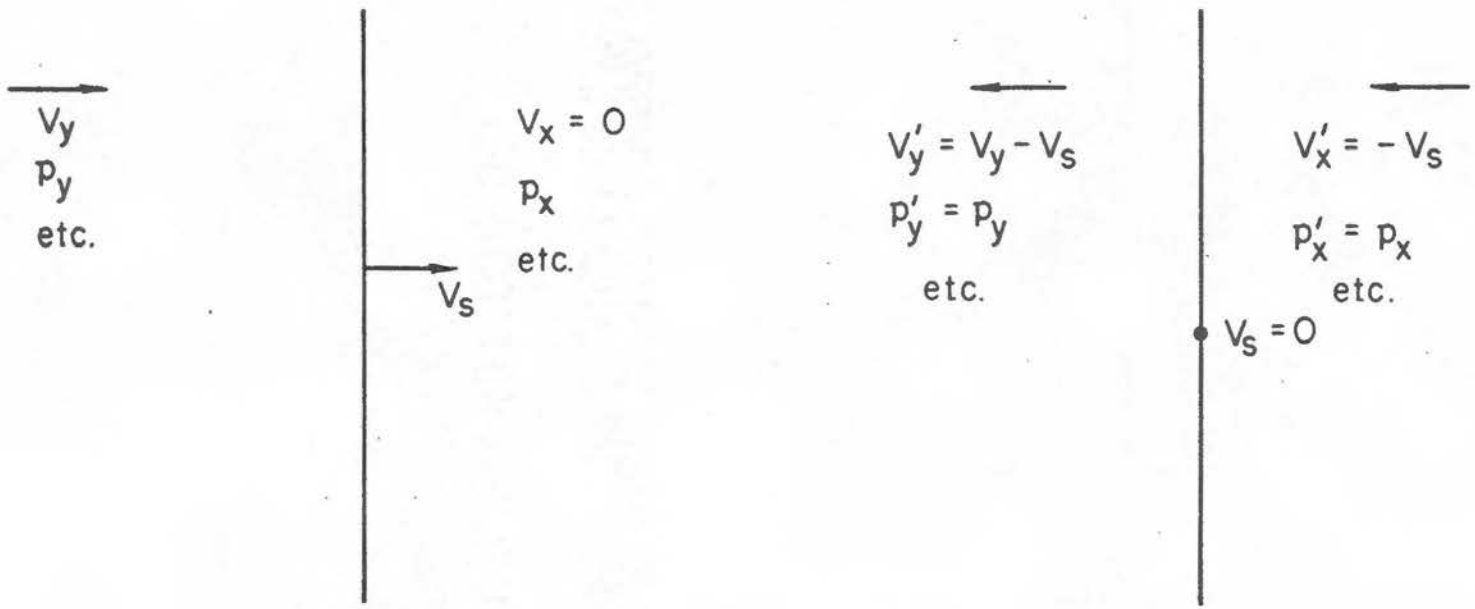

Figure 38. Coordinate Transformations

$$V_x' V_y' = a_*'^2\left(\frac{\gamma - 1}{\gamma + 1} M_x'^2 + \frac{2}{\gamma + 1}\right)$$

$$V_y' = \frac{540^2}{1695}\left(\frac{1.1 - 1.0}{1.1 + 1.0} 3.14^2 + \frac{2}{1.1 + 1.0}\right)$$

$$V_y' = 244.7 \text{ fps} \qquad (1)$$

or $$V_y = -V'_y + V_s = 1450.3 \text{ fps}$$

and from normal shock relation:

$$M'_y = 0.3722. \qquad (2)$$

Combination of (1) and (2) gives $a_y = a'_y = 604.0$ fps.

Relative Velocity After Model Penetration

The velocity relative to the model is next obtained graphically as in Figure 39. The measured velocity is 3180 fps, resulting in the Mach number of the flow relative to the model of 5.26, and is at an angle of 22° to the model axis.

Pressure Rise Across Bow Wave

The bow shock angle on the high-pressure side measured from Figure 34 is 22°. Hence, the bow shock is making an angle of 22° + 22° = 44° with the flow direction. Assuming locally two-dimensional flow for the meridian plane, one can use relations for oblique shocks to obtain pressure ratio across this shock wave. This method gives the following relation:

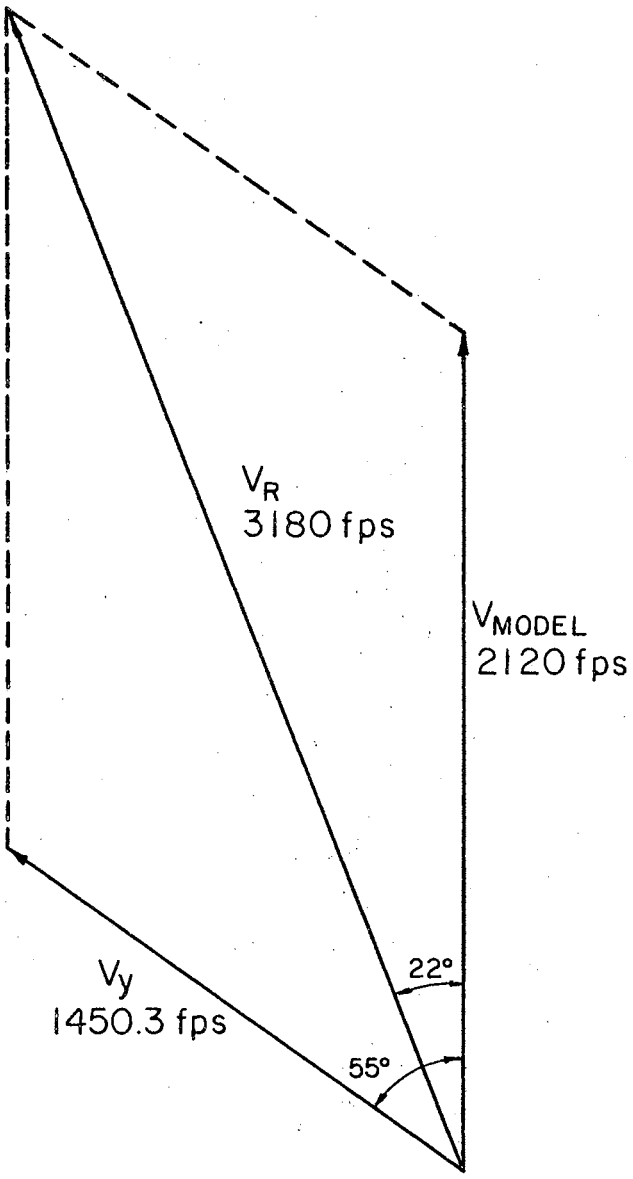

Figure 39. Vector Diagram for Obtaining Relative Flow Direction After Interaction Behind the Blast Wave

$$P_w = 13.98\ P_r \tag{3}$$

P_r = pressure rise across the bow shock (receiver pressure being taken as 1.00)

$$= 10.27. \tag{4}$$

From (3) and (4):

$$P_w = 143.5. \tag{5}$$

Surface Pressure on the Low Pressure Side

Prediction of the pressure on this side becomes difficult because of the numerous slip lines and the curved bow shock present in this region. However, it seems that the pressure on this side should not be much different from the pressure behind the blast wave as the relative flow direction almost coincides with the general bow shock angle. There would have been an expansion wave on this side if the model were a wedge, but the conical shape allows relief of pressure from the high pressure side and the bow shock to be formed, as explained earlier.

Finally, the computed transient pressure of 143.5 times that of the local atmosphere on the high pressure side of the conical forebody points out the strength of the shock-on-shock interaction. The steady-state pressure on the same conical forebody before interaction was estimated at 2.86 times the free-stream pressure and the incident blast pressure ratio was 10.27. A simple product of the pressures would give 29.28, so the wave reflected

from the body surface must account for a further multiplication factor of 4.88. The large pressure difference between the two sides of the borebody should affect the trajectory of the projectile upon entering the blast region. The usefulness of the schlieren photographs in making such order-of-magnitude estimates is, thus, clearly seen.

CHAPTER V

CONCLUSIONS AND RECOMMENDATIONS

The experimental technique of using a rifle-launched model and a blast wave from a short shock tube for the study of oblique interaction between a supersonic cone-cylinder body and a blast wave is found to be feasible. The shape of the model is not restricted to a cone-cylinder except that some portion of the model should be cylindrical to permit loading into standard rifle cases. Repeatability in timing was the biggest stumbling block to the success of this technique, and this has been achieved by using the signal from the launched model to trigger electrically the shock wave. The electronic delays which were used performed well but showed considerable dependence on temperature and, hence, needed constant readjustment.

The use of Freon-114 as the driven gas in the shock tube improved the visualization of shock phenomena at low pressures, in addition to greatly increasing the model Mach number due to its high molecular weight and low specific heat ratio. To the author's knowledge, this is the first published work involving a shock tube using this gas. The curve showing shock Mach number versus diaphragm

pressure ratio for a helium/Freon-114 combination (Figure 27) should prove useful for further work.

The schlieren photographs of the interaction of an oblique blast and a cone-cylinder body are the first to be obtained for a free-flight model. The interaction pattern does not have any entirely unexpected geometry on the side first encountering the blast wave. Nevertheless, the shock angles are not theoretically predictable because of the finite-body effects involved when the entire flow picture is considered. The shock geometry on the lee side of the model is quite different and unpredictable from any theory presently known. The value of taking photographs is apparent.

An estimate of the pressures on the conical forebody, based on the measured shock angles, gives an idea of the enormous pressure rise caused by the passage of a nearly side-on blast wave. The transient pressure was found to be at least 50 times the steady-state pressure before interaction for a model traveling at Mach 3.94 encountering a blast wave having a pressure rise of 10.27 across it. Furthermore, there is pressure unbalance between the two sides of the body in the meridian plane so that the trajectory would be altered upon encounter with the blast wave.

Recommendations for Future Work

One of the limitations of this technique was that the

shock wave was always curved and somewhat non-uniform at the time of intersection with the model. If a larger diameter shock tube were used for the same model size, a larger opening could be provided and the shock wave curvature reduced. The present work could then be extended easily to cover truly side-on interactions.

A method of obtaining sequential photographs of each interaction should be developed. Records of successive changes in shock geometry for the same model and blast wave at different time instants would greatly enhance the value of the results, in addition to the saving in number of runs required for the record of a sequence. A multiple-spark light source with multiple paths of light intersecting in the test section is described in Reference (23). Events as close as 10 microseconds could be photographed by this method on different areas of the same film plate. The disadvantage of this method is that the different angles at which the light beams travel through the interaction region would introduce distortion. An alternative method that can be suggested is to use a rotating mirror camera along with a very high intensity steady light source. Recently, laser techniques have been developed for obtaining photographs of events as close as five microseconds apart (24).

Further results for the oblique interaction could be obtained for stronger blasts and faster models. The medium in which the interaction takes place would have to be

air, however, because Freon-114 would be too dense under the circumstances to give sufficiently detailed photographs of the region between the shock and the body. Even at a Mach number of 3.94, the 19.5 degree cone of the model gave a bow shock angle of only 25 degrees and details between the cone surface and the bow shock after interaction were rendered difficult to observe. A word of caution about using models machined out of commercial bullets is also in order here. Excessive powder loads are likely to cause distortion of the brass jacket resulting in a frozen jecket inside the rifle bore. The next shot would then result in the destruction of the weapon. It is best to leave some portion of the brass jacket on the conical part of the model for this reason. Also, it is essential to check the bore of the rifle for any obstructions after each experiment.

SELECTED BIBLIOGRAPHY

(1) Smyrl, J. L. "Impact of a Shock Wave on a Thin Two-Dimensional Aerofoil Moving at Supersonic Speed." J. of Fluid Mech., Vol. 15, 1963, 223-240.

(2) Brown, E. A., Jr., and G. J. Mullaney. "A Technique for Studying the Shock-on-Shock Problem." Boeing Scientific Research Laboratories, Flight Sciences Laboratory Report No. 99, June 1965.

(3) Pierce, D. "Simulation of Blast Waves in a Supersonic Wind Tunnel." Royal Aircraft Establishment, Farnborough, England; TN AERO 2665, Jan. 1960.

(4) Merritt, D. L., and P. M. Aronson. "Study of Blast-Bow Wave Interactions in a Wind-Tunnel." AIAA preprint 65-5, Jan. 1965.

(5) Bingham, G. G, and T. E. Davidson. "Investigation of Simulation of Shock-Shock Interaction in Hypersonic Gasdynamic Test Facility." Wright-Patterson Air Force Base Tech Report FDL-TDR-64-9, 1964.

(6) Tyler, L. D., and G. W. Zumwalt. "Numerical Solutions of the Flow-Field Produced by a Plane Shock Wave Emerging Into a Crossflow." Oklahoma State University Research Report SBW-10 (Available as Research Report SC-DC-65-1916 from Sandia Corporation, Albuquerque, New Mex.), Aug. 1965.

(7) Brown, E. A., Jr., and G. J. Mullaney. "Experiments on the Head-on Shock-Shock Interaction." AIAA Journal, Vol. 3, No. 11, 1965, 2168-2170.

(8) Merritt, D. L., and P. M. Aronson. "Free-Flight Shock Interaction Studies." AIAA paper 66-57, Jan. 1966.

(9) Walker, W. F., and L. D. Tyler. "Literature Survey on Shock Wave Interactions With Shocks and Bodies." Oklahoma State University Report SBW-7 (prepared for Sandia Corp. Aerothermodynamic Division, Albuquerque, N. M.), 1964.

(10) Miles, J. W. "Notes on the Diffraction of Blasts by Flying Vehicles." Aerospace Corporation Report TDR-269 (4230-30)-1, Aug. 1963.

(11) Whitham, G. B. "A New Approach to Problems of Shock Dynamics, Part I, Two-Dimensional Problem," J. Fluid Mechanics, Vol. 2, 1957, 145-171.

(12) Wolff, W. S. "Transient Flow Field Analysis Around a Conical Body Exposed to a Blast Wave." Lockheed Missiles and Space Co. Report No. 4-70-64-1, 1964.

(13) Inger, G. R. "Blast Wave Impingement on a Slender Wedge Moving at Hypersonic Speeds," AIAA Journal, Vol. 4, No. 3, March 1966, 428-435.

(14) Lax, P. "Weak Solutions of Nonlinear Hyperbolic Equations and Their Numerical Computation." Comm. Pure and Appl. Math., Vol. VII, 1954, p. 159.

(15) Rusanov, V. V. "The Calculation of the Interaction of Non-Stationary Shock Waves and Obstacles."* Akademiya Nauk, SSSR 1, Vol. 1, No. 2, p. 267, 1961. (National Research Council of Canada Library Tech. Translation 1027 by D. A. Sinclair, 1962.) *(Zhurnal Vychislitelnoi Fiziki)

(16) Jackomis, W. N., and G. W. Zumwalt. "Transient Flow-Field Analysis of a Plane Blast Wave Intercepting a Stationary Cone at Zero Angle of Attack." Oklahoma State University Research Report SBW-9 (Available as Research Report SC-DC-66-1319 from Sandia Corporation, Albuquerque, N. M.), Aug. 1965.

(17) Eaton, R. R. "A Numerical Solution for the Flow Field of a Supersonic Cone-Cylinder Entering and Leaving a Blast Sphere Diametrically." (Unpublished Ph.D. thesis, School of Mechanical Engineering, Oklahoma State University, 1967.)

(18) Lyman Gunsight Corporation Staff. Lyman Reloading Handbook. 43rd Edition, 1964.

(19) Lazalier, G. R. "Design and Construction of a Shock Tube Facility for the Study of Shock Waves Emerging From Openings." (Unpub. M. S. thesis, School of Mechanical Engineering, Oklahoma State University, 1965.)

(20) Bradley, J. N., R. N. Butlin, and J. G. Quinn. "An Electrical Breaking Method for Shock Tube Diaphragms." J. Scientific Instruments, Vol. 42, 1965, 901-902.

(21) Fitzpatrick, J. A., J. C. Hubbard, and W. J. Thaler. "A High Intensity Short Duration Spark Light Source," Journal of Applied Physics, Vol. 21, Dec. 1950, 1269-1271.

(22) Wilson, M. R., and R. J. Hiemenz. "High-Speed Multiple-Spark Light Source," Review of Scientific Instruments, Vol. 29, No. 11, Nov. 1958, 949-951.

(23) DeLeeuw, J. H., I. I. Glass, and L. E. Heuckroth. "A High-Speed Multi-Source Spark Camera." Institute of Aerophysics, University of Toronto, UTIA Technical Note No. 26, Feb. 1962.

(24) Steel, G. B. "High-Speed Schlieren Photography Using a Kerr Cell Modulated Laser Light Source," AIAA Student Journal, Vol. IV, No. 3, Oct. 1966.

(25) Glass, I. I., and J. G. Hall. "Handbook of Supersonic Aerodynamics, Section 18, SHOCK TUBES." NAVORD Report 1488, Vol. 6, 1959.

(26) Obert, E. F. Concepts of Thermodynamics. New York: McGraw-Hill Book Company, 1960.

APPENDIX I

MONOSTABLE MULTIVIBRATOR

The Engineered Electronics Z-8889 packaged 'one-shot' unit employs a type 5963 dual-triode tube. It can be described as a cathode-coupled one-shot multivibrator. In the circuit shown in Figure 40, the two triode sections are designated as V_1 and V_2. The plate of V_1 is capacitively coupled to the grid of V_2. The coupling from V_2 to V_1 is through the common cathod resistor R_o, whence the classification "cathode-coupled."

The voltage E_{cc} on the grid of V_1 is set by the potentiometer R_p to a value such that V_1 is cut off. Tube V_2 is clamped ON since its grid resistor R_{g2} is connected to the plate supply E_{bb}. When a positive pulse of sufficiently large amplitude is applied to the grid of V_1, V_1 starts conducting and the potential at point 7 is abruptly lowered. This is coupled immediately to the grid of V_2, where it decreases the plate current and causes the voltage drop across the cathode resistor R_c to decrease. This decrease in cathode voltage increases the conduction in V_1 still further and regenerative switching occurs so that V_2 goes OFF and V_1 goes ON. Capacitor C_1 will now discharge. When C_1 has discharged so that the grid bias of V_2 is less

than cutoff, the plate current in V_2 increases the cathode voltage, which increases the grid bias of V_1 and decreases its plate current. This increases the plate voltage of V_1, which is coupled to the grid of V_2, so that V_1 is again OFF and V_2 ON. This completes the cycle ON-OFF-ON for V_2 and OFF-ON-OFF for V_1, which was instigated by the positive trigger pulse at the grid of V_1. This one-shot multivibrator action can also be triggered by a negative pulse at the plate of V_1.

One useful feature of the above circuit is that the period T between the start and completion of a cycle is a linear function of Ecc over a considerable range. It can be approximated by the following formula:

$$T = C_1(0.08\ E_{cc} - 0.6)$$

where C_1 is in pica-farads, E_{cc} in volts and T is given in microseconds.

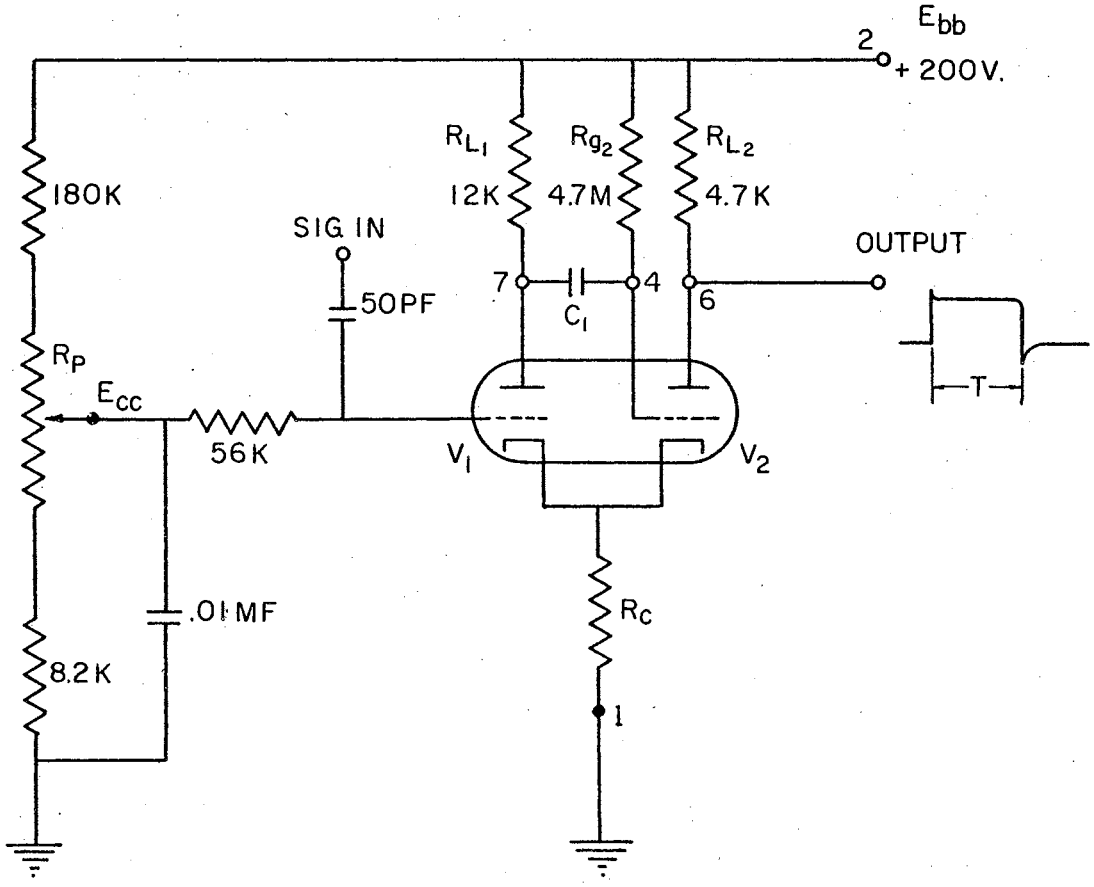

Figure 40. Monostable Multivibrator

APPENDIX II

PROPERTIES OF FREON-114 ($C\ Cl\ F_2$-$C\ Cl\ F_2$)

The physical properties of Freon-114 are presented below to aid in calculations related to the use of this gas as a driven medium in a shock tube.

Molecular Weight	170.93	
Boiling Point	38.4° F	at 1 atm.
Freezing Point	-137° F	
Critical temperature	294.3° F	
Critical pressure	474	psi absolute
Density of saturated vapor at boiling point	0.488	lb/cft
Specific Heat of vapor at constant pressure (1 atm) at 86° F.	0.160	Btu/lb °F
Specific Heat Ratio at 86° F and 1 atm	1.088	

Non-flammable and has faint ethereal odor.

Figure 41 gives the ratio of specific heats for Freon-114 at different temperatures and pressures. It is clear that any calculations involving large temperature changes would need to take this variation into account.

Figures 42 and 43 show the corresponding variation of the specific heats at constant pressure and constant volume, respectively.

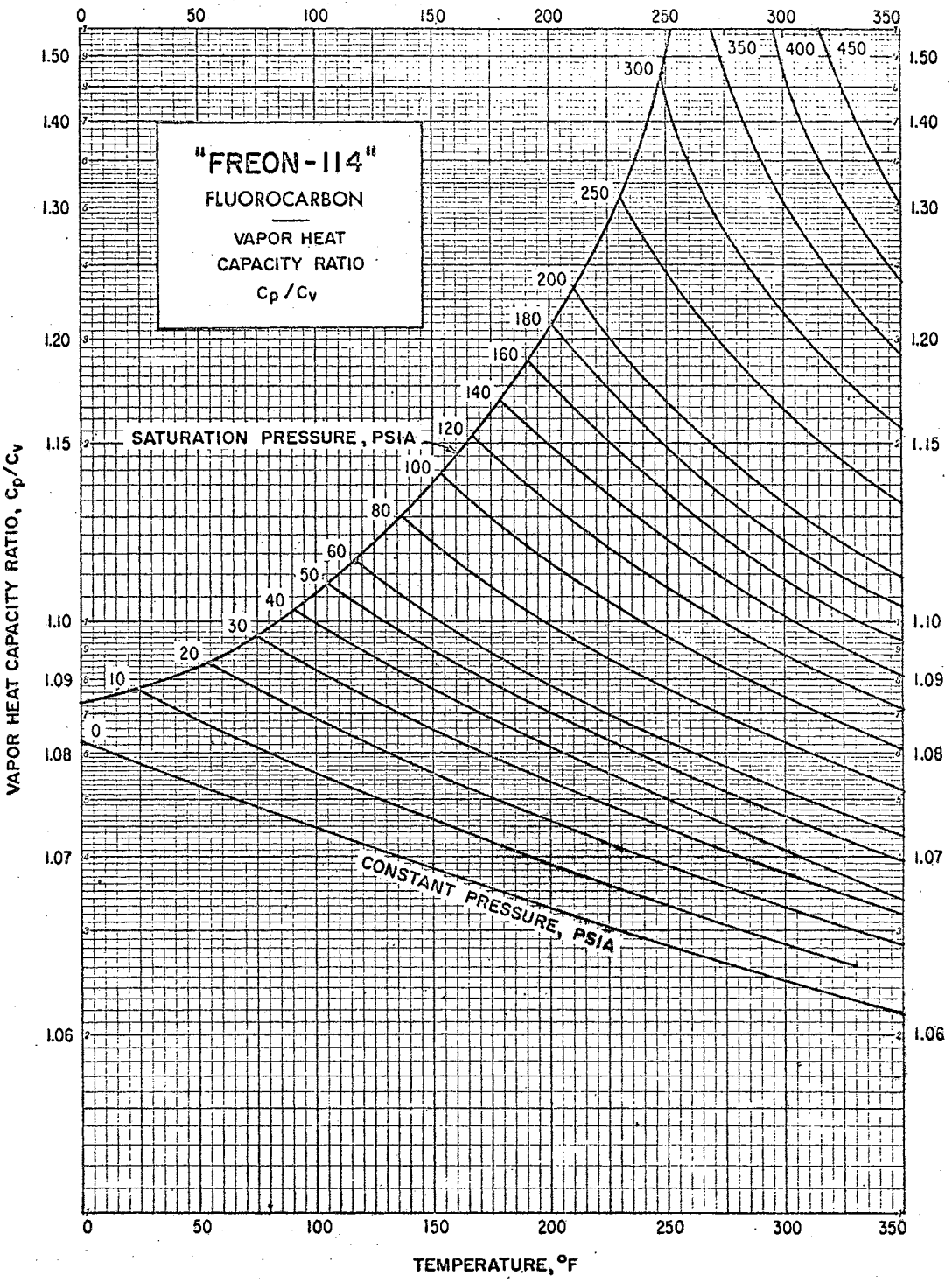

Figure 41. Variation of γ for Freon F-114

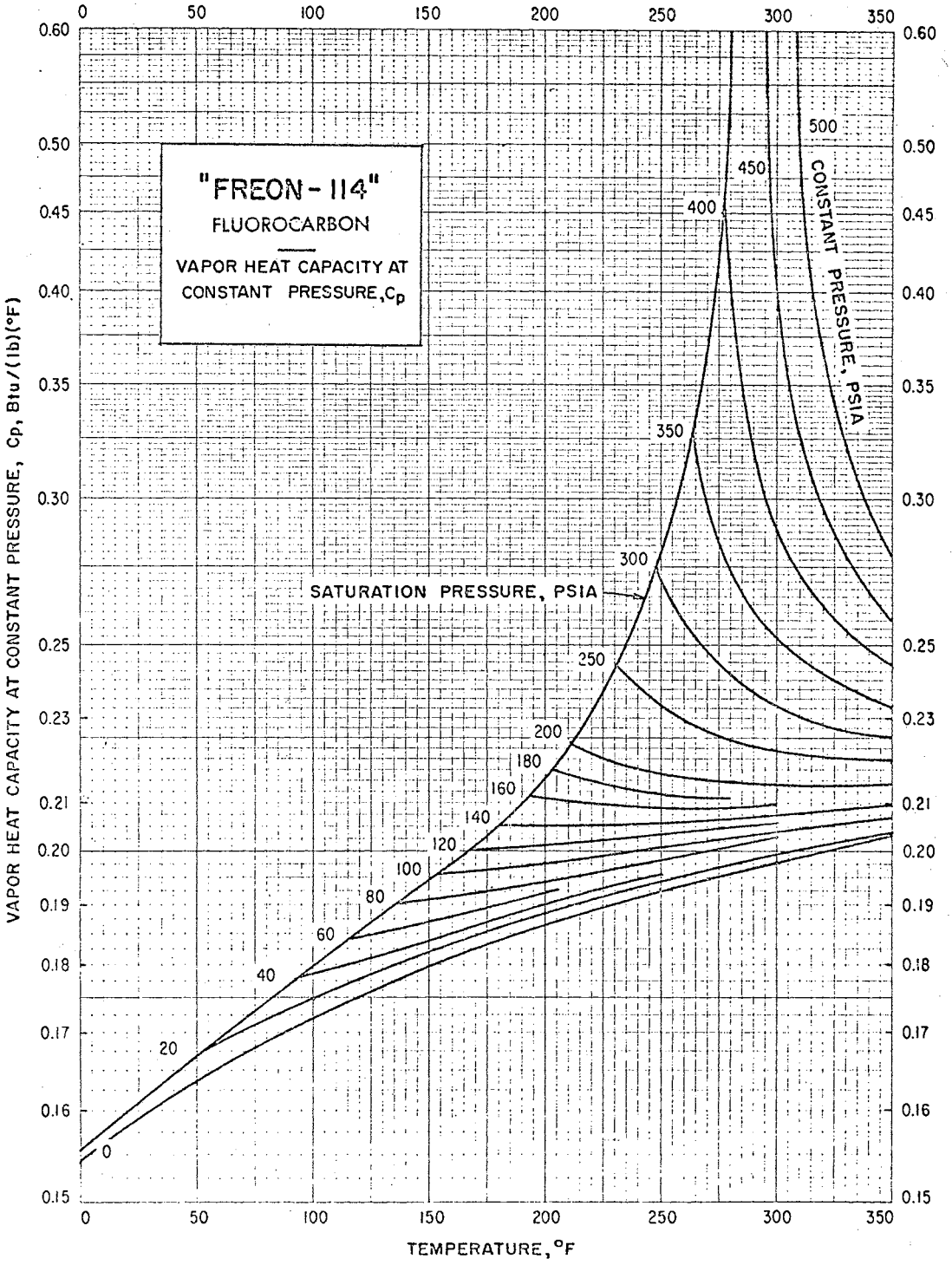

Figure 42. Variation of C_p for Freon F-114

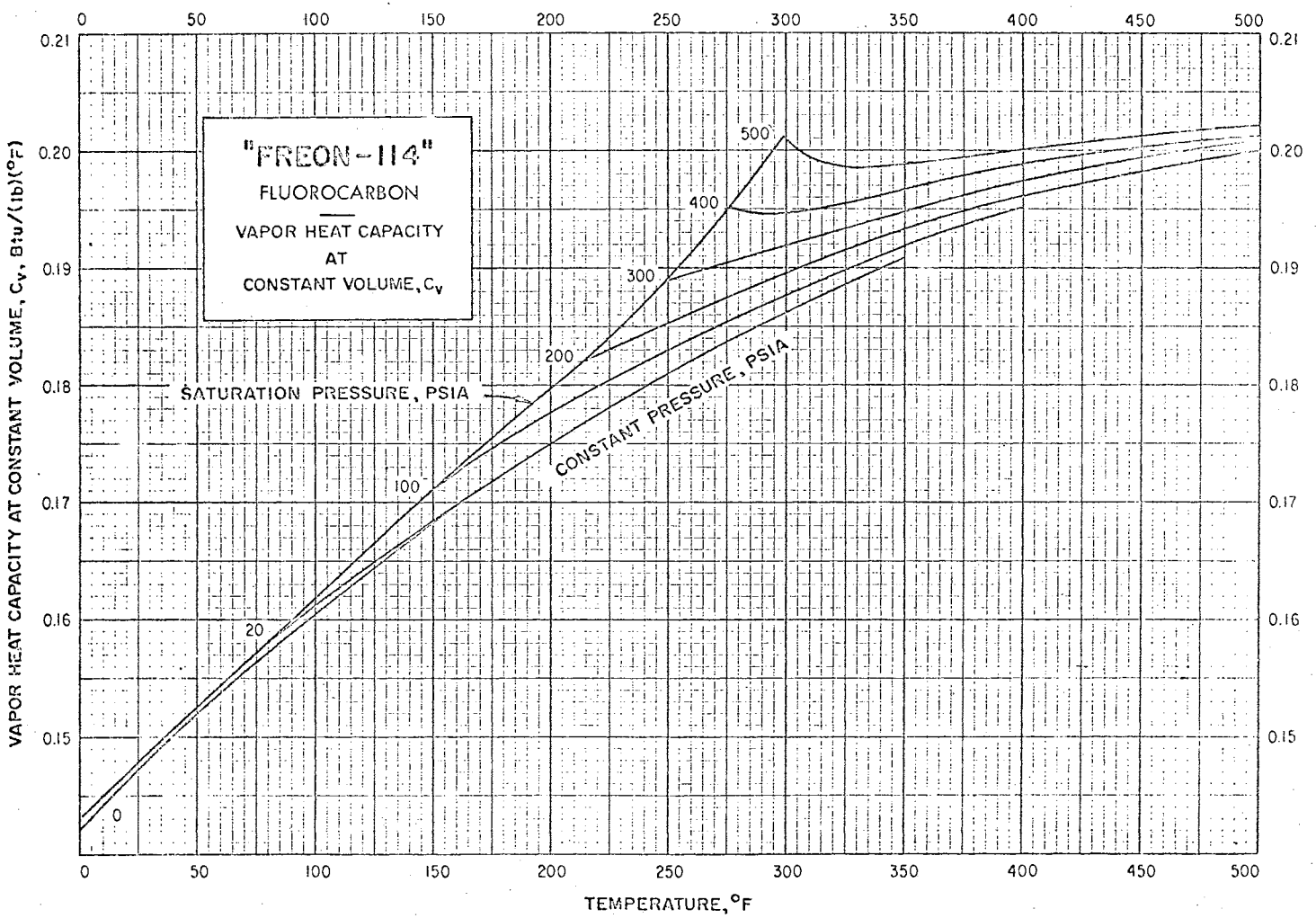

Figure 43. Variation of C_v for Freon F-114

VITA

Rusi Jal Damkevala

Candidate for the Degree of

Doctor of Philosophy

Thesis: A TECHNIQUE FOR STUDYING INTERACTIONS BETWEEN A SUPERSONIC BODY AND BLAST WAVES APPROACHING OBLIQUELY

Major Field: Mechanical and Aero-Space Engineering

Biographical:

Personal Data: Born in Bombay, India, December 7, 1939, the son of Jal E. and Banoo Damkevala.

Education: Attended schools in Bombay, India, graduating from Bharda New High School in 1955; received the Bachelor of Engineering degree in Civil Engineering from Gujarat University, Ahmedabad, India, in April 1960; received the Master of Engineering in Aeronautical Engineering from the Indian Institute of Science, Bangalore, in Aug. 1962; completed the requirements for the Doctor of Philosophy degree in December 1966.

Experience: Civil engineer for City and Suburban Construction Company, Bombay, India, during the summers of 1959 and 1960. Junior Aeronautical Engineer at Hinduatan Aircraft Limited, Bangalore, India from Sept. 1962 to Aug. 1963. Research Assistant at Oklahoma State University, Stillwater, Oklahoma, from Feb. 1964 to Dec. 1966.

Professional Organizations: The author is a member of the American Institute of Aeronautics and Astronautics.